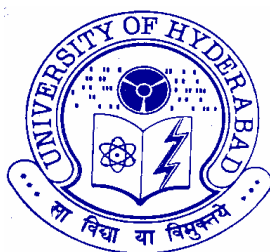


Structure, Phase Behavior and Membrane Interactions of *N*-Acylethanolamines and *N*-, *O*-Diacylethanolamines

A Thesis
Submitted for the Degree of
DOCTOR OF PHILOSOPHY

By
K. RAVIKANTH

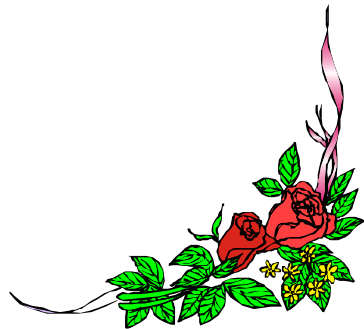


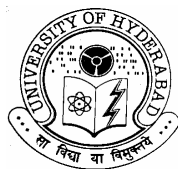
School of Chemistry
University of Hyderabad
Hyderabad – 500 046
INDIA

September 2006



*Dedicated to
my beloved
family & friends*





**School of Chemistry
University of Hyderabad
Hyderabad – 500 046**

STATEMENT

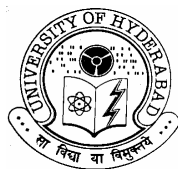
I hereby declare that the matter embodied in this thesis is the result of investigations carried out by me in the School of Chemistry, University of Hyderabad, Hyderabad, under the supervision of **Prof. Musti J. Swamy**.

In keeping with the general practice of reporting scientific observations, due acknowledgements have been made whenever the work described is based on the finding of other investigators. Any omission which might have occurred by oversight or error is regretted.

Hyderabad

September 2006

K. Ravikanth



**School of Chemistry
University of Hyderabad
Hyderabad – 500 046**

CERTIFICATE

Certified that the work embodied in this thesis entitled “**Structure, Phase Behavior and Membrane Interactions of *N*-Acylethanolamines and *N*-, *O*-Diacylethanolamines**” has been carried out by **Mr. K. Ravikanth**, under my supervision and the same has not been submitted elsewhere for any degree.

Hyderabad

September 2006

**Prof. Musti J. Swamy
(Thesis Supervisor)**

**Dean
School of Chemistry**

ACKNOWLEDGEMENTS

I sincerely thank and express my deep gratitude to my supervisor Prof. M. J. Swamy, for his excellent guidance and encouragement given throughout the Ph.D. program. I appreciate his patience, kindness and very understanding and humanistic approach.

My sincere thanks to Prof. D. Marsh, Max-Planck Institut für biophysikalische Chemie, Göttingen, Germany for the access to his laboratory facilities such as DSC and ESR. I am fortunate to be associated with him. I also thank his coworkers Frau B. Angerstein, who synthesized all spin-labels used in the present study, and Frau Inge Dreger for the kind understanding and care extended to me and for making my life comfortable during my stay in Göttingen. I thank Dr. Tibor Páli and Mr. Dieter Kurad for their understanding and help during my stay there.

I am grateful to Prof. T. P. Radhakrishnan and his student Dr. Sharath Chandra for the help in carrying out the monolayer and BAM studies reported in Chapter 4, to Prof. Samudranil Pal for advice in X-ray data analysis and to Dr. B. Gopalakrishnan (Tata Consultancy Services, Hyderabad) for helpful suggestions regarding the work presented in Chapter 2 and for critically reading the related manuscript.

I thank Prof. M. Periasamy, Dean, School of Chemistry as well as past Deans of the School for providing the infrastructure for carrying out the research work and all the faculty members for the help and encouragement at different times. A special word of thanks to Prof. D. Basavaiah who helped me in various ways. I also thank all my teachers, who have guided me up to this stage.

I am very grateful to my labmates Anuradha, Rajani, Kavitha, Narahari, Pradip and Rajeshwar for providing a good working atmosphere in the lab. I would like to specially thank my seniors Dr. Ramakrishnan, Dr. Roopa, Dr. Nabil and Dr. Anbu for the fruitful discussions and suggestions.

I thank my friends Basavoju, Devender, Malla, Gupta, Anbu, Shekar, Vasulu, Pavan, Srinivas Reddy, Balu, Ram Prasad, Jagadish, Bhuvan, Satish, Padmanaban, Suresh, ShyamRaj, Narsi, Venu and Vamshi.

I thank HareKrushna, Jyothi and Pratap for making my stay in Germany a memorable one.

I thank all the research scholars of School of Chemistry and specially members of the COSIST lab for providing a cheerful atmosphere around me.

I thank all non-teaching staff of the School of Chemistry and CIL for their help and cooperation.

I thank to Saibaba's, Shekar's and Kavitha's families for being wonderful human beings and caring of my family when I am very late to home and in emergency times.

Words can never be enough to express the support which was given by my wife, son and my family members and all friends at M'Nagar. I would like place on record my appreciation to Roopa & Jay Krishna, my beloved wife and son; Ramchanderji Rao, Urmila Bai & P.M.G. Nambiar, Radhamani, my beloved parents and in-laws. My uncles VijayaRaj's and Ramakrishna's families, my brother, sisters, brothers-in-law, sisters-in-law, co-brothers and my friends Raghu, Srikanth and Dr. Kiran for their love and affection.

Ravikanth. K

LIST OF ABBREVIATIONS

General

ANS	8-Anilinonaphthalene-1-sulfonate
Ca ²⁺	Calcium ions
CoA	Coenzyme A
EDTA	Ethylenediamine tetra acetic acid
HEPES	<i>N</i> -(2-hydroxyethyl)Piperazine- <i>N'</i> -2-ethanesulfonic acid
HPLC	High-pressure liquid chromatography
NaCl	Sodium chloride
<i>Sn</i>	Stereo specific numbering
TLC	Thin layer chromatography
Tris	Tris (hydroxymethyl) aminomethane

Lipids

5-SASL	Stearic acid spin labeled on the 5 th C-atom
DAE	<i>N</i> -, <i>O</i> -Diacylethanolamine
DMPE	1,2-Dimyristoyl- <i>sn</i> -glycero-3-phosphoethanolamine
DMPG	Dimyristoylphosphatidylglycerol
DPPE	1,2-Dipalmitoyl- <i>sn</i> -glycero-3-phosphoethanolamine
FA	Fatty acid
<i>N</i> -14 DMPE	1,2- Dimyristoyl- <i>sn</i> -glycero-3-(<i>N</i> -myristoyl)phosphoethanolamine
<i>N</i> -acyl PE	
NAE	<i>N</i> -Acylethanolamine
NAEA	<i>N</i> -Arachidonylethanolamine
NAPE	<i>N</i> -Acylphosphatidylethanolamine
NLEA	<i>N</i> -Lauroylethanolamine
NMEA	<i>N</i> -Myristoylethanolamine
<i>n</i> -PCSL	Phosphocholine spin label; 1-acyl-2-(<i>n</i> -(4,4-dimethyloxazolidine- <i>N</i> -oxyl)stearoyl)- <i>sn</i> -glycero-3-phosphocholine

NPEA	<i>N</i> -Palmitoylethanolamine
NSEA	<i>N</i> -Steroylethanolamine
PC	Phosphatidylcholine
PE	Phosphatidylethanolamine
PG	Phosphatidylglycerol
PS	Phosphatidylserine
SA	Stearic acid
StCar	D, L-Stearoylcarnitine

Techniques

ΔH_t	Transition enthalpy
ΔS_t	Transition entropy
$2A_{\max}$	Outer hyper fine splitting between the spectral extrema
^{31}P -NMR	Phosphorus-31 nuclear magnetic resonance
^1H -NMR	Proton
a_0	Isotropic hyperfine splitting constant
CMC	Critical micellar concentration
DSC	Differential scanning calorimetry
ESR	Electron magnetic resonance
FAB-MS	Fast-atom-bombardment mass spectrometry
H_I	Hexagonal phase I
H_{II}	Hexagonal phase II
LB film	Langmuir blotting film
NMR	Nuclear magnetic resonance
pK_a	Acid dissociation constant
ppm	Parts per million
T_t	Transition temperature

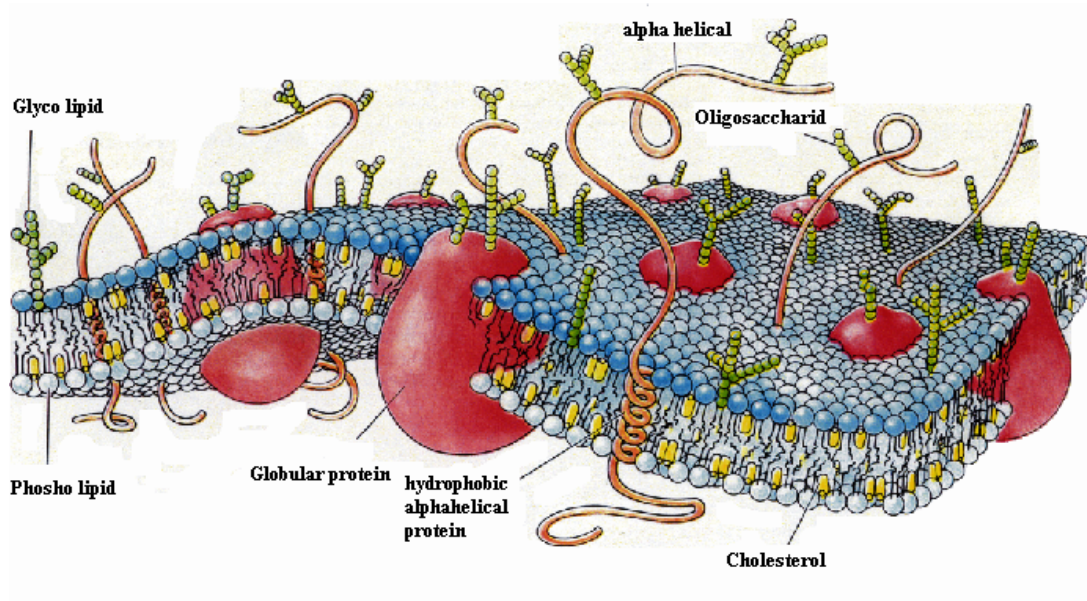
$\Delta T_{1/2}$ The width of the phase transition at half-height

CONTENTS

Statement	i
Certificate	ii
Acknowledgments	iii
Abbreviations	v
Chapter 1: A General Introduction to Biomembranes	1
Chapter 2: Crystal Structure, Molecular Packing and Intermolecular Interactions in Two Structural Polymorphs of <i>N</i> -Palmitoylethanolamine	33
Chapter 3: Differential Scanning Calorimetric and Computational Modeling Studies on the Interaction of <i>N</i> -Acylethanolamines with Cholesterol	59
Chapter 4: Interaction of <i>N</i> -Myristoylethanolamine with Cholesterol: Monolayer and Brewster Angle Microscopic Studies	75
Chapter 5: Miscibility and Phase Behavior of <i>N</i> -acylethanolamine/ Diacylphosphatidylethanolamine Binary mixtures of Matched Acyl Chainlengths (n = 14, 16)	93
Chapter 6: Synthesis, Characterization and Differential Scanning Calorimetry of <i>N</i> -, <i>O</i> -Diacylethanolamines of Matched Acyl Chainlengths (n = 10-20) and Crystal Structure of <i>N</i> -, <i>O</i> -Dilauroylethanolamine	121
Chapter 7: General Discussion and Conclusions	153
Chapter 8: Appendix	161
References	181
Curriculum Vitae	193

Chapter 1

A General Introduction to Biomembranes



The cell membrane

Lipids are as important for life as proteins, sugars, and nucleic acids. The science of lipids is called **lipidomics**. It involves a quantitative experimental and theoretical study of lipid and membrane self-assembly, lipid-protein interactions, lipid-gene interactions, and the biophysical properties of lipid structure, function, and dynamics (Mouritsen, 2005, <http://www.memphys.sdu.dk/fat-flyer.pdf>). The molecules we encounter in this chapter, the **lipids**, carry out multiple functions. Some— the fats— are used for energy storage and heat insulation. However, the largest fraction of lipids in most cells is used to form **membranes**.

1.1. BIOMEMBRANES

A **biological membrane** or **biomembrane** is a membrane which acts as a barrier within or around a cell. It is, almost always, a lipid bilayer (except for Archaea which have isoprene membrane) composed of a double layer of amphiphilic lipid molecules, a majority of which are phospholipids in the eukaryotes. A variety of proteins are associated with this bilayer, some of which function as channels. Such membranes typically define enclosed spaces or partitions in which cells may maintain a chemical or biological environment that differs from the outside, organize complex reaction sequences, and act in signal reception and energy transformation. Most organelles are defined by such membranes, and are called **membrane-bound** organelles (<http://en.wikipedia.org/wiki/Biomembrane>; Lehninger et al., 1993). The membranes are much more than passive walls; they contain highly selective gates that promote the passage of certain materials in certain directions and block others altogether. It is this property of **selective membrane permeability** that allows each of the different parts of the cell to carry out its specific operation.

The two most important energy conversion processes in biological systems are carried out by membrane systems that contain highly ordered arrays of enzymes

and other proteins. **Photosynthesis**, in which light is converted into chemical bond energy, occurs in the inner membrane of chloroplasts, while **oxidative phosphorylation**, in which adenosine triphosphate (ATP) is formed by the oxidation of fuel molecules, takes place in the inner membranes of mitochondria.

1.1.1. The Molecular Structure of Lipids

In contrast to the proteins, nucleic acids and polysaccharides, lipids are not polymers. They are rather small molecules that have strong tendency to associate through noncovalent forces. A highly schematized general structure of a lipid shown in Figure 1.1 contains a polar, hydrophilic “head” connected to a nonpolar, hydrophobic hydrocarbon ‘tail’.

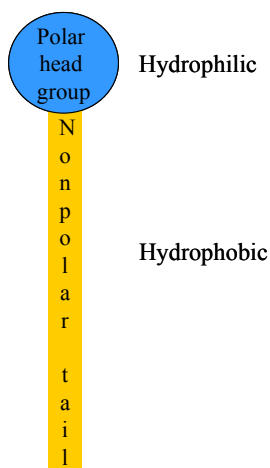


Fig. 1.1: A schematic general structure of a lipid

Lipids are an extremely diverse group of molecules. The emphasis of the present chapter is on the molecular constituents of biomembranes and their chemical architecture, the classification of membrane lipids and the currently accepted model of biomembranes, namely the **fluid-mosaic model**. In addition, the polymorphic phase behavior of hydrated lipids and the phase transitions involving

them are discussed in some detail. Finally, contemporary knowledge on *N*-acylethanolamines (NAEs), *N*-acylphosphatidylethanolamines (NAPEs) and *N*-, *O*-diacylethanolamines (DAEs) which form the main subject of study of this thesis, has been discussed. At the end of this chapter objectives and scope of the work undertaken in this study are given.

1.2. THE MOLECULAR CONSTITUENTS OF BIOMEMBRANES

In order to understand the function of biomembranes it is essential to study membrane composition. The functional variety of biomembranes arises primarily from the diversity of their constituents. Although the organizational principle underlying all biomembranes is essentially the same, membranes do differ morphologically, physiologically, biochemically and compositionally. The composition of membrane *in vivo* is preserved metabolically by biosynthesis and degradation, as well as by fusion and recycling.

Table 1.1: Major components of plasma membranes of different species*.

	Protein (%)	Phospho-lipid (%)	Other lipids	Sterol (%)	Sterol type
Mouse liver	45	27	-	25	Cholesterol
Corn leaf	47	26	Galactolipids	7	Sitosterol
Yeast	52	7	Triacylglycerols Stery esters	4	Ergosterol
<i>Paramecium</i>	56	40	-	4	Stigmasterol
<i>E. coli</i>	75	25	-	0	-

Taken from Lehninger et al. (1993). *Values are given as weight percentages.

Membranes contain primarily lipids and proteins. In addition, carbohydrates, which are covalently attached to the membrane proteins and lipids, are also present on the surface. In general, membrane protein content varies between 25 and 75% by weight, whereas the lipid comprises the rest. The

carbohydrates, which are covalently attached to proteins and lipids, typically make up less than 10% of the membrane by weight. By employing different fractionating procedures the membrane components can be separated. The relative proportion of protein and lipid differ in different membranes (Table 1.1), reflecting the diversity of biological roles associated with different membranes (Lehninger et al., 1993).

The density of isolated membranes (usually 1.05-1.35 g/ml) is directly proportional to their protein content (Jain, 1988). The protein content is found to increase with the number of metabolic functions carried out by the membrane. Thus the density of isolated membranes increases in the order: myelin < plasma membrane < endoplasmic reticulum < mitochondria (Jain, 1988). Chemical analysis of membranes isolated from various sources reveals certain common properties. Membrane lipid composition (Table 1.2) is characteristic for each kingdom, each species, each tissue, and each organelle within given cell type (Lehninger, 1993).

Table 1.2: Lipid composition of organelle membranes of rat liver cell*.

	Chol	PC	PE	PS	PI	PG	CL	SM
Plasma membrane	30	18	11	9	4	0	0	14
Golgi complex	8	40	15	4	6	0	0	10
Smooth endoplasmic reticulum	10	50	21	0	7	0	2	12
Rough endoplasmic reticulum	6	55	16	3	8	0	0	3
Nuclear membrane	10	55	20	3	7	0	0	3
Lysosomal membrane	14	25	13	0	7	0	5	24
Mitochondrial membrane	3	45	24	1	6	2	18	3
Inner								
Outer	5	45	23	2	13	3	4	5

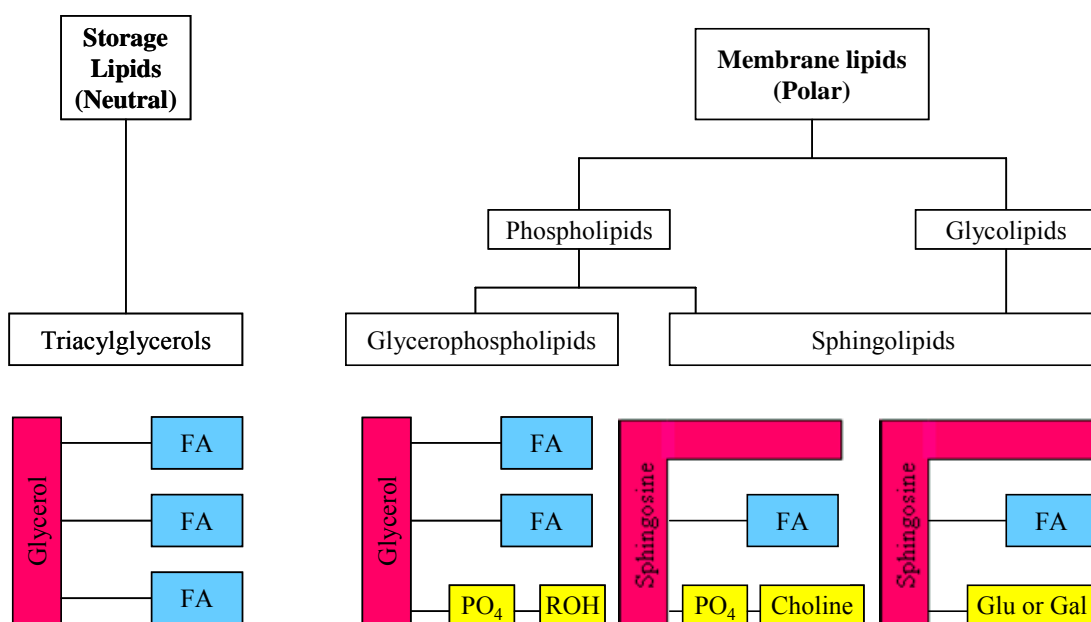
Taken from Lehninger et al. (1993). *Values are given as weight percentages. Chol = Cholesterol; PC = Phosphatidylcholine; PE = Phosphatidylethanolamine; PS = Phosphatidylserine; PI = Phosphatidylinositol; PG = Phosphatidylglycerol; CL = Cardiolipin; SM = Sphingomyelin.

1.2.1. Membrane Lipids

Lipids are the major structural elements of biomembranes. The universal description of a lipid is an amphiphilic organic compound of biological origin, which is water insoluble or slightly soluble in water. Lipids encompass a diverse range of compounds including waxes, fatty acids, fatty-acid derived phospholipids, sphingolipids, glycolipids, and terpenoids such as retinoids and steroids. Some lipids are linear aliphatic molecules, while others have ring structures. Some are aromatic, while others are not. Some are flexible, while others are rigid (Gunstone et al., 1986). In one of the recent classifications, lipids have been divided into eight categories depending on their structure, i.e., fatty acids, glycerolipids, glycerophospholipids, sphingolipids, sterol lipids, prenol lipids, saccharolipids, and polyketides containing distinct classes and subclasses of molecules (Fahy et al., 2005).

Lipids may be divided into two major classes of lipids based on their reactivity with strong bases, i.e., **saponifiable** and **nonsaponifiable**. The nonsaponifiable classes include the "fat-soluble" vitamins (A, E) and cholesterol. Saponification is the process that produces soaps from the reaction of lipids and a strong base. The saponifiable lipids contain long chain carboxylic acids, or **fatty acids**, esterified to a "backbone" molecule, which is either **glycerol** or **sphingosine**. The major saponifiable lipids are triacylglycerides, glycerophospholipids, and the sphingolipids. The first two use glycerol as the backbone. Triacylglycerides have three fatty acids esterified to the three -OH groups on glycerol. Glycerophospholipids have two fatty acids esterified at carbons 1 and 2 of glycerol, and a phospho-X groups esterified at C3. Sphingosine, the backbone of sphingolipids, has a long alkyl group connected at C1 and a free amine at C2, as the backbone. In sphingolipids, a fatty acid is attached through an amide link at C2, and a hydrogen atom or an esterified phospho-X group is found at C3.

A general diagram showing the difference in these structures is given below in Figure 1.2. The four major classes of membrane-forming lipids are glycerophospholipids, phosphosphingolipids, glycosphingolipids, and glycoglycerolipids, which differ principally in the nature of the head group.

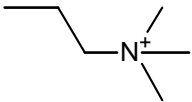
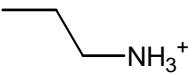
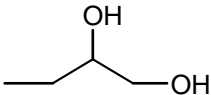
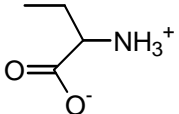
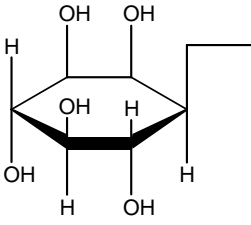


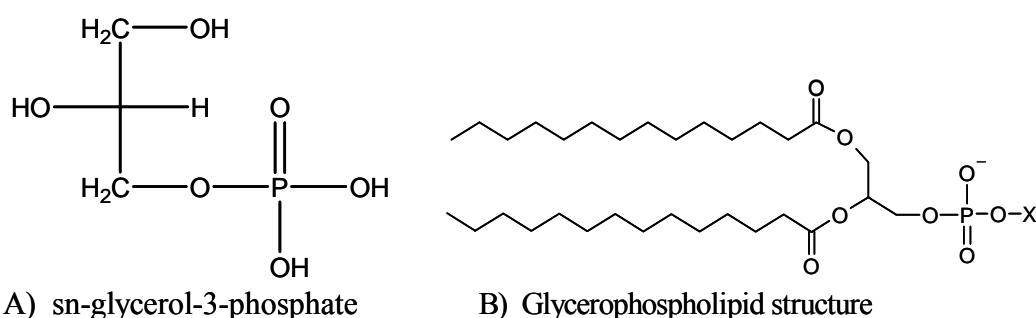
Taken from Lehninger et al. (1993).

Fig. 1.2: Classification of common phospholipids, glycolipids, and triacylglycerides based on their structural features.

Glycerophospholipids: Glycerophospholipids are the major class of naturally occurring phospholipids, which contain a phosphate moiety in the head group. These lipids are considered to be derivatives of glycerol-3-phosphate.

Table 1.3: Structures of membrane phospholipids. The variety of polar head groups found in phospholipids is illustrated.

Name of the Glycerophospholipid	R ₃	Charge	Remarks
Phosphatidic acid	-H	-1	<i>Strongly acidic, Important metabolic intermediate, occurring in trace amounts.</i>
Phosphatidylcholine (Lecithin)		Neutral	<i>Major animal phospholipid, found in large amounts in plants and in small quantities in some bacteria.</i>
Phosphatidylethanolamine (Cephalin)		Neutral	<i>Widespread and major lipid in plants, animals and in some microorganisms.</i>
Phosphatidylglycerol		-1	<i>Head group glycerol has an sn1 configuration. Trace constituent of most of the tissues but has important function in lung surfactant and in the chloroplasts.</i>
Phosphatidylserine		-1	<i>Weakly acidic, serine is an L-isomer. Widespread but minor lipid.</i>
Phosphatidylinositol		-1	<i>Inositol is the myo- isomer. Widespread and usually minor lipid. The higher inositides have been detected in animals and yeast.</i>
Diphosphatidylglycerol (Cardiolipin, DPG)	Phosphatidylglycerol	-2	<i>Acidic lipid. Common in bacteria. Heart muscle is a rich source. Localized in inner mitochondrial membrane of erythrocytes.</i>

**Fig. 1.3: Structures of Glycerophospholipids.**

In Glycerol-3-phosphate (Figure 1.3a) carbon 2 is a chiral center, and the naturally occurring glycerophospholipids are derivatives of the L enantiomer. The general structure of a glycerophospholipid with the hydrophobic tails drawn to the left and hydrophilic head group to the right is shown in Figure 1.3b. The acyl side chains derived from fatty acids; often one is saturated, and the other unsaturated.

Table 1.4: Lipid compositions of some biological membranes.

Lipid	Percentage of Total Composition in			
	Human Erythrocyte Plasma Membrane	Human Myelin	Beef Heart Mitochondria	<i>E. coli</i> Cell Membrane
Phosphatidic acid	1.5	0.5	0	0
Phosphatidyl choline	19	10	39	0
Phosphatidylethanolamine	18	20	27	65
Phosphatidylglycerol	0	0	0	18
Phosphatidylinositol	1	1	7	0
Phosphatidylserine	8	8	0.5	0
Sphingomyelin	17.5	8.5	0	0
Glycolipids	10	26	0	0
Cholesterol	25	26	3	0
Others	0	0	23.5	17

Taken from Tanford (1973).

The hydrophilic X group varies significantly, which confers enormous variation in properties among the glycerophospholipids. A gallery of the most common glycerophospholipids is shown in Table 1.3, and their relative abundance in some biological membranes is given in Table 1.4.

Sphingolipids and Glycosphingolipids: The second major class of membrane constituents is built on the long-chain amino alcohol **sphingosine**, rather than on glycerol. If a fatty acid is linked via an amide bond to the —NH_2 group, the class of **sphingolipids** referred to as **ceramides** is obtained. Ceramides consist only of sphingosine and a fatty acid. Addition of groups further to the C-1 hydroxyl of sphingosine leads to a variety of other sphingolipids.

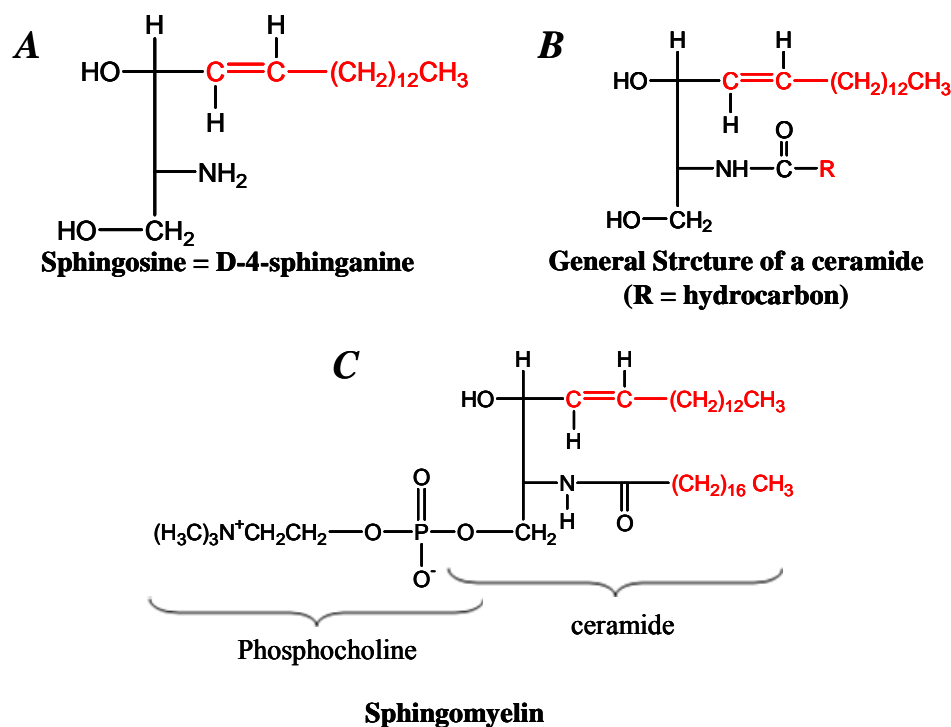


Fig. 1.4: Molecular structures of sphingolipids shown in Fischer projection.
(A) Sphingosine, (B) Ceramide, (C) Sphingomyelin.

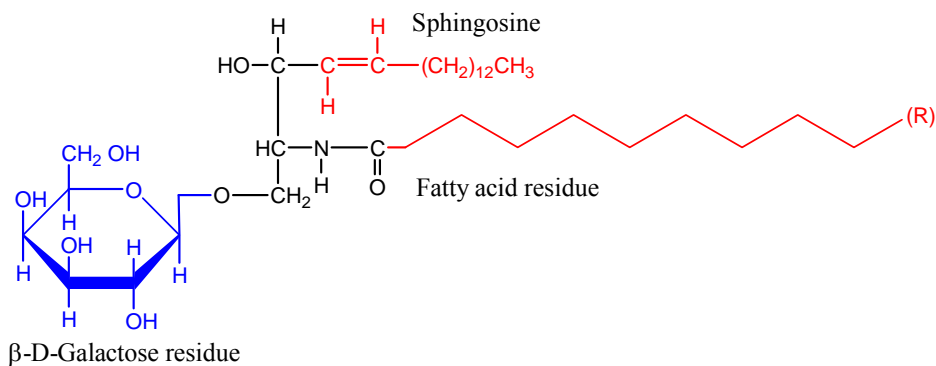
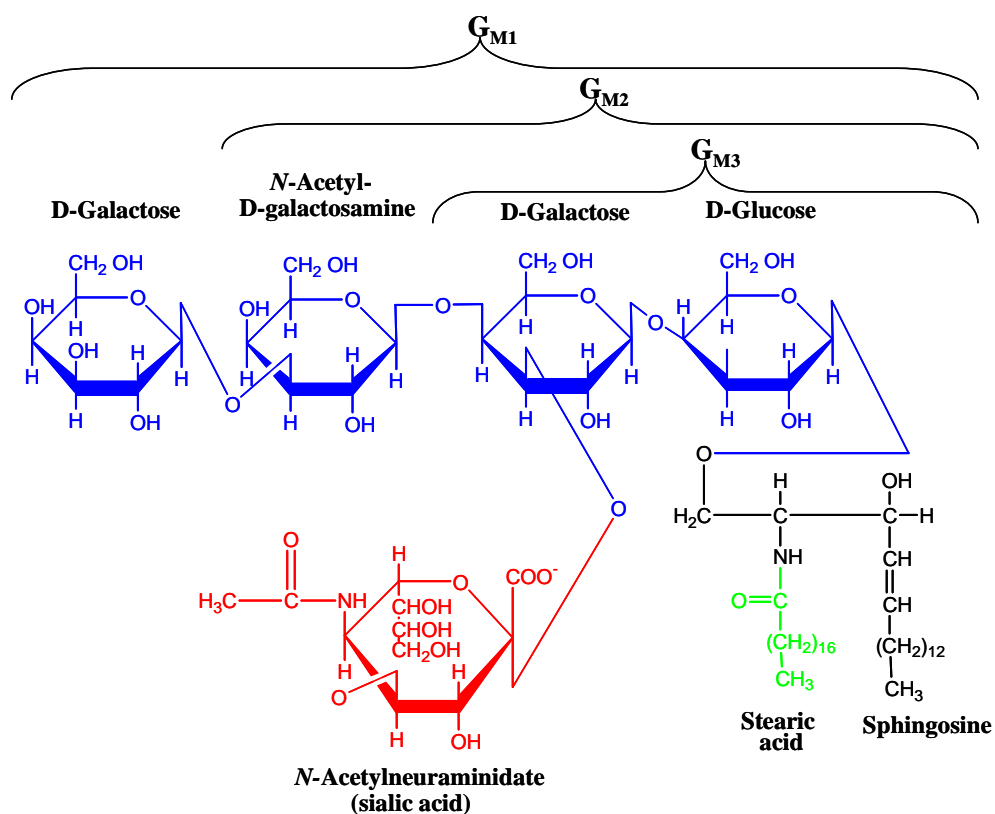


Fig. 1.5: Structure of a galactocerebroside. Cerebrosides are important constituents of the neuronal cell membranes in the brain.



Taken from Voet and Voet (1995).

Fig. 1.6: Structure of ganglioside G_{M1} .

Sphingomyelins, the most common sphingolipids are ceramides containing either a *phosphocholine* group or a phosphoethanolamine moiety attached to the C-3 hydroxyl of sphingosine.

Glycosphingolipids constitute the third major class of membrane lipids. Their general structure includes molecules such as the cerebrosides (monoglycoceramides) and gangliosides, anionic glycosphingolipids containing one or more sialic acid residues. They are especially widespread in the membranes of brain and nerve cells. **Cerebrosides**, the simplest glycosphingolipids, are ceramides with head groups that consist of a single sugar residue. The structure of **galactocerebroside**, having a β -D-galactose head group is shown in Figure 1.5.

Gangliosides form the most complex group of glycosphingolipids. They are ceramide oligosaccharides that include among the sugar groups at least one sialic acid residue (*N*-acetylneuraminic acid and its derivatives). The structures of gangliosides G_{M1} , G_{M2} and G_{M3} , three of the over 60 that are known, are shown in Figure 1.6. Gangliosides are primarily components of cell surface membranes and constitute a significant fraction (ca. 6%) of brain lipids.

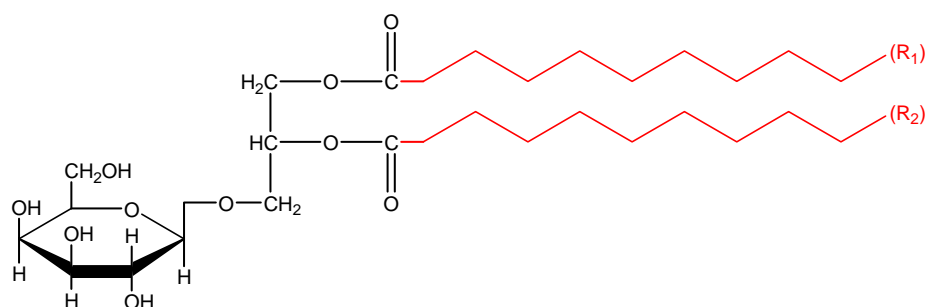


Fig. 1.7: Structure of monogalactosyldiglyceride.

Glycoglycerolipids: The glycoglycerolipids are minor constituents of animal membranes but are widespread in plant and bacterial membranes. The most notable example of this class is monogalactosyldiglyceride (Figure 1.7), which is the most

abundant polar lipid in chloroplast membranes, constituting about half the polar lipid in these membranes. These lipids are also the major membrane components in archaeobacteria.

Sterols: These are found in many plant, animal and microbial membranes. These molecules are made up of a compact, rigid hydrophobic entity with a polar hydroxyl group. **Cholesterol** (Figure 1.8a) is the most common and important constituent of many membranes (about 30% of the mass of the membrane lipids of many animal cell plasma membranes). It is found in animal cell plasma membranes, lysosomes, endosomes, and golgi. Cholesterol is the metabolic precursor of steroid hormones, substances that regulate a great variety of physiological functions including sexual development and carbohydrate metabolism.

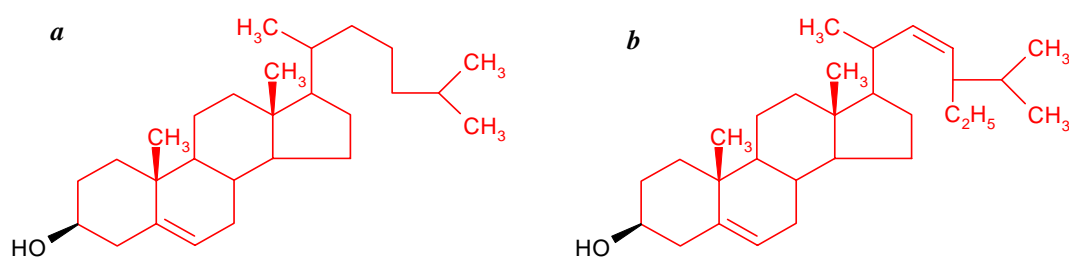


Fig. 1.8: Structures of sterols. a) Cholesterol, b) Stigmasterol.

Other sterols, notably **sitosterol** and **stigmasterol** (Figure 1.8b) are found in higher plants. They have an additional chain at position C-24 and/or a double bond at position C-22. **Ergosterol** is often found in yeast and other eukaryotic microorganisms. Some sterol-like lipids, *hopanoids* are also present in bacteria and some plants (Prince, 1987). Hopanoids are pentacyclic triterpenoid lipids and are important for bacterial membrane stability and functioning.

1.2.2. Self-association of Lipids

Normally, membrane lipids are virtually insoluble in water. When mixed with water, these amphiphilic compounds form microscopic lipid aggregates in a phase separate from their aqueous surroundings. Lipid molecules cluster with their hydrophobic moieties in contact with each other and their hydrophilic groups interacting with the surrounding water. When amphiphilic lipids are mixed with water basically three types of aggregates namely micelles, bilayers and liposomes or vesicles (Figure 1.9) can form depending on the precise conditions (such as the lipid concentration, temperature, pressure, ionic strength, and pH) and nature of lipids used.

Micelles: Micelles are comparatively small, spherical structures involving a few dozen to a few thousand molecules arranged so that hydrophobic regions aggregate in the interior, excluding water, and their hydrophilic head groups are at the surface, in contact with the water. Micelle formation is favored when the cross-sectional area of the head group is greater than that of acyl side chains. Examples include free fatty acids, lysophospholipids, and detergents such as sodium dodecyl sulfate (SDS).

Bilayers: Bilayer is the type of lipid aggregate in water in which two lipid monolayers combine to form a two-dimensional sheet. Its formation occurs most readily when the cross-sectional areas of the head group and side chains are similar, as in glycerophospholipids and sphingolipids. The hydrophobic portions of the two monolayers interact, excluding water. The hydrophilic head groups interact with water at the two surfaces of the bilayer.

Liposomes: A liposome or a vesicle is a hollow spherical structure that forms when a lipid bilayer folds back on itself. By forming vesicles, bilayer sheets lose their

hydrophobic edge regions, achieving maximal stability in their aqueous environment. These bilayer vesicles enclose water, creating a separate aqueous compartment.

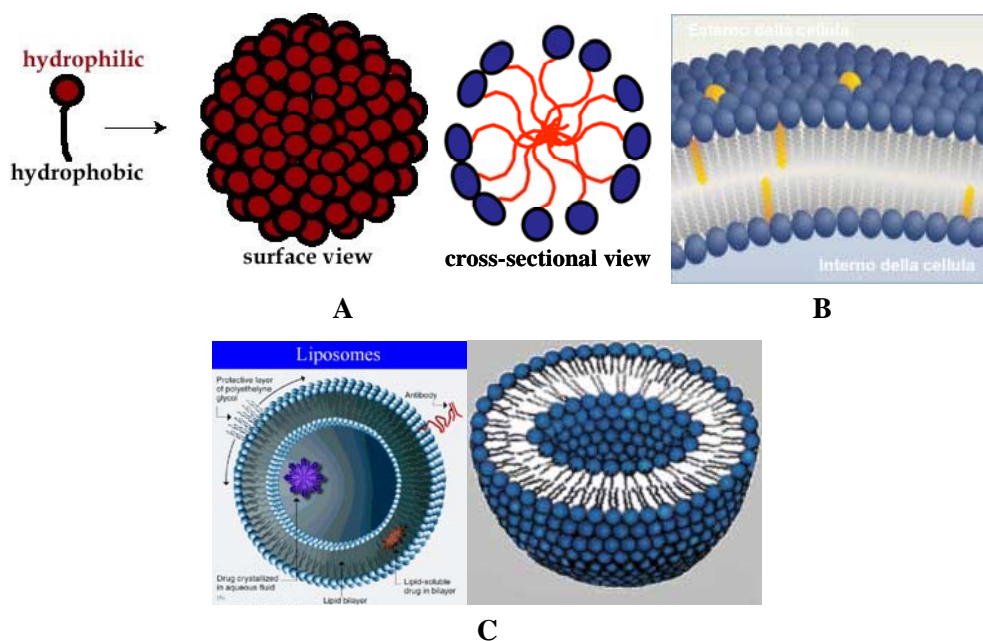


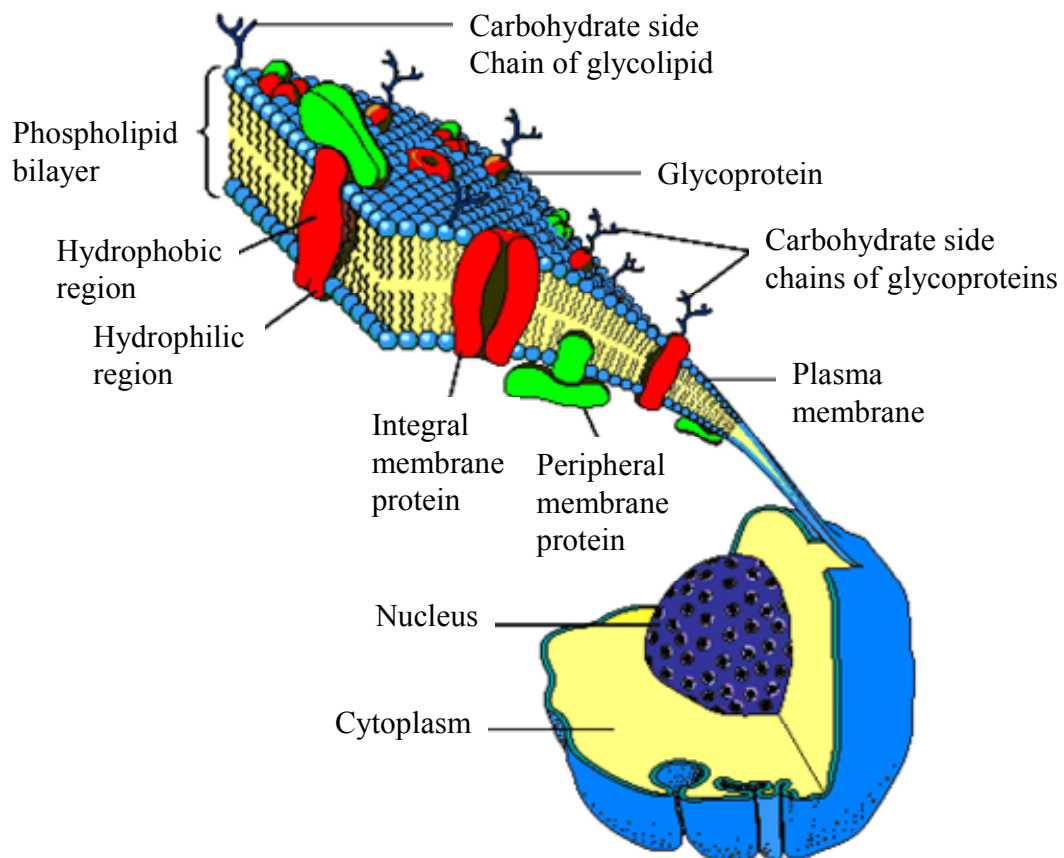
Fig. 1.9: Self-organization of lipids. A) Surface and cross-sectional views of a micelle (Taken from <http://en.wikipedia.org/wiki/Micelle>). B) A bilayer (Taken from www.biologia-it.arizona.edu). C) Two different cross-sectional views of a liposome (Taken from www.livonlabs.com/LV/apps/images/liptra2.JPG; www.uic.edu).

1.2.3. Membrane Proteins

A typical biomembrane, which is made up of a phospholipid bilayer, contains specific proteins embedded in it or bound to its surface. Many of these proteins bear oligosaccharide groups that project into the surrounding aqueous medium. The different types of membrane proteins are discussed below (section 1.3.1).

1.3. THE STRUCTURE AND PROPERTIES OF MEMBRANES

The membranes of living cells are incredible pieces of molecular structural design, with many and varied functions. In its simplest form, a membrane is essentially a phospholipid bilayer, which has a basic structure akin to a biological membrane, but there is much more to the plasma membrane found in the living cells. A more realistic representation of a typical eukaryotic cell membrane is shown in Figure 1.10.

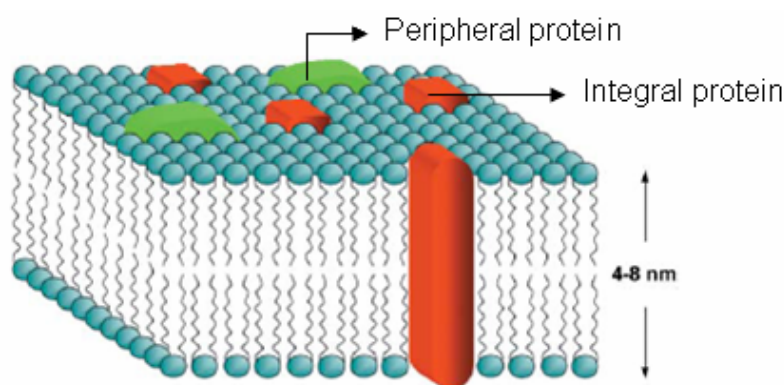


Taken from Mathews et al. (2000).

Fig. 1.10: Structure of a typical cell membrane. In this schematic view, a strip of the plasma membrane of a eukaryotic cell has been peeled off. Proteins embedded in and attached to the surface of the phospholipid bilayer are shown; some of them are glycoproteins, carrying oligosaccharide chains. The membrane is about 6 nm thick.

1.3.1. Fluid Mosaic Model

It is now some 34 years since the widely accepted structural model, namely the **fluid mosaic model**, was proposed for the biological membrane by Singer and Nicholson (1972). The essence of their model is that membranes are *two-dimensional solutions of oriented globular proteins and lipids* (Figure 1.11). It comprises of a tail-to-tail arrangement of amphipathic lipid molecules, forming a bilayer. The ‘tails’ of the lipid molecules, the hydrophobic fatty acyl chains, are associated together in the interior of the bilayer in a favourable like-with-like arrangement that keeps them segregated from the hydrophilic aqueous medium on either side of the membrane. The ‘heads’ of the lipid molecules, which are hydrophilic groups such as choline, are present on the outside of the membrane in a favorable disposition for solvation by water.



Taken from Sanderson (2005).

Fig. 1.11: The Singer-Nicolson fluid mosaic model. Peripheral proteins are indicated in green and integral proteins in red.

Proteins present in this model are peripheral membrane proteins and integral membrane proteins. **Peripheral membrane proteins** are exposed only at one membrane surface or the other. They are held to the membrane surface by interaction with lipid heads or integral membranes proteins. **Integral membrane proteins** span the lipid bilayer with parts of the protein exposed on both surfaces of

the membrane. Integral membrane proteins are often involved in transmitting either specific substances or chemical signals through the membrane.

The whole membrane is a mosaic of lipids and proteins. Their proposal is supported by a wide range of experimental observations. The major attributes of this model are:

1. Most of the membrane phospholipids and glycolipids are in a bilayer form. This lipid bilayer has a dual role; it is both a solvent for integral membrane proteins and a *permeability barrier*.
2. A small proportion of membrane lipids interact specifically with particular membrane proteins and may be crucial for their function.
3. Membrane proteins are free to circulate laterally in the lipid matrix unless restricted by special interactions, while they are not free to rotate from one side of a membrane to the other.

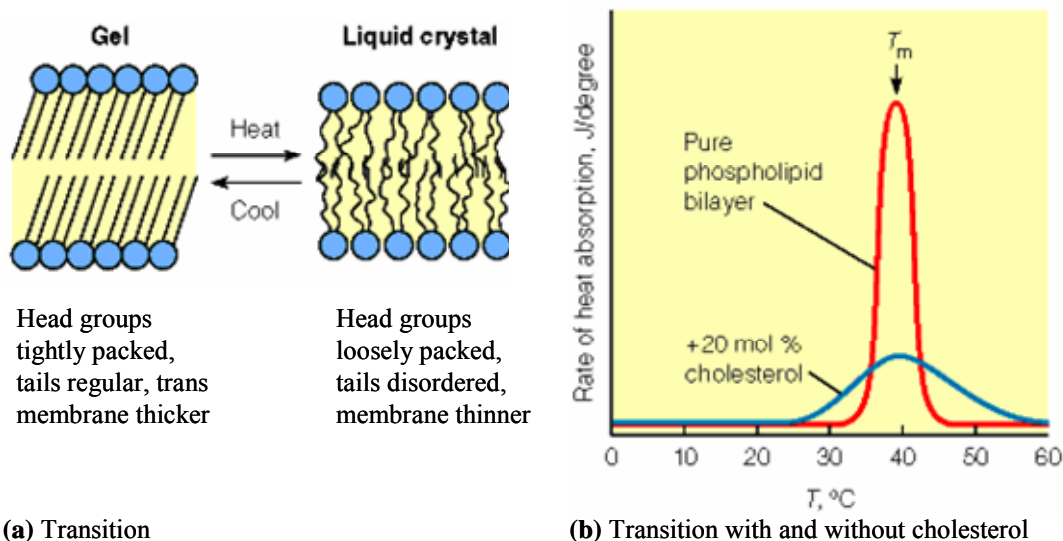
1.3.2. Motions in Biological Membranes

A functioning biological membrane is not a firm, frozen structure. Many of the membrane lipid and protein components are in constant motion. The key motions exhibited by membrane lipids are described in detail below.

Lateral Diffusion: Membrane lipids diffuse laterally, parallel to the membrane surface. The speed of such two-dimensional diffusion depends on the membrane fluidity, which in turn depends on temperature and lipid composition.

Thermal Motion: At low temperature, relatively little lipid motion occurs and the bilayer exists as a nearly crystalline array or gel phase. Above a temperature that is characteristic for each membrane, lipids can undergo rapid motion, where membrane melts to adopt a semi-fluid, liquid crystalline phase (Figure 1.12a). The temperature at which this happens is called the transition temperature. Saturated

fatty acids pack well in a crystalline array, but the twists in unsaturated fatty acids interfere with this in the solid state. Therefore the solid-to-fluid transition temperature of the membrane increases with increase in the proportion of saturated fatty acids.



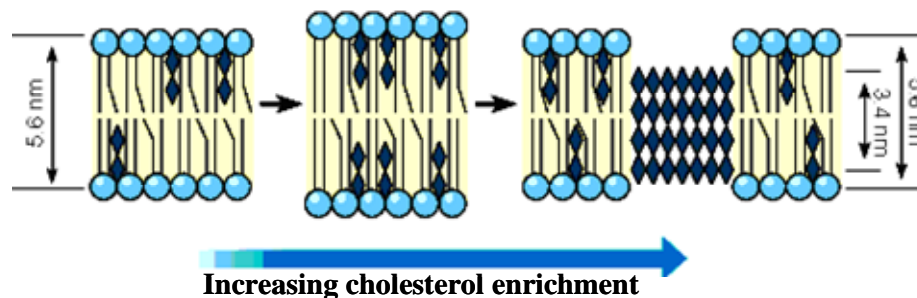
Taken from Mathews et al. (2000).

Fig. 1.12: The gel-liquid crystalline transition in a synthetic lipid membrane.

Transbilayer Diffusion (Flip-Flop): In disparity to the simplicity of lateral movement, the “flip-flop” of lipid molecules across synthetic lipid bilayers, from one side to another, is much slower. In this, the hydrophilic head group of the phospholipid has to pass through the inhospitable medium of the hydrocarbon tail region. Such a movement is very unfavorable from an energetic point of view, and hence the process is slow. A class of enzymes known as *translocases* normally catalyze flipping and maintain membrane asymmetry. In contrast to phospholipids, the transport of fatty acids across membranes is much faster, as unlike the phosphate groups of phospholipids, the carboxylates on fatty acids are protonated and uncharged in the highly nonpolar atmosphere of the lipid bilayer. Thus they

can be better accommodated in the membranes than an ionized molecule and undergo flip-flop motion relatively fast.

Effect of Cholesterol on Membrane Fluidity: Cholesterol has a specific and complex effect on membrane fluidity. In a membrane containing phospholipids and cholesterol, the cholesterol molecules are inserted in between fatty acyl side chains. As Figure 1.12b shows for a synthetic membrane, cholesterol does not influence the transition temperature, but broadens the transition. This broadening occurs because cholesterol prevents the highly ordered packing of fatty acyl chains and thus fluidizes the membrane below the transition temperature, and above the thermal transition point, the rigid ring system of cholesterol reduces the freedom of neighboring fatty acyl chain to move by rotation at carbon-carbon bonds, and thus reduces the fluidity in the core of the bilayer.



Taken from Mathews et al. (2000).

Fig. 1.13: A Schematic model of the effect of cholesterol on plasma membrane structure. The data indicate an initial effect of the cholesterol/phospholipids ratio, Chol:PL, on membrane width.

The effect of cholesterol on plasma membrane is shown in Fig. 1.13. At cholesterol/phospholipid (Chol:PL) ratio of (0.8:1) or below, the bilayer width increases with increasing Chol:PL ratio. At Chol:PL mole ratios above 0.9:1, as the membrane saturates with cholesterol two separate lamellar phases form by phase

separation. One of these two phases represents a liquid crystalline lipid bilayer and the other an immiscible cholesterol phase (Tulenko et al., 1998).

1.3.3. Membrane Dynamics and Time Scale

The fluid-mosaic model likens biological membranes to a sea of lipids organized in a bilayer format in which the embedded proteins are freely moving in the plane of the bilayer (Singer and Nicolson, 1972; Singer, 1992). Over the past three to four decades a vast amount of data has accumulated in the literature regarding the quantitative and qualitative aspects of the dynamics of membrane lipids and proteins. The dynamic properties of membrane proteins and lipids can be divided broadly into two groups (Marsh, 1988). One is the *lateral diffusion* in the plane of the membrane and the other is the *rotational motion* around the molecular axis, normal to the bilayer. Both these dynamic motions are shown in Figure 1.14 and are considered while interpreting the data obtained from various biophysical techniques.

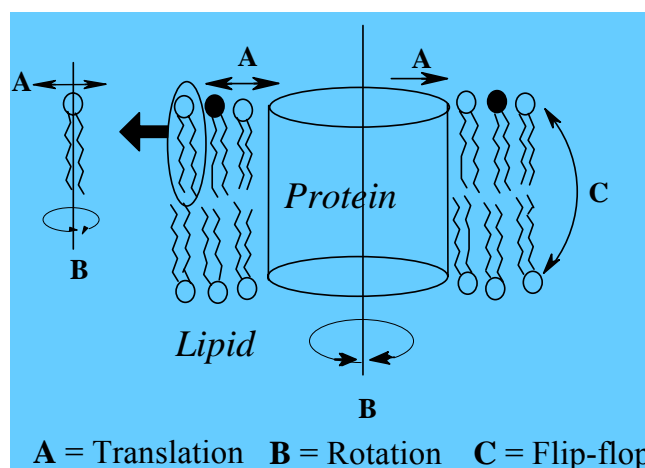


Fig. 1.14: Schematic representation of various translational and rotational motions within membranes.

Typical time scales of assorted membrane events in which various biophysical techniques are sensitive to molecular motions are indicated in Figure

1.15 (adapted from Gennis, 1989). Spin labeled and fluorescently labeled lipid probes can be used to get information on rotational motions in the nanosecond scale in the fluid-lipid membranes. Lateral diffusion or translational motion of protein and lipid molecules in fluid-lipid membranes are characterized by lateral diffusion coefficients in the region of $D_{lat} \sim 10^{-8} \text{ cm}^2/\text{s}$. Rotational diffusion is characterized by the rotational correlation times, which are given by the Debye equation, $\tau_R = \eta v/kT$, where η corresponds to viscosities in the range of $\eta \sim 0.1\text{--}1.0$ poise.

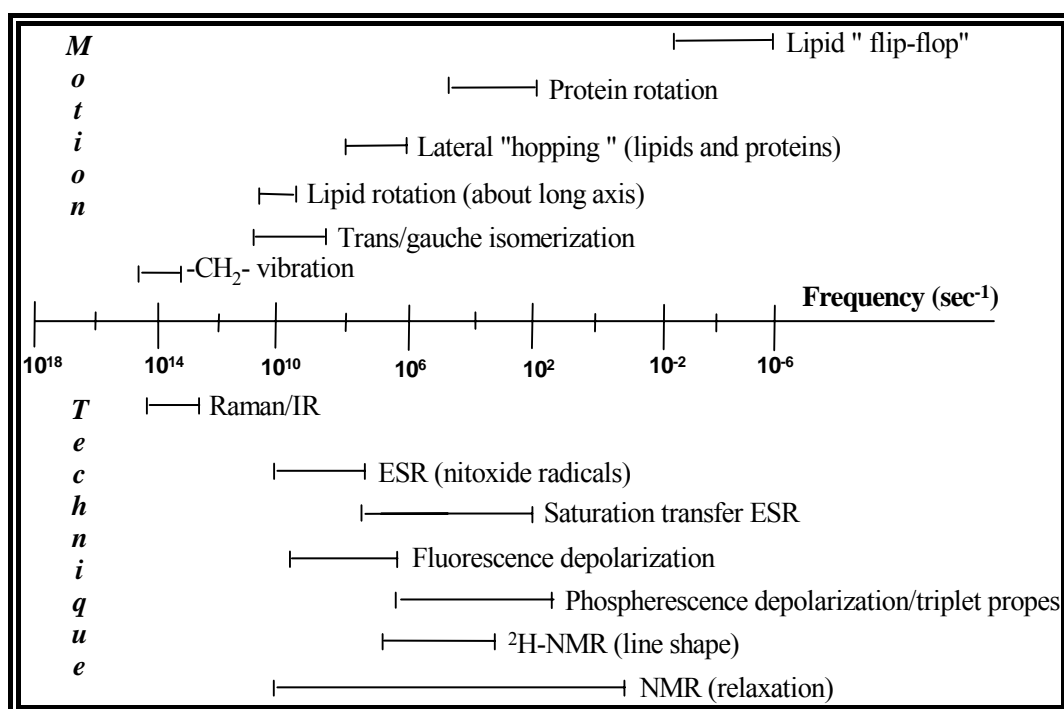


Fig. 1.15: Characteristic frequencies of molecular motions of membrane proteins and lipids and the techniques to study them. The frequencies of molecular motions are compared with the frequency ranges in which various spectroscopic techniques are sensitive to the molecular motion. The characteristic times are obtained by taking the reciprocal of the indicated frequencies. Boundaries are very approximate.

From Figure 1.15 it can be seen that the major techniques used for characterizing the dynamic aspects of the membrane proteins and lipids are ESR, NMR, fluorescence, phosphorescence, IR and Raman spectroscopies. Among

these, ESR spectroscopy requires the incorporation of a free radical probe in the system, usually by covalent attachment to the lipid or protein although a small stable free radical such as TEMPO is sometimes used without attaching it to membrane constituents. Membrane proteins usually have tryptophan or tyrosine residues and their fluorescence is quite often used to derive information on their dynamic properties. Application of fluorescence spectroscopy to investigate the dynamics of membrane lipids, however, requires the incorporation of a fluorescent probe in the membrane. This is often achieved by covalently attaching a fluorescent label to a membrane lipid. While these two techniques have yielded a significant amount of information on the dynamic properties of membrane proteins and lipids, one drawback they suffer from is that the probe used in these techniques can perturb the properties of the membrane. Therefore, when such techniques are used it is important to ensure that the changes observed are not due to the perturbations caused by the spectroscopic probe. The other techniques such as FTIR, NMR, and Raman spectroscopy, mentioned above do not require any probes to be attached and hence do not have such drawbacks.

A more detailed discussion on these topics is not within the scope of this dissertation, but can be found in a number of excellent text books; reviews and monographs (cf. Grell, 1981; Hesketh et al., 1982; Campbell and Dwek, 1984).

1.4. *N*-ACYLPHOSPHATIDYLETHANOLAMINES, *N*-ACYLETHANOLAMINES AND *N*-, *O*-DIACYLETHANOLAMINES.

N-Acylphosphatidylethanolamines (NAPEs) and *N*-acylethanolamines (NAEs) are naturally occurring membrane constituents, which exhibit interesting biological and pharmacological properties. NAPEs are negatively charged glycerophospholipids in which the amino group of phosphatidylethanolamine (PE) is acylated with a fatty acid chain. NAEs are amphiphilic derivatives of 2-ethanolamine, wherein the amino

group is derivatized with a long acyl chain. NAPes are the precursors of NAEs as NAEs are generally produced *in vivo* by the cleavage of NAPes by a phospholipase-D-type enzyme. It has been suggested that *N*-, *O*-diacylethanolamines (DAEs) may also be present in biological membranes, although their presence is not conclusively proven. In this section NAPes and NAEs will be discussed together first, followed by DAEs.

1.4.1. Occurrence

N-Acyl PEs were first discovered as minor membrane constituents in wheat flour by Bomstein (1965). Later on, a large number of reports by many groups have shown that NAPes are present in a variety of organisms, e.g., animals (Hack and Helmy, 1975, 1982; Natarajan et al., 1985), plants (Bomstein, 1965; MacMurray and Morrison, 1970; Dawson et al., 1969; Hargin and Morrison, 1980) and microorganisms (Hazlewood and Dawson, 1975; Clarke et al., 1976; Ellingson, 1974, 1980). Thus, both NAPes and NAEs appear to be ubiquitous molecules with their presence in a wide variety of animals, plants, bacteria, fungi and viruses being well established (Schmidt et al., 1990; Hansen et al., 2000).

The content of long-chain NAEs and NAPes increases quite dramatically in the parent organisms under conditions of stress (Schmid et al., 1996). For example, both NAEs and NAPes accumulate in animal tissues during stress conditions such as post decapitative ischemia in rat brain (Natarajan et al., 1986; Moesgaard et al., 1999) and traumatic brain injury (Hansen et al., 2001a, b) and their content rises to very high levels when extensive membrane degradation occurs, such as in myocardial infarction (Epps et al., 1979, 1980; Schmid et al., 1990, 1996; Marsh and Swamy, 2000; Chapman, 2000). They also accumulate in a variety of human tumors and surrounding normal tissues. Since NAEs have been shown to inhibit the growth of different cell lines *in vitro*, this suggests that their accumulation in the

tumor tissue may be due to the production of NAEs by the adjacent tissues to fight the cancerous growth (Schmid et al., 2002). These observations have led to the postulate that increase in the levels of NAEs and NAPEs is probably due to a stress or disease-fighting response of the parent organisms.

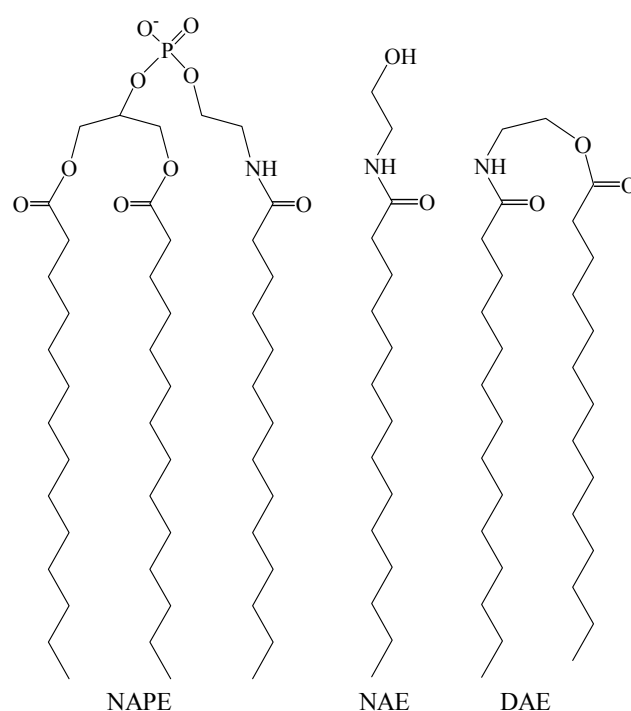


Fig. 1.16: Structures of *N*-Acylphosphatidylethanolamine, *N*-acylethanolamine, and *N*-, *O*-diacylethanolamine.

A large number of reports have appeared in the last two decades describing the occurrence of these lipids in various species (see Table 1.5A and 1.5B). From this Table it is clear that NAEs and NAPEs are minority lipids, present only in small traces when their level is compared to that of other membrane lipids.

Table 1.5A: *In vivo* levels of NAPEs.

Tissue	Species	Total NAPEs pmol/g tissue	References
Microorganisms	<i>Butyrivibrio</i>	40%	Clarke et al., 1976
	<i>Dictyostelium discoideum</i>	-	Clarke et al., 1976
Plants	Wheat flour	4%	Bomstein, 1965
	Pea Seeds	5%	Quarles and Dawson, 1969
	Spring bean	2.9%	Quarles and Dawson, 1969
	Soy bean	3.5%	Aneja et al., 1969
	Oat	13.3%	Dawson et al., 1969
Brain	Rat	12072	Sugiura et al., 1996b
		3666	Cadas et al., 1997
		-	Yang et al., 1999
		-	Bisogno et al., 1999
		-	Berrendro et al., 1999
			Gonzalez et al., 1999
			Natarajan et al., 1985
Retinal	Fish	0.1%	Natarajan et al., 1985
	Bovine	-	Bisongo et al., 1999b
Spinal cord	Rat	-	Yang et al., 1999
	Fish	0.9%	Natarajan et al., 1985
Kidney	Rat	610	Deutsch et al., 1997
Spleen	Rat	-	Yang et al., 1999
Testis	Rat	2525	Sugiura et al., 1996a
		2887	Kondo et al., 1998
Uterus	Murine	713-4095	Schmid et al., 1997
Erythrocytes	Bovine	5%	Matsumoto and Miwa, 1973
Stomach	Hog	-	Slomiany et al., 1973

Table 1.5B: *In vivo* levels of NAEs.

Tissue	Species	Total NAEs pmol/g tissue	References
Plants	Soybean lecithin		Schmid, 1990
	Tobacco		Chapman et al., 1998
	Cotton seeds		Schmid et al, 1990
Brain	Human	-	Felder et al., 1996
	Rat	-	Felder et al., 1996
		597	Sugiura et al., 1996a
		513-1397	Koga et al., 1997
		136	Cadas et al., 1997
		-	Bisongo et al., 1999a
		-	Berrendero et al., 1999
		-	Gonzalez et al., 1999
		400	Bacher et al., 1965
	Murine	-	Schmid et al., 1995
	Porcine	-	Devane et al., 1992
		2037	Schmid et al., 1995
	Bovine	957	Schmid et al., 1995
	Sheep	835	Schmid et al., 1995
Retina	Rat	185	Straiker et al., 1999
	Bovine	-	Bisongo et al., 1999b
Heart	Human	-	Felder et al., 1996
Liver	Rat		Koga et al., 1997
Kidney	Rat	186	Deutsch et al., 1997
Spleen	Human	-	Felder et al., 1996
	Rat	-	Felder et al., 1996
Thymus	Rat	210	Koga et al., 1997
Testis	Rat	122	Sugiura et al., 1996a
		109	Koga et al., 1997
		97	Kondo et al., 1998
Uterus	Murine	2719-22269	Schmid et al., 1997
Skin	Rat	-	Felder et al., 1996
		741	Calignano et al., 1998
ECF (brain)	Rat	3.7 pmol/ 300 micro l	Giuffrida et al., 1999
		-	Walker et al., 1999
CSF	Human	3.0 pmol/ml	Giuffrida and Piomelli, 1998
	Human	3.0 pmol/ml	Leweke et al., 1999
Plasma	Rat	30 pmol/ml	Giuffrida and Piomelli, 1998

1.4.2. Biological and Medicinal Properties of NAPes and NAEs

Besides their increased levels in various organisms under conditions of stress, NAEs also exhibit several interesting biological and medicinal properties. It has been shown that *N*-arachidonyl ethanolamine (anandamide) acts as an endogenous ligand of type-I cannabinoid receptors, inhibits gap-junction conductance and reduces the fertilizing capacity of sperm (Devane et al., 1992; Schuel et al., 1994; Venance et al., 1995), whereas *N*-palmitoyl ethanolamine acts as an agonist for the type-2 cannabinoid receptor, CB-2 (Facci et al., 1995). *N*-Myristoyl ethanolamine (NMEA) and *N*-lauroyl ethanolamine are secreted into the culture medium of tobacco cells when challenged by the fungal elicitor, xylanase (Chapman et al., 1998). NAEs also exhibit anti-inflammatory, antibacterial and antiviral properties, which are of considerable application potential (Ganley et al., 1958; Schmid et al., 1990).

In addition to their interesting biological and medicinal properties mentioned above, NAEs and NAPes have also been reported to exhibit membrane stabilizing property. Recent studies suggest that *N*-acyl egg PE and *N*-palmitoyl dipalmitoyl phosphatidylethanolamine (*N*-16 DPPE) stabilize liposomes against leakage (Domingo et al., 1993; Mercadal et al., 1995). Especially, *N*-16 DPPE has been shown to stabilize liposomes even in the presence of human serum. NAEs have been shown to stabilize the bilayer structure in the sense of inhibiting the formation of inverted hexagonal phase (Ambrosini et al., 1993).

1.4.3. Metabolism

Considerable work has already been carried out on the metabolism of NAPes and NAEs and it has been shown that the former are continuously synthesized by a calcium and energy-dependent transacylase and are hydrolyzed by a phospholipase D-type enzyme to phosphatidic acid and NAEs, which are further degraded by fatty

acid amidohydrolase (for reviews, see Schmid et al., 1996; Cravatt and Lichtman, 2003). More recently, it has been demonstrated that NPEA and anandamide can also be synthesized by the sequential action of phospholipase A2 and lysophospholipase D on *N*-acyl PE (Sun et al., 2004). Many of the enzymes involved in the biosynthesis and degradation of NAPEs and NAEs have been purified, characterized and cloned (Sun et al., 2004; Okamoto et al., 2004; Tsuboi et al., 2005).

1.4.4. N-, O-Diacylethanolamines (DAEs)

Recent biochemical and pharmacological studies have led to the characterization of different fatty acid amides as a new family of biologically active lipids. Anandamide (*N*-arachidonylethanolamine) and other ethanolamides of polyunsaturated fatty acids have been reported to displace radioactive cannabinoid ligands from specific binding sites in brain membranes, to inhibit adenylate cyclase and *N*-type calcium channels and to produce hypothermia, catalepsy, analgesia and hypoactivity (the latter four tests known as the cannabinoid tetrad). Studies of the structure-activity relationships of anandamide and oleamide analogous revealed the importance of their fatty acid moieties for biological activity (Bezuglov et al., 2001).

Furutani et al. (1997) have shown that *N*-acylethanolamines can be *O*-acylated in organic solvents by a lipase catalyzed reaction. It was also shown that rat heart cell-free preparation can catalyze *O*-acylation of NAE in the presence of fatty acid and acyl Co-A-generating factors (Schmid et al., 1990). These observations suggest that, *N*-, *O*-diacylethanolamines may be present in biological membranes along with NAEs in minor quantities. But there have been no reports so far on their chemical synthesis and biophysical characterization.

1.4.6. Objectives

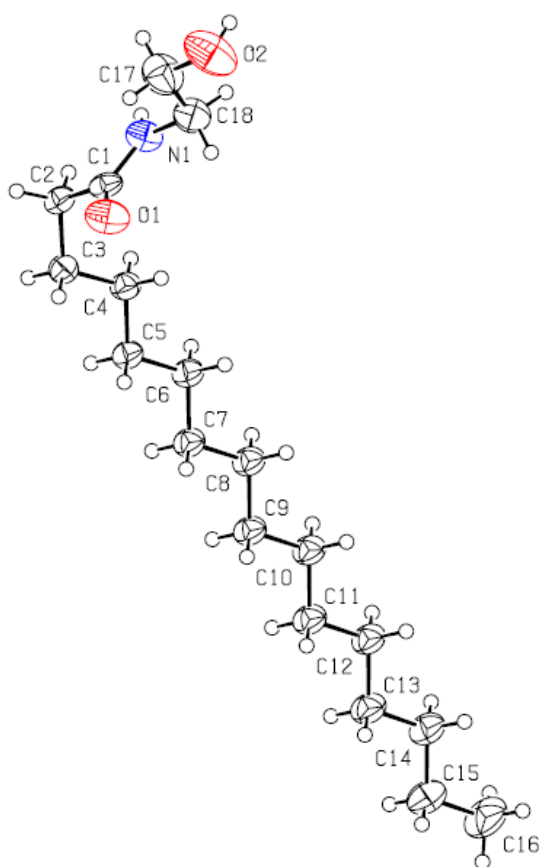
As NAEs and NAPEs have been reported to exhibit various interesting biological and medicinal properties, it is important to carry out systematic investigations on NAEs and NAPEs directed at understanding their metabolism, physicochemical properties (e.g., phase transitions and supramolecular structure) as well as their interaction with other membrane lipids and proteins. In earlier studies from this laboratory, the chain-melting phase transitions of homologous series of these two classes of compounds were investigated by differential scanning calorimetry, (Ramakrishnan et al., 1997; Ramakrishnan and Swamy, 1998, Swamy et al., 1997; Marsh and Swamy, 2000), and reported the crystal structure of *N*-myristoylethanolamine (NMEA), and analyzed the intermolecular interactions and molecular packing in the crystal (Ramakrishnan and Swamy, 1999). Studies employing DSC, fast-atom-bombardment mass spectrometry and computational modeling have indicated that NMEA forms a 1:1 (mol/mol) complex with cholesterol (Ramakrishnan et al., 2002). In another study, the interaction of *N*-palmitoylethanolamine (NPEA) with DPPC was investigated by DSC, ³¹P-NMR and small-angle X-ray scattering (Swamy et al., 2003).

While these studies as well as those carried out in other laboratories have yielded much valuable and interesting information, it is necessary to carry out additional studies in order to understand the biophysical properties and membrane interactions of NAEs and NAPEs better. In addition, the physico-chemical properties of DAEs have not been studied so far. In view of this, studies have been performed on synthetic NAEs, NAPEs and DAEs with the following specific objectives.

- To investigate the structural polymorphism, molecular packing and intermolecular interactions in *N*-acylethanolamines by single-crystal X-ray diffraction analysis.
- To investigate the interaction of other long chain NAEs i.e., NPEA and NSEA with cholesterol by DSC.
- To investigate the interaction of NMEA and cholesterol at different compositions by computational modeling and monolayer behavior by using Langmuir-Blodgett film balance technique and Brewster angle microscopy and their mixtures in dry form by DSC.
- To investigate the interaction of NAEs with phosphatidylethanolamines (PEs) of similar acyl chainlength by DSC, spin-label ESR and ^{31}P -NMR spectroscopy and to construct temperature-composition binary phase diagrams.
- To synthesize and characterize a homologous series of *N*-, *O*-diacylethanolamines (DAEs) with matched *N*- and *O*-acyl chains and to investigate their phase transitions in the dry and hydrated conditions. Also to investigate the molecular packing and intermolecular interactions in these compounds by analyzing their structures in the solid state by single-crystal X-ray diffraction analysis.

Chapter 2

Crystal Structure, Molecular Packing and Intermolecular Interactions in the Two Structural Polymorphs of *N*-Palmitoylethanolamine



Molecular packing and intermolecular interactions in two structural polymorphs of *N*-palmitoylethanolamine, a type 2 cannabinoid receptor agonist.

Kamlekar, R.K. and Swamy, M.J. 2006. *J. Lipid. Res.* **47**: 1424-1433.

2.1. SUMMARY

The molecular structure, packing properties and intermolecular interactions of two structural polymorphs of *N*-palmitoylethanolamine (NPEA) – a type-2 cannabinoid receptor agonist – have been determined by single crystal X-ray diffraction. Polymorph α crystallized in the monoclinic space group $P2_1/c$ ($Z = 4$, $a = 43.410(13)$, $b = 4.8850(15)$, $c = 9.003(3)$ Å), whereas polymorph β crystallized in the orthorhombic space group $Pbca$ ($Z = 8$, $a = 4.8979(4)$, $b = 8.9974(7)$, $c = 86.419(7)$ Å). In both polymorphs, the NPEA molecules are organized in a tail-to-tail fashion, resembling a bilayer membrane. While the molecular packing in polymorph α is similar to that in crystal structures of *N*-myristoylethanolamine and *N*-stearoylethanolamine, polymorph β is a new form. The acyl chains in both polymorphs are tilted by $\sim 35^\circ$ with respect to the bilayer normal and their hydrocarbon moieties are packed in an orthorhombic subcell ($O'\perp$). In both structures, the hydroxy group of NPEA forms two hydrogen bonds with the hydroxy groups of molecules in the opposite leaflet, resulting in extended, zig-zag type hydrogen bonded networks along the b -axis in polymorph α and a -axis in polymorph β . In addition, the amide N–H and C=O groups of adjacent molecules are involved in N–H \cdots O hydrogen bonds that connect adjacent molecules along the b -axis and a -axis, respectively, in polymorphs α and β . Whereas in polymorph α , the L-shaped NPEA molecules in opposite layers are arranged to yield a ‘Z’ like organization, in polymorph β one of the two NPEA molecules is rotated by 180° , leading to a ‘W’ like arrangement. Differential scanning calorimetric studies indicate two minor transitions at ca. 76.8 and 86.2°C with enthalpies of 3.1 and 1.3 kcal/mol, before the main chain-melting transition at 97.3°C with a corresponding enthalpy value of 11.3 kcal/mol. Lattice energy calculations indicate that polymorph α is more stable than polymorph β by ca. 2.65 kcal.mol⁻¹, which is in

good agreement with the enthalpy of the first minor transition occurring at 76.8°C. These results suggest that polymorph α is the form that is stable at low temperature.

2.2. INTRODUCTION

From the Introduction (Section 1.4) it is seen that *N*-acylethanolamines are ubiquitous molecules with their presence in a wide variety of animals, plants, as well as microbes such as bacteria, fungi and viruses being well established (Schmid et al., 1990; Hansen et al., 2000). The content of long-chain NAEs and their precursors, NAPEs, increases quite dramatically in the parent organisms under conditions of stress, injury or disease, leading to the postulate that increase in the levels of these two classes of amphiphiles is probably due to a stress-fighting response of the parent organisms. Additionally, NAEs also exhibit interesting medicinal properties, which are of considerable application potential (Schmid et al., 1990). NAEs and NAPEs may also be useful in developing liposomal formulations for drug delivery and targeting, in view of their ability to stabilize bilayer structure (Ambrosini et al., 1993; Domingo et al., 1993; Mercadal et al., 1995).

In view of their interesting biological and medicinal properties, putative role in stress-combating response of organisms as well as their potential in developing liposomal drug delivery systems, it is important to systematically investigate NAEs and NAPEs with an aim to understand their metabolism, physicochemical properties and interaction with other membrane lipids and proteins. The metabolism of NAPEs and NAEs has already been studied in considerable detail and a number of the enzymes involved in the biosynthesis and degradation of NAPEs and NAEs have been purified, characterized and cloned (see Section 1.4.3).

In earlier studies from this laboratory, the chain-melting phase transitions of homologous series of these two classes of compounds by differential scanning

calorimetry have been investigated, which indicated that the longer chainlength NAEs exhibit one or two minor transitions before the main chain-melting phase transition, suggesting that they exhibit structural polymorphism in the solid state (Ramakrishnan et al., 1997; Ramakrishnan and Swamy, 1998; Swamy et al., 1997; Marsh and Swamy, 2000). In another study the crystal structure of *N*-myristoyethanolamine (NMEA) was determined and the intermolecular interactions and molecular packing in the crystal were analyzed (Ramakrishnan and Swamy, 1999). Although these earlier studies suggest that NAEs exhibit polymorphism, so far there have been no reports on the structures of different polymorphs, which could shed light on the differences between them. In this Chapter single-crystal X-ray diffraction studies on two structural polymorphs of NPEA is reported and analyzed the molecular packing and intermolecular interactions in the crystal lattice. It is observed that although in both polymorphs the molecular structure of NPEA is similar to that observed earlier with NMEA and *N*-stearoylethanolamine, in one of the two polymorphs the molecules pack in a different way. However, the hydrogen bonding pattern is remarkably similar in both forms.

2.3. MATERIALS AND METHODS

2.3.1. Crystallization and X-ray Diffraction

Thin plate type colorless crystals of *N*-palmitoylethanolamine were grown at room temperature from isobutanol. A crystal of $0.03 \times 0.42 \times 0.50$ mm size was used for the data collection. Diamond shaped, colorless crystals of *NPEA* were grown at room temperature from a 1:1 (vol/vol) mixture of dichloromethane and toluene, containing a trace of ethanol. A crystal of $0.24 \times 0.14 \times 0.12$ mm size was used for data collection in the present study. As will be discussed below, these two types of crystals gave two different polymorphic structures. Therefore, henceforth they will

be referred to as polymorph α and polymorph β , respectively. X-ray diffraction measurements were carried out at room temperature (ca. 25°C) with a Bruker SMART APEX CCD area detector system using a graphite monochromator and Mo-K α ($\lambda = 0.71073$ Å) radiation obtained from a fine-focus sealed tube.

2.3.2. Structure Solution and Refinement

For polymorphs α and β , the data collected in the range of $\theta = 1.41$ – 26° and $\theta = 1.41$ – 25° , respectively, were used for structure solution. Data reduction was done using Bruker SAINTPLUS program. Structure solution was carried out in the monoclinic space group for α and orthorhombic space group for β . Absorption correction was applied using SADABS program. The structures were solved successfully by direct methods in the space group $P2_1/c$ for α and $Pbca$ for β . In both cases refinement was done by full matrix least-squares procedure using the SHELXL97 program (Sheldrick, 1997). For polymorph α , the refinement was carried out using 2264 observed [$>2\sigma(F_o)$] reflections and converged into a final $R_I = 0.058$, $wR_2 = 0.1604$ and goodness of fit = 1.032, whereas for polymorph β , 2679 observed [$>2\sigma(F_o)$] reflections upon refinement converged into a final $R_I = 0.0978$, $wR_2 = 0.2635$ and goodness of fit = 1.036. For both structures, two hydrogen atoms on the amide and hydroxy groups were refined isotropically, whereas all the carbon atoms and heteroatoms were refined anisotropically. All hydrogen atoms on the acyl chains and other carbon atoms were included in the structure factor calculation with fixed thermal parameters at idealized positions but were not refined.

2.3.3. Crystal Parameters of *N*-Palmitoylethanolamine

Polymorph α : Molecular formula, $C_{18}H_{37}NO_2$; Molecular formula weight, 299.49; Crystals were thin plate type and colorless; Crystal system, Monoclinic; Space

group, $Sg = P2_1/c$; Ambient temperature, $T = 298(2)$ K; Radiation wavelength (λ) = 0.71073 Å; Radiation type, Mo-K α ; Radiation source, Fine-focus sealed tube; Radiation monochromator, graphite; Number of reflections collected, 18314; Unique reflections, 3685; Reflection with $I > 2\sigma(I)$, 2264; Number of parameters, 192.

Unit cell dimensions (with standard deviation in parentheses): $a = 43.410(13)$, $b = 4.8850(15)$, $c = 9.003(3)$ Å; $\alpha = 90$, $\beta = 94.075(6)$, $\gamma = 90$; Volume of the cell, $V = 1904.4(10)$ Å³(5); Density, $D_{\text{Calc}} = 1.045$ gm.cm⁻¹; Number of molecules in the unit cell, $Z = 4$; Angle of tilt of acyl chains, $\theta = 34.5^\circ$; Cross sectional area of the unit cell, $\Sigma = 43.979$ Å²; Area per molecule, $S = 21.989$ Å²; $F_{(000)} = 672$; Absorption Coefficient, $\mu = 0.066$ mm⁻¹; $T = 298(2)$ K.

Polymorph β : Molecular formula, C₁₈H₃₇NO₂; Crystals were colorless and diamond shaped; Crystal system, orthorhombic; space group, $Sg = Pbca$. Ambient temperature, $T = 298(2)$ K; Radiation wavelength (λ) = 0.71073 Å; Radiation type, Mo-K α ; Radiation of source, Fine-focus sealed tube; Radiation monochromator, graphite; Number of reflections collected, 33801; unique reflections, 3586; reflections with $I > 2\sigma(I)$, 2679; number of parameters, 198.

Unit cell dimensions (with standard deviation in parentheses): $a = 4.8979(4)$, $b = 8.9974(7)$, $c = 86.419(7)$ Å; Volume of the cell, $V = 3808.3(5)$ Å³; Density, $D_{\text{Calc}} = 1.045$ gm.cm⁻¹; Number of molecules in the unit cell, $Z = 8$; Angle of tilt of acyl chains, $\theta = 35.5^\circ$; Cross sectional area of the unit cell, $\Sigma = 44.068$ Å²; Area per molecule, $S = 22.034$ Å²; $F_{(000)} = 1344$; Absorption Coefficient, $\mu = 0.066$ mm⁻¹. $T = 298(2)$ K.

2.3.4. Lattice Energy Calculations

Lattice energy calculations for polymorphs α and β were performed using the COMPASS force field in Cerius² suite of programs (Accelrys Inc., San Diego, CA, USA, and website: <http://www.accelrys.com>). Lattice energies were reported after normalizing the values obtained for a single molecule.

2.3.5. Differential Scanning Calorimetry

Differential scanning calorimetric scans were recorded on a TA instruments Universal V2.6D differential scanning calorimeter. Samples of dry NPEA (~1-2 mg) were loaded into aluminium sample pans were covered with an aluminium lid and sealed by crimping. Reference pans were prepared in a similar manner, but without any sample in the pan. DSC measurements were performed by heating the samples at a scan rate of 0.5°/min or 1.5°/min. Transition enthalpies (ΔH_t) were estimated by integrating the areas under the peaks corresponding to the individual transitions. Transition entropies (ΔS_t) were determined from the transition enthalpies according to the expression (Marsh, 1990):

$$\Delta H_t = T_t \cdot \Delta S_t \quad (1)$$

2.4. RESULTS AND DISCUSSION

2.4.1. Description of the Structure

The molecular structure of *N*-palmitoylethanolamine as found in polymorph α is shown in the ORTEP plot given in Fig. 2.1, along with the atom numbering for all the non-hydrogen atoms. The atomic coordinates and equivalent isotropic displacement parameters for all non-hydrogen atoms and the two hydrogen atoms on heteroatoms (N-H and O-H) are given in Table 2.1. The bond distances, bond

angles and torsion angles involving all the non-hydrogen atoms are given in Tables 2.2, and 2.3, respectively. It is clearly seen from Fig. 2.1, that the hydrocarbon portion (C3–C16) of the acyl chains of the molecule is in an all-*trans* conformation. The torsion angle observed for acyl chain region – excepting the C1–C2–C3–C4 angle, which is 68.11° – are all close to 180° and are fully in agreement with above observation. The gauche conformation at the C2–C3 bond results in a bending of the molecule, giving it an ‘L’ shape. The carbonyl group and the amide N–H are also in *trans* geometry. Earlier studies have shown that *N*-myristoylethanolamine and *N*-stearoylethanolamine also have very similar molecular structure in the crystalline state (Ramakrishnan and Swamy, 1999; Dahlén et al., 1977).

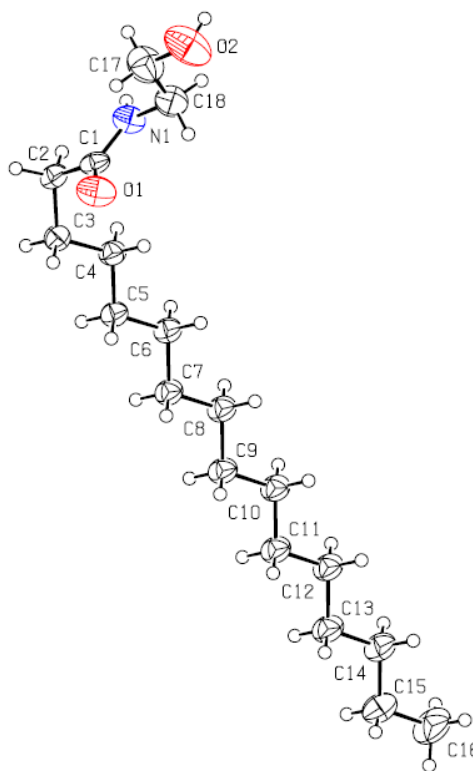


Fig. 2.1: ORTEP plot of *N*-palmitoylethanolamine. The atom numbering is indicated in the figure. Hatched symbols indicate atoms that are refined anisotropically.

Table 2.1: Fractional atomic coordinates ($\times 10^4$) and equivalent isotropic displacement parameters ($\text{\AA}^2 \times 10^3$) the α form of *N*-palmitoylethanolamine. U(eq) is defined as one third of the trace of the orthogonalized U_{ij} tensor [$U(\text{eq}) = \frac{1}{3} \sum_i \sum_j U_{ij} a_i \cdot a_j \cdot a_i a_j \cos(a_i, a_j)$].

Atom	x	y	z	U(eq)
N(1)	5884(1)	8627(3)	4575(2)	46(1)
O(1)	6017(1)	12984(2)	4991(2)	61(1)
O(2)	5121(1)	10477(3)	2808(2)	94(1)
C(1)	6051(1)	10553(3)	5286(2)	39(1)
C(2)	6285(1)	9599(3)	6481(2)	40(1)
C(3)	6609(1)	10696(3)	6273(2)	41(1)
C(4)	6755(1)	9536(3)	4925(2)	41(1)
C(5)	7077(1)	10634(3)	4755(2)	41(1)
C(6)	7238(1)	9426(3)	3457(2)	42(1)
C(7)	7559(1)	10589(3)	3301(2)	43(1)
C(8)	7724(1)	9388(4)	2015(2)	45(1)
C(9)	8043(1)	10578(4)	1864(2)	45(1)
C(10)	8211(1)	9396(4)	584(2)	47(1)
C(11)	8530(1)	10581(4)	446(2)	48(1)
C(12)	8699(1)	9399(4)	-829(2)	49(1)
C(13)	9020(1)	10577(4)	-949(2)	54(1)
C(14)	9191(1)	9424(4)	-2219(2)	54(1)
C(15)	9511(1)	10559(5)	-2327(2)	69(1)
C(16)	9678(1)	9437(5)	-3611(3)	86(1)
C(17)	5352(1)	9975(5)	3995(3)	75(1)
C(18)	5647(1)	9219(4)	3379(2)	58(1)
H(1)	59166	69482	48281	55
H(2)	50460	90178	25132	140

Table 2.2: Bond lengths [Å] and Bond angles (degrees) of the α form of *N*-palmitoylethanolamine.

Bond lengths [Å]			Bond angles (degrees)		
O(1) - C(1)	1.2238(18)		C(1) - N(1) - C(18)	123.17(15)	
O(2) - C(17)	1.434(3)		O(1) - C(1) - N(1)	122.02(16)	
N(1) - C(1)	1.325(2)		O(1) - C(1) - C(2)	121.53(15)	
N(1) - C(18)	1.464(2)		N(1) - C(1) - C(2)	116.45(13)	
C(1) - C(2)	1.500(2)		C(1) - C(2) - C(3)	112.64(13)	
C(2) - C(3)	1.527(2)		C(2) - C(3) - C(4)	113.96(13)	
C(3) - C(4)	1.518(2)		C(3) - C(4) - C(5)	112.88(13)	
C(4) - C(5)	1.518(2)		C(4) - C(5) - C(6)	114.67(13)	
C(5) - C(6)	1.523(2)		C(5) - C(6) - C(7)	113.55(13)	
C(6) - C(7)	1.520(2)		C(6) - C(7) - C(8)	114.21(14)	
C(7) - C(8)	1.522(2)		C(7) - C(8) - C(9)	113.73(15)	
C(8) - C(9)	1.518(3)		C(8) - C(9) - C(10)	114.26(15)	
C(9) - C(10)	1.520(3)		C(9) - C(10) - C(11)	113.96(15)	
C(10) - C(11)	1.515(3)		C(10) - C(11) - C(12)	114.17(15)	
C(11) - C(12)	1.519(3)		C(11) - C(12) - C(13)	113.82(15)	
C(12) - C(13)	1.519(3)		C(12) - C(13) - C(14)	114.46(15)	
C(13) - C(14)	1.515(3)		C(13) - C(14) - C(15)	114.58(16)	
C(14) - C(15)	1.508(3)		C(14) - C(15) - C(16)	114.24(18)	
C(15) - C(16)	1.510(3)		O(2) - C(17) - C(18)	110.00(2)	
C(17) - C(18)	1.479(3)		N(1) - C(18) - C(17)	110.84(16)	

Table 2.3: Torsion angles (degrees) for the α form of *N*-palmitoylethanolamine.

C(18) N(1) C(1) O(1)	0.30(3)
C(18) N(1) C(1) C(2)	-179.80(15)
C(1) N(1) C(18) C(17)	-83.10(2)
O(1) C(1) C(2) C(3)	-53.30(2)
N(1) C(1) C(2) C(3)	126.84(15)
C(1) C(2) C(3) C(4)	-68.13(17)
C(2) C(3) C(4) C(5)	-179.32(13)
C(3) C(4) C(5) C(6)	177.33(13)
C(4) C(5) C(6) C(7)	179.23(13)
C(5) C(6) C(7) C(8)	179.59(14)
C(6) C(7) C(8) C(9)	179.62(14)
C(7) C(8) C(9) C(10)	-180.00(14)
C(8) C(9) C(10) C(11)	-179.65(15)
C(9) C(10) C(11) C(12)	179.79(15)
C(10) C(11) C(12) C(13)	-179.41(15)
C(11) C(12) C(13) C(14)	-179.83(15)
C(12) C(13) C(14) C(15)	-179.13(16)
C(13) C(14) C(15) C(16)	-178.98(18)
O(2) C(17) C(18) N(1)	-178.50(16)

N-Palmitoylethanolamine was found to adopt an essentially similar structure in the polymorph β also. Only very minor differences were seen between the molecular features of NPEA in these two polymorphs. For example, the C1–C2–C3–C4 torsion angle in polymorph β is found to be 66.9° , which is very close to the value of 68.11° mentioned above for the polymorph α . The atomic coordinates and equivalent isotropic displacement parameters for all non-hydrogen atoms in polymorph β are given in Table 2.4. The bond distances, bond angles and torsion angles involving all the non-hydrogen atoms are given in Tables 2.5 and 2.6, respectively.

Table 2.4: Fractional atomic coordinates ($\times 10^4$) and equivalent isotropic displacement parameters ($\text{\AA}^2 \times 10^3$) for the β form of *N*-palmitoylethanolamine. U(eq) is defined as one third of the trace of the orthogonalized U_{ij} tensor [$U(\text{eq}) = \frac{1}{3} \sum_i \sum_j U_{ij} a_i \cdot a_j \cdot a_i a_j \cos(a_i, a_j)$].

Atoms	x	y	z	U(eq)
O(1)	2007(4)	-1288(4)	1998(1)	68(1)
O(2)	4617(9)	823(6)	2434(1)	96(1)
N(1)	6397(6)	-956(4)	2064(1)	58(1)
C(1)	4458(6)	-1589(4)	1980(1)	47(1)
C(2)	5375(7)	-2716(4)	1863(1)	47(1)
C(3)	4296(7)	-2398(4)	1701(1)	48(1)
C(4)	5436(7)	-1009(4)	1627(1)	45(1)
C(5)	4365(7)	-728(4)	1466(1)	45(1)
C(6)	5569(7)	623(4)	1385(1)	45(1)
C(7)	4425(7)	892(4)	1225(1)	45(1)
C(8)	5593(7)	2226(4)	1142(1)	47(1)
C(9)	4436(7)	2486(4)	982(1)	48(1)
C(10)	5588(7)	3823(4)	898(1)	49(1)
C(11)	4445(7)	4062(4)	737(1)	49(1)
C(12)	5584(8)	5398(4)	653(1)	51(1)
C(13)	4444(8)	5624(4)	493(1)	57(1)
C(14)	5558(8)	6947(4)	406(1)	57(1)
C(15)	4482(10)	7168(5)	246(1)	72(1)
C(16)	5541(12)	8504(5)	162(1)	88(2)
C(17)	4950(11)	-414(6)	2323(1)	84(1)
C(18)	5816(9)	242(5)	2178(1)	72(1)
H(1A)	8190(8)	-1290(4)	2010(0)	5(1)
H(1B)	5880(9)	990(5)	2470(1)	6(2)

Table 2.5: Bond lengths [Å] and Bond angles (degrees) of the β form of *N*-palmitoylethanolamine.

Bond lengths [Å]			Bond angles (degrees)		
O(1) - C(1)	1.240(4)		C(1) - N(1) - C(18)	122.3(3)	
O(2) - C(17)	1.480(6)		O(1) - C(1) - N(1)	122.5(3)	
N(1) - C(1)	1.322(5)		O(1) - C(1) - C(2)	121.0(3)	
N(1) - C(18)	1.488(6)		N(1) - C(1) - C(2)	116.5(3)	
C(1) - C(2)	1.504(5)		C(1) - C(2) - C(3)	113.0(3)	
C(2) - C(3)	1.522(5)		C(2) - C(3) - C(4)	114.6(3)	
C(3) - C(4)	1.507(5)		C(3) - C(4) - C(5)	113.6(3)	
C(4) - C(5)	1.508(5)		C(4) - C(5) - C(6)	115.2(3)	
C(5) - C(6)	1.518(5)		C(5) - C(6) - C(7)	114.1(3)	
C(6) - C(7)	1.516(5)		C(6) - C(7) - C(8)	115.1(3)	
C(7) - C(8)	1.509(5)		C(7) - C(8) - C(9)	114.6(3)	
C(8) - C(9)	1.509(5)		C(8) - C(9) - C(10)	115.2(3)	
C(9) - C(10)	1.515(5)		C(9) - C(10) - C(11)	114.7(3)	
C(10) - C(11)	1.509(5)		C(10) - C(11) - C(12)	114.9(3)	
C(11) - C(12)	1.513(5)		C(11) - C(12) - C(13)	114.6(3)	
C(12) - C(13)	1.501(5)		C(12) - C(13) - C(14)	115.5(3)	
C(13) - C(14)	1.508(5)		C(13) - C(14) - C(15)	116.1(3)	
C(14) - C(15)	1.498(5)		C(14) - C(15) - C(16)	115.8(4)	
C(15) - C(16)	1.496(6)		O(2) - C(17) - C(18)	106.8(4)	
C(17) - C(18)	1.449(6)		N(1) - C(18) - C(17)	109.5(4)	

Table 2.6: Torsion angles (degrees) for the β form of *N*-palmitoylethanolamine.

C(18) N(1) C(1) O(1)	-4.5(6)
C(18) N(1) C(1) C(2)	176.2(3)
C(1) N(1) C(18) C(17)	83.6(5)
O(1) C(1) C(2) C(3)	53.6(4)
N(1) C(1) C(2) C(3)	-127.0(3)
C(1) C(2) C(3) C(4)	66.9(4)
C(2) C(3) C(4) C(5)	179.2(3)
C(3) C(4) C(5) C(6)	-177.2(3)
C(4) C(5) C(6) C(7)	-179.1(3)
C(5) C(6) C(7) C(8)	-179.8(3)
C(6) C(7) C(8) C(9)	-179.8(3)
C(7) C(8) C(9) C(10)	179.9(3)
C(8) C(9) C(10) C(11)	179.2(3)
C(9) C(10) C(11) C(12)	179.9(3)
C(10) C(11) C(12) C(13)	179.8(3)
C(11) C(12) C(13) C(14)	-179.8(3)
C(12) C(13) C(14) C(15)	178.7(3)
C(13) C(14) C(15) C(16)	178.5(4)
O(2) C(17) C(18) N(1)	175.5(4)

2.4.2. Molecular Packing

Packing diagrams of *N*-palmitoylethanolamine along the *c*-axis and *b*-axis in polymorph α are given in Fig. 2.2A and 2.2B, respectively. The NPEA molecules are packed head-to-head (and tail-to-tail) in stacked bilayers. The hydroxy groups from the opposite layers form O–H \cdots O hydrogen bonds, which appear to drive the formation of such bilayer-like supramolecular arrangement. These O–H \cdots O hydrogen bonds form an extended, zig-zag type network along the *b*-axis, with each O–H group being involved in two hydrogen bonds, one as donor and the other as acceptor. In addition, the amide groups of adjacent molecules are involved in N–H \cdots O hydrogen bonds, which also connect adjacent molecules along the *b*-axis. The carbonyl oxygen atoms of adjacent molecules point in opposite direction, thus providing the appropriate juxtaposition of the amide carbonyl and hydrogen atoms to interconnect adjacent molecules by hydrogen bonds. The methyl ends of the stacked bilayers are in van der Waals contacts, with the closest methyl-methyl (C16–C16) distance between opposite layers and the same layer being 3.922 Å and 4.885 Å, respectively.

The bilayer thickness (O2–O2 distance) in the α polymorph is 45.57 Å and the all-*trans* acyl chains are tilted by 34.5° with respect to the bilayer normal. This is identical to the tilt angle in NSEA and rather similar to that observed in NMEA (37°) (Ramakrishnan et al., 1999; Dahlén et al., 1977). Other long chain molecules such as long chain carboxylic acids and n-alcohols also pack in a bilayer form with tail-to-tail hydrocarbon alignment with tilted chains (Larsson, 1986).

Packing diagrams corresponding to the β polymorph of *N*-palmitoylethanolamine along the *b*-axis and *a*-axis are given in Fig. 2.2C and 2.2D, respectively. Although the NPEA molecules are packed in a tail-to-tail fashion akin to that found in a lipid bilayer in this polymorph also, with O–H \cdots O hydrogen

bonds between the hydroxyl groups from opposite layers forming extended, zig-zag type network along the *a*-axis, a very significant difference is seen in the alignment between the opposing leaflets. While in polymorph α the L-shaped NPEA molecules in opposite layers are arranged to yield a Z-like organization, in polymorph β one of the two NPEA molecules is rotated by about 180° , such that the organization of two molecules yields a W-like shape. This is schematically shown in Fig. 2.3. Despite this difference in the orientation of the acyl chains with respect to polymorph α , the hydrogen bonding network involving the amide N-H and carbonyl groups of adjacent molecules in polymorph β is remarkably similar to that in polymorph α . In addition, the β form contains 8 molecules of NPEA in the orthorhombic unit cell. This is because as seen in Fig. 2.2C the hydrogen bonded leaflets in polymorph β are arranged in two different orientations; while the methyl termini of the upper two layers in the unit cell point to the left, the methyl termini of the lower pair of layers point to the right. The distance between the terminal methyl groups (C16–C16) of the bilayer in polymorph β is 3.918 Å, whereas between adjacent molecules in the same layer is 4.898 Å. These values closely match the corresponding values obtained for the α polymorph, mentioned above.

In an earlier study, Lambert and coworkers (Wouters et al., 2002) studied the polymorphism of *N*-stearoylethanolamine by DSC, powder X-ray diffraction and FTIR spectroscopy. Although the polymorph observed in the crystal structure of NSEA (which is similar to polymorph α of NPEA, Dahlén et al., 1977) is identified by them as the most stable one, based on powder diffraction and FTIR data, they proposed that two other polymorphic forms differ from the above form in the chain tilt angles, with the head group region remaining essentially unaltered (see Fig. 6 in Wouters et al., 2002).

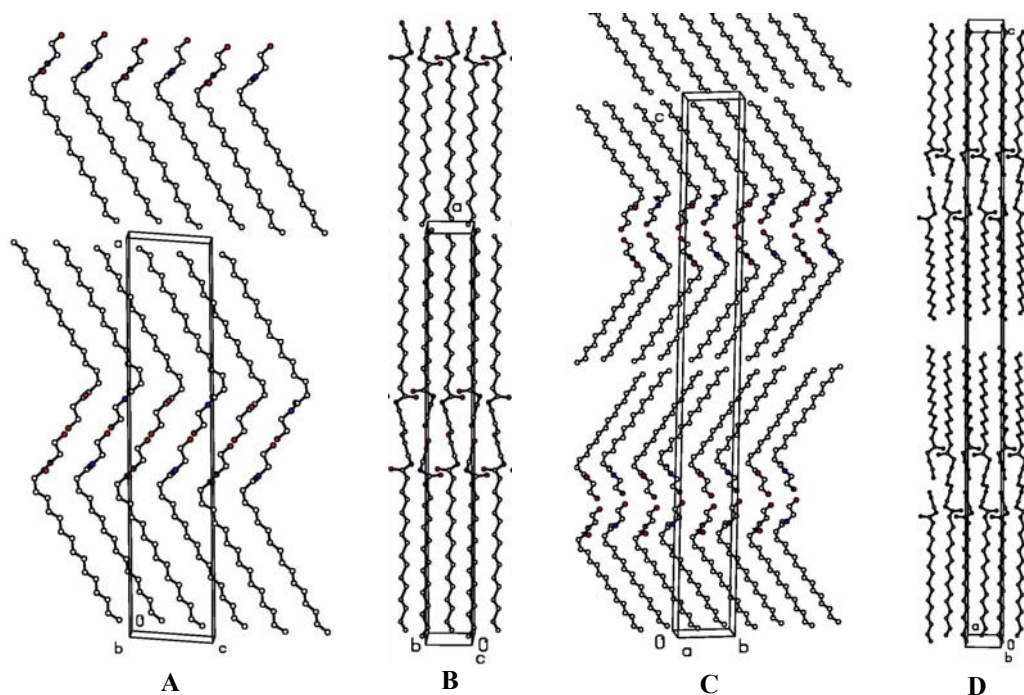


Fig. 2.2: Packing diagrams of *N*-palmitoylethanolamine, (A) View along the *c*-axis of the α polymorph, (B) View along with the *b*-axis of the α polymorph, (C) View along the *b*-axis of polymorph β , (D) View along with the *a*-axis of polymorph β .

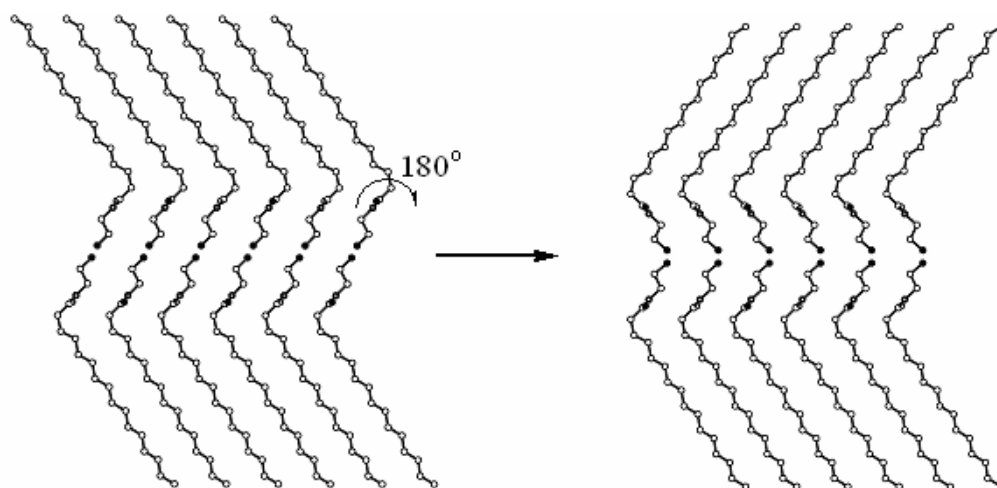


Fig. 2.3: A model for the interconversion of *N*-palmitoylethanolamine polymorphs α and β . This model suggests that a simple rotation of all the molecules in one of the two leaflets of the bilayer by 180° (indicated by the curved arrow) results in the conversion of polymorph α to polymorph β (and *vice versa*).

Our present results do not concur with this and indicate that reorientation of acyl chain region in one layer with respect to the opposite layer as shown in Fig. 2.3, resulting from a rotation of the NAE molecules by 180° , would most likely lead to the conversion of the stable form (polymorph α) to a second form (polymorph β). Although our results are obtained with NPEA, similar conversion is highly likely in the other long chain NAEs as well, especially NMEA and NSEA for which an equivalent to the α polymorph has been observed by single-crystal X-ray diffraction.

Besides the similarities in the hydrogen bonding patterns between the two polymorphs, the bilayer thickness and angle of tilt of the acyl chains are also very similar. Thus in polymorph β , the O2–O2 distance is 45.2 Å and matches very well with the distance of 45.57 Å observed in polymorph α , whereas the chain tilt angle of 35.5° for polymorph β is in good agreement with the value of 34.5° estimated for polymorph α .

2.4.3. Subcell Structure

The hydrocarbon chains in lipid crystals adopt a variety of lateral packing modes, which may be described by subcells that specify the relations between equivalent positions within the chain and its neighbors. Analysis of a large number of lipid crystal structures has shown that the chain packing modes fall into a relatively small number of hydrocarbon subcells with triclinic, monoclinic, orthorhombic and hexagonal symmetry and their polymethylene planes can be mutually parallel or perpendicular with respect to their neighbors (Abrahamsson et al., 1978; Maulik et al., 1988). The subcells have been further divided into simple and hybrid types, with the latter type involving more than two different asymmetric units in a subcell. Examination of the hydrocarbon chain packing in the α and β polymorphs of NPEA revealed that the subcells in both these polymorphs is of the orthorhombic type

(O' \perp) in the *Pbnm* space group. The unit cell dimensions of these subcells have been found to be: $a = 7.435 \text{ \AA}$, $b = 4.885 \text{ \AA}$, and $c = 2.544 \text{ \AA}$ for polymorph α and $a = 7.45 \text{ \AA}$, $b = 4.898 \text{ \AA}$, and $c = 2.547 \text{ \AA}$ for polymorph β . These then yielded the area per chain as 18.16 \AA^2 for the α polymorph and as 18.25 \AA^2 for the β polymorph. These parameters are in the range that is typically observed for the orthorhombic type O' \perp (Larsson, 1966).

2.4.4. Molecular Area

The area per each NPEA molecule in the bilayer plane in the crystal structures of polymorphs α and β is 21.99 \AA^2 and 22.03 \AA^2 , respectively. These values are in the same range as those found for other NAEs whose 3-dimensional structures have been determined earlier, namely NMEA (21.95 \AA^2) and NSEA (21.99 \AA^2) as well as some other single-chain lipids such as 3(11-bromoundecanoyl)-D-glycerol, 3-lauroyl-D-glycerol and 3-Stearoyl-D-glycerol, whose molecular areas are in the range of $21.5\text{--}22.7 \text{ \AA}^2$ (Ramakrishnan and Swamy, 1999; Dahlén et al., 1977; Larsson et al., 1966; Goto et al., 1985, 1988; Pascher et al., 1992). Other single chain lipids such as lysophosphatic acid and lysophosphatidylethanolamine have somewhat larger molecular areas (33.6 and 34.8 \AA^2 , respectively). Such large molecular areas observed in these two molecules are due to the very high tilt angle of the acyl chains with respect to the bilayer normal (Pascher et al., 1985, 1981).

2.4.5. Hydrogen Bonding and Intermolecular Interactions

The molecular packing in the crystal structure of NPEA was examined from various angles in order to understand the intermolecular interactions. Results obtained for polymorph α , which is similar to the crystal structure of NMEA (Ramakrishnan and Swamy, 1999) will be presented first and then the results from the analysis of polymorph β will be discussed in comparison.

The hydrogen bonding pattern observed in the crystal lattice of polymorph α is shown in Fig. 2.4. Fig. 2.4A gives a view of the molecular packing together with the hydrogen bonds between hydroxyl group in the opposite leaflets as well as those between the amide hydrogen and the carbonyl oxygen atoms of adjacent layers in the same leaflet of the bilayer. In Fig. 2.4B, a closer picture of the hydrogen bonding pattern is given, which shows the view along the *b*-axis. Each hydroxy group is involved in two hydrogen bonds, one as a donor and the other as an acceptor. All these hydrogen bonds connect the NPEA molecules only along the *b*-axis. Therefore, in the unit cell containing 4 NPEA molecules, organized in a bilayer, the hydroxy group of each molecule forms one hydrogen bond within the same unit cell and the second hydrogen bond with another molecule of NPEA in an adjacent unit cell along the *b*-axis. All the O–H \cdots O hydrogen bonds in the α polymorph are 2.701(2) Å in length, with the H \cdots O distance and the angle subtended at the hydrogen atom being 1.73 Å and 169°, respectively.

Besides the hydrogen bonds between the hydroxy groups, strong hydrogen bonds are also formed between the amide N–H and carbonyl oxygen of adjacent NPEA molecules along the *b*-axis. All these hydrogen bonds are again identical, with an N–O distance of 2.836(2) Å, a H \cdots O distance of 1.84 Å and an N–H \cdots O angle of 167°. Fig. 2.4B clearly shows that the O–H \cdots O hydrogen bonds form an extended network along the *b*-axis, which stabilizes the bilayer-type packing in the crystal lattice. The hydroxy groups are arranged in a zig-zag network, with the angle between two hydrogen bonds (O2–O2–O2 angle) being 129.5°. The N–H \cdots O hydrogen bonds join adjacent NPEA molecules in the same plane along the *b*-axis. While the N–H group of each NPEA molecule forms a hydrogen bond with another NPEA molecule in the adjacent unit cell on one side, the carbonyl oxygen of the same molecules forms a hydrogen bond with the amide N–H of another NPEA molecule in the adjacent unit cell on the other side (Fig. 2.4B).

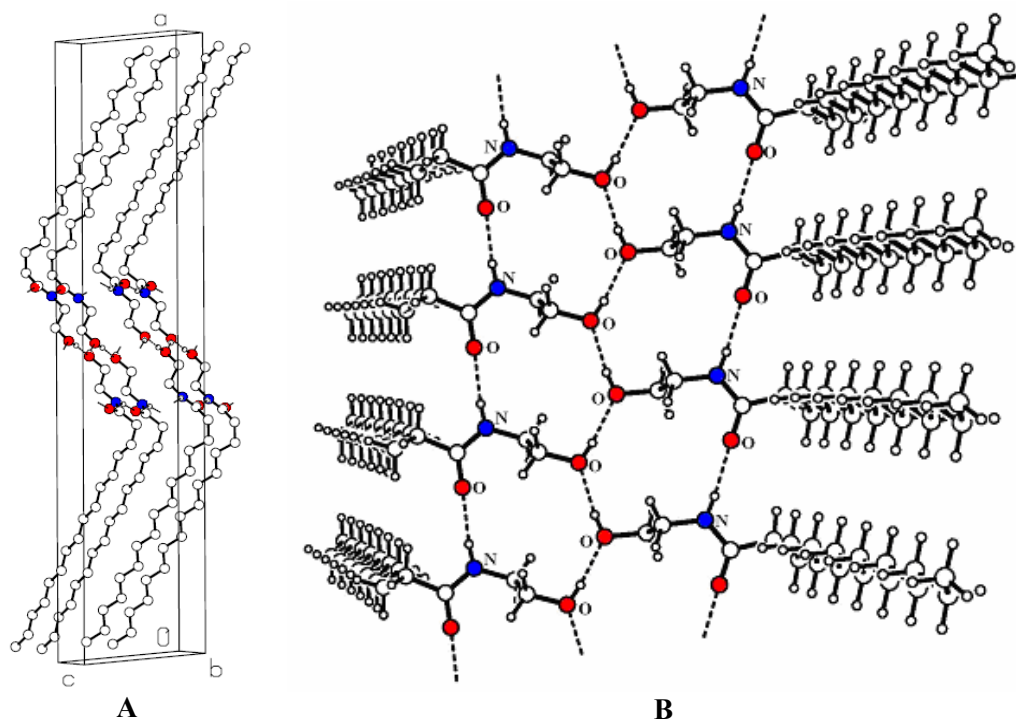


Fig. 2.4: Hydrogen bonding pattern in the crystal lattice of α form of *N*-palmitoylethanolamine. (A) A view of the bilayer displaying both the $\text{O-H}\cdots\text{O}$ and $\text{N-H}\cdots\text{O}$ type hydrogen bonds, (B) A close-up view along the b -axis. The hydrogen bonds ($\text{N-H}\cdots\text{O}$ and $\text{O-H}\cdots\text{O}$) are indicated by dashed lines. (○) hydrogen, (●) carbon, (●) oxygen, (●), nitrogen.

Hydrogen bonding patterns observed in polymorph β are presented in Fig. 2.5. Fig. 2.5A shows both the packing arrangement as well as hydrogen bonding in polymorph β . In the unit cell containing eight NPEA molecules in two head-to-head bilayers stacked one above the other, the hydroxy group of each molecule forms one hydrogen bond within the same unit cell and a second hydrogen bond with another molecule from one of the adjacent unit cells along the a -axis.

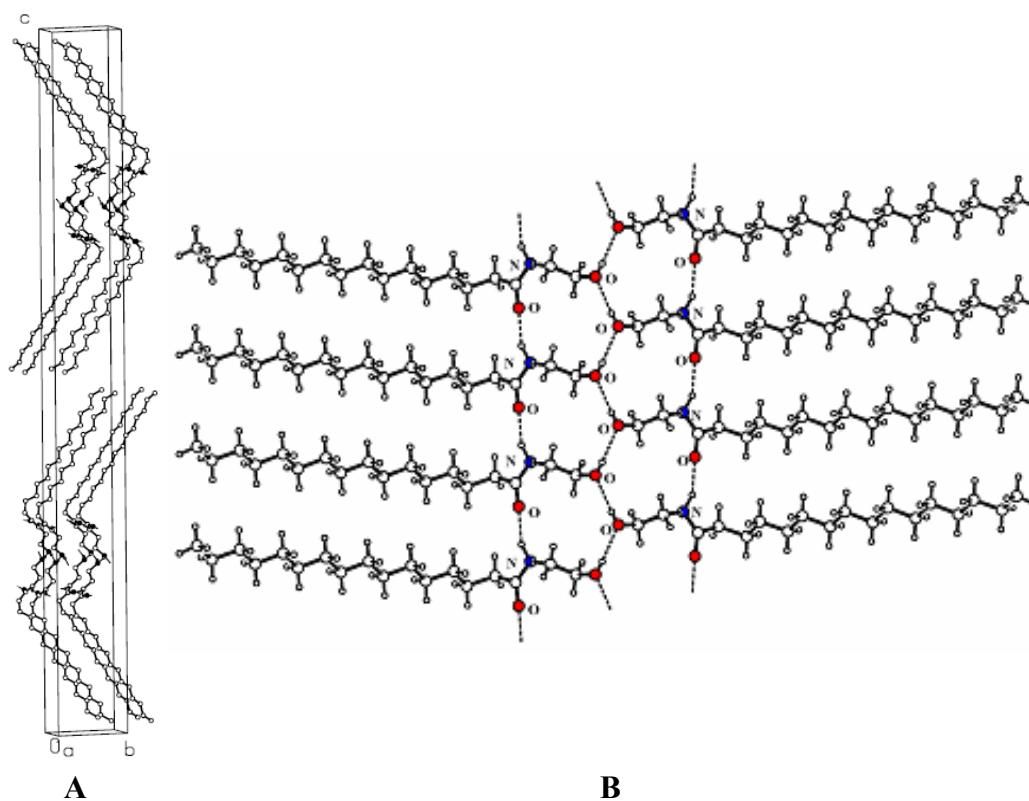


Fig. 2.5: Hydrogen bonding pattern in the crystal lattice of β form of *N*-palmitoylethanolamine. (A) A view of the bilayer displaying both the $\text{O-H}\cdots\text{O}$ and $\text{N-H}\cdots\text{O}$ type hydrogen bonds, (B) A close-up view along the a -axis. The hydrogen bonds ($\text{N-H}\cdots\text{O}$ and $\text{O-H}\cdots\text{O}$) are indicated by dashed lines. (o) hydrogen, (O) carbon, (●) oxygen, (●) nitrogen.

A comparison of Fig. 2.5B with Fig. 2.4B clearly shows that despite the significantly different arrangement of the acyl chains in the opposite leaflets of the bilayer, the hydrogen bonding pattern in the β polymorph is very similar to that observed in the α polymorph. All the $\text{O-H}\cdots\text{O}$ hydrogen bonds in polymorph β of NPEA have the same $\text{H}\cdots\text{O}$ distance of 1.75 Å and the distance between the two oxygen atoms is 2.699(6) Å. These hydrogen bonds are also non-linear with angle between the covalent bond and the hydrogen bond being 160°.

In polymorph β the hydrogen bonds between the amide N–H and carbonyl oxygen of adjacent NPEA molecules are seen along the a -axis. Here the distance between hydrogen bonded carbonyl oxygen and the amide hydrogen atom is 1.89 Å and the N \cdots O distance is 2.823(4) Å. The angle between the covalent bond and the hydrogen bond (N–H \cdots O angle) is 152°, which clearly deviates significantly from linearity and hence is expected to be somewhat weaker compared to the N–H \cdots O hydrogen bonds in the α polymorph.

Similar to the α polymorph (Fig. 2.4B), the O–H \cdots O hydrogen bonds in polymorph β also form extended, zig-zag networks (Fig. 2.5B), which stabilize the bilayer arrangement. These networks are seen along the a -axis, and the angle between the two hydrogen bonds (O2–O2–O2 angle) at each oxygen atom is 130.3°. The N–H \cdots O hydrogen bonds connect adjacent NPEA molecule in the same plane along the a -axis. The amide N–H group of each NPEA molecule forms a hydrogen bond with another molecule in the adjacent unit cell on one side, whereas the carbonyl oxygen atom from the same molecule is involved in another hydrogen bond with the amide N–H of an NPEA molecule in the unit cell on the other side (Fig. 2.5B).

As is seen clearly in Figs. 2.4B and 2.5B, the interconnecting hydrogen bonds at the head-to-head bilayer interface result in the formation of 14-membered loops. Each loop contains one N–H \cdots O hydrogen bond and two O–H \cdots O hydrogen bonds. Two adjacent molecules of NPEA in each leaflet, which are connected by an N–H \cdots O hydrogen bond, and one NPEA molecule from the opposite leaflet – which forms one hydrogen bond each with the above two NPEA molecules via its hydroxy group – are involved in the formation of the 14-membered, hydrogen bonded loop.

2.4.6. Lattice Energy Calculations

The lattice energy of polymorphs α and β was computed using the COMPASS force field in Cerius² program package in order to estimate their relative energies. These calculations yielded an overall energy of -46.53 kcal/mol for the α polymorph, which is made up of -39.61 kcal/mol van der Waals' energy and -6.92 kcal/mol electrostatic energy. For the β polymorph the overall computed energy is -43.88 kcal/mol, with the van der Waals' and electrostatic components being -39.63 and -4.25 kcal/mol. These results indicate that the crystal lattice energy of polymorph α is lower than that of polymorph β by about 2.65 kcal/mol, which appears to be arising solely from the electrostatic component. Since the N-H \cdots O bond angle is significantly lower in the β polymorph as compared to the polymorph α (167° vs. 152°), it is likely that this difference can be largely accounted for by the weaker N-H \cdots O hydrogen bond in the former.

2.4.7. Differential Scanning Calorimetry

Previous differential scanning calorimetric studies from this laboratory have shown that based on the thermal history NPEA and other long-chain NAEs give one or two minor transitions before the major chain-melting transition, which were attributed to solid-solid phase transitions, indicating structural polymorphism (Ramakrishnan and Swamy, 1999). In order to investigate this, additional DSC experiments have been carried out in the present study. Thermogram **a** in Fig. 2.6 gives the first heating scan of the α form of dry NPEA and thermogram **b** gives the cooling scan obtained immediately after the heating. Thermogram **c** corresponds to the second heating scan of the same sample.

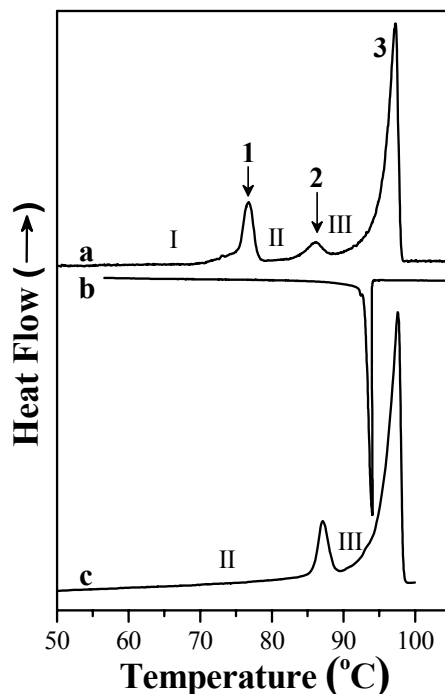


Fig.2.6: DSC thermograms of the α polymorph of *N*-palmitoylethanolamine. a) First heating scan, b) cooling scan, and c) second heating scan performed in succession.

The first heating scan shows three endothermic transitions at ca. 76.8, 86.2 and 97.3°C, with enthalpies of 3.1, 1.3 and 11.3 kcal/mol, respectively and the enthalpy of transition 3 is in good agreement with the value of 11.54 kcal/mol reported earlier for the melting transition of NPEA (Ramakrishnan and Swamy, 1999).

These results show that NPEA exists in at least three polymorphic forms in the solid state; polymorph I exists below transition 1, polymorph II exists between transitions 1 and 2, and polymorph III exists between transitions 2 and 3. Since the DSC scans were performed with the polymorph α , these results establish that polymorph I is the same as α form. Heating the polymorph α to 80°C and 90°C (i.e., to a temperature above transition 1 and transition 2, respectively), followed by

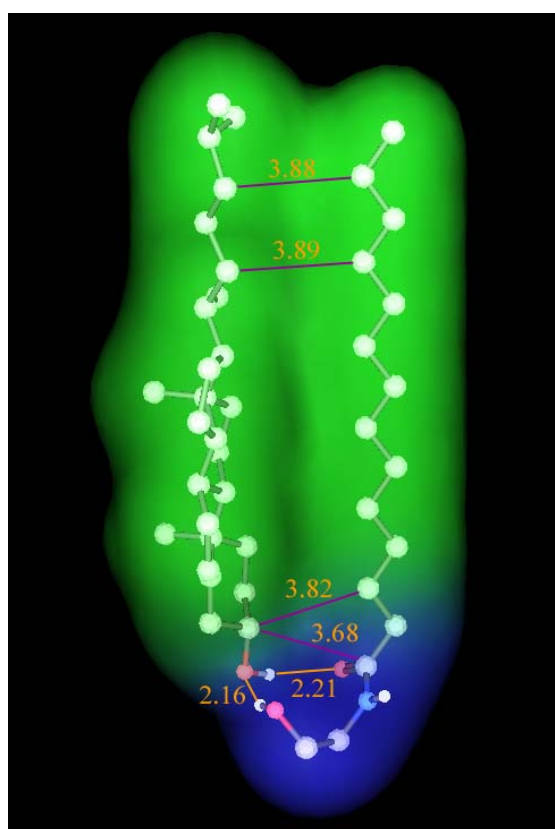
cooling to room temperature and then reheating gave thermograms that are identical to thermogram **c** (Fig. 2.6). This shows that transition **1** is not reversed once it is completed irrespective of whether transitions **2** and **3** are also completed or not, whereas transition **2** could be readily reversed by cooling from a temperature below transition **3** or above it. These observations suggest the polymorph II is metastable at room temperature.

The enthalpy value of 3.1 kcal/mol for transition **1** occurring at $\sim 77^\circ\text{C}$ (thermogram **a**, Fig. 2.6) is in good agreement with the energy difference of 2.65 kcal/mol between the α and β polymorphs, obtained from lattice energy calculations described above and suggests that polymorph II is most likely the β form.

It has been suggested earlier that NAEs may stabilize the bilayer structure of diacyl phosphatidylethanolamines because addition of NAEs such as *N*-lauroylethanolamine and *N*-oleoylethanolamine to egg PE shifted its bilayer-inverse hexagonal phase transition to higher temperatures (Ambrosioni et al., 1993). The present study together with earlier studies on the crystal structures of *N*-myristoylethanolamine and *N*-stearoylethanolamine suggest that such stabilization is probably driven by the strong tendency of the NAEs to form bilayer structure. This is further strengthened by the observation of bilayer arrangement in both the polymorphic forms of NPEA in the present study. Since intermolecular hydrogen bonds between the head groups of neighboring molecules are found in the crystal structures of PEs (Pascher et al., 1981, 1992) as well as all the NAEs for which crystal structures are known, namely NMEA (Ramakrishnan and Swamy, 1993), NSEA (Dahlén et al., 1977) and NPEA (Kamlekar and Swamy, 2006), it appears likely that hydrogen bond formation between PE and NAE may play an important role in such stabilization. DSC, spin-label ESR and ^{31}P -NMR investigations aimed at understanding the mixing behaviour of NAEs and PEs are reported in Chapter 5.

Chapter 3

Differential Scanning Calorimetric and Computational Modeling Studies on the Interaction of *N*-Acylethanolamines with Cholesterol



N-Myristoyl ethanolamine—Cholesterol (1:1) Complex: First Evidence from Differential Scanning Calorimetry, Fast-Atom-Bombardment Mass Spectrometry and Computational Modelling.

Ramakrishnan, M., Kenoth, R., **Kamlekar, R.K.**, Chandra, M.S., Radhakrishnan, T.P. and Swamy, M.J. 2002. *FEBS Lett.* **531**, 343-347.

3.1. SUMMARY

In previous work from this laboratory, the interaction of *N*-myristoylethanolamine (NMEA) with cholesterol in aqueous dispersion was investigated by DSC and fast-atom-bombardment mass spectrometry (FAB-MS), which suggested the formation of a 1:1 (mol/mol) complex between them (Ramakrishnan et al, 2002). In this study, this interaction has been further investigated by DSC studies on mixtures of NMEA and cholesterol in the solid state as well as by computational modeling. DSC on solid mixtures indicate that addition of cholesterol to NMEA leads to a new phase transition at ca. 86.5°C besides the chain-melting transition of NMEA at 95°C. The intensity of the peak corresponding to the new transition increases with cholesterol content up to 50 mol%, but decreases thereafter, whereas the intensity of the peak corresponding to NMEA decreases with increasing cholesterol content with concomitant and gradual shift to lower temperatures and vanishes at 50 mol% cholesterol. These results are consistent with the formation of a 1:1 molar complex between NMEA and cholesterol proposed earlier and indicates that these two amphiphiles are associated in the solid state as well. Molecular modeling studies support this experimental finding and provide a plausible structural model for the complex, which highlights multiple H-bond interactions between the hydroxy group of cholesterol and the hydroxy and carbonyl groups of NMEA besides appreciable dispersion interaction between the hydrocarbon domains of the two molecules. DSC studies on hydrated mixtures of NPEA and NSEA with cholesterol show that these two long chain NAEs also form 1:1 (mol/mol) complexes with cholesterol.

3.2. INTRODUCTION

As discussed in Chapter 1, long-chain *N*-acylethanolamines and their precursors, *N*-acylphosphatidylethanolamines accumulate in plants and animals when the parent organism is subjected to stress such as injury in animals or dehydration in plants. Besides, NAEs exhibit a variety of interesting biological properties such as binding to type-I and type-II cannabinoid receptors, inhibition of gap-junction conductance and reduction of sperm fertilizing capacity as well as anti-inflammatory, antibacterial and antiviral properties, which are also of considerable interest and potential application (see for reviews, Schmid et al., 1990, 1996; Hansen et al., 2000; Chapman, 2004).

In order to develop structure-function relationships for NAEs, it is important to characterize their physical properties and interaction with other membrane constituents such as cholesterol, phospholipids and integral membrane proteins. In previous work from this laboratory and elsewhere, the 3-dimensional structures of NSEA and NMEA were determined by single crystal X-ray diffraction studies and the molecular packing and intermolecular interactions in the solid phase were analysed (Dahlen et al., 1977; Ramakrishnan and Swamy, 1999). In the studies reported in Chapter 2, two structural polymorphs of *N*-palmitoylethanolamine were investigated by single crystal X-ray diffraction and their molecular packing and intermolecular interactions were analysed in detail (Kamlekar and Swamy, 2006). These studies revealed that in the crystal lattice NAE molecules pack in a bilayer format, analogous to that found in phospholipid membranes (Ramakrishnan and Swamy, 1999; Kamlekar and Swamy, 2006).

The interaction of NPEA with DPPC in aqueous dispersion, investigated by DSC, ^{31}P -NMR and small-angle X-ray diffraction, indicated that both components mix well up to 60 mol% of NPEA with phase separation occurring at higher

contents of the NAE. DSC and fast-atom-bombardment mass spectrometric studies on the interaction of NMEA with cholesterol indicated the formation of a 1:1 (mol/mol) complex between them (Ramakrishnan, 2001; Ramakrishnan et al., 2002). In this chapter this interaction has been further investigated by DSC studies on solid mixtures of NMEA and cholesterol and by computational modeling. In addition, DSC studies have also been carried out on hydrated mixtures of two other NAEs, namely *N*-palmitoylethanolamine (NPEA) and *N*-stearoylethanolamine (NSEA), with cholesterol. The results obtained suggest that NPEA and NSEA also form 1:1 stoichiometric complex with cholesterol.

3.3. MATERIALS AND METHODS

3.3.1. *Materials*

The NAEs were synthesized and characterized as described in (Ramakrishnan et al., 1997). Cholesterol was purchased from Avanti Polar Lipids (Alabaster, AL, USA).

3.3.2. *Sample Preparation*

Dry mixtures of NMEA and cholesterol for DSC measurements were prepared by weighing out appropriate amounts of the two lipids into a dry glass test tube to give the desired ratio and then dissolving the mixture (total weight of 5 – 10 mg) in ca. 0.5 mL of dichloromethane with mild vortexing to ensure uniform mixing of the dissolved components. The solvent was then removed by blowing dry nitrogen gas slowly on the surface of the sample while the sample tube was maintained in a warm water bath. The sample was then kept for at least three hours in desiccator connected to a vacuum pump. The dry mixture was then transferred to a pre-weighted aluminium DSC pan, which was sealed by crimping and weighed again. Mixtures of NPEA and NSEA with cholesterol were also prepared essentially in the

same manner. However, after preparation of the dry mixture, the samples (1-3 mg) were transferred into pre-weighted stainless steel DSC pans and the pan was weighed again. Then about 30 μ L of double distilled water was added and the sample pan was sealed by crimping. Reference pan contained only water.

3.3.3. Differential Scanning Calorimetry

DSC measurements were performed on a Perkin-Elmer DSC-4 calorimeter equipped with a data station. For dry samples, the DSC scans were carried out by placing the DSC pan containing the appropriate lipid or lipid mixture in the sample compartment of the calorimeter with an empty pan in the reference compartment. Then two heating and two cooling scans were performed between 30°C and 100°C at a scan rate of 2.5 degrees/min.

DSC measurements on hydrated samples were performed essentially as described earlier (Ramakrishnan et al., 2002). Briefly, the DSC pans containing the lipid or lipid mixture were hydrated by incubation at 90°C for 30 minutes in the calorimeter and then cooled to 35°C. After incubation at this temperature for 20 minutes, two heating scans and two cooling scans were performed at a scan rate of 2.5 degrees/min. After each scan, the sample was incubated for 10 minutes at the extreme. Transition enthalpies were evaluated by integrating the area under each peak using the software supplied by the instrument manufacturers.

3.3.4. Computational Methodology

Molecular modeling studies were carried out using a combination of empirical force field available in the MOE program and the AM1 semiempirical quantum chemical method. The MOE program (The Molecular Operating Environment, Version 2001.01) is available from Chemical Computing Group Inc. (1010 Sherbrooke Street West, Montreal, Canada H3A 2R7; website:

<http://www.chemcomp.com>). AM1 computations were carried out using the MOPAC93 program (© Fujitsu Inc., Japan). Geometries of NMEA and cholesterol were optimized using the empirical potentials followed by the AM1 method. Default options in MOE were employed in systematic conformational search on conformations arising out of bond rotations at 10° intervals in the hydrophilic region of NMEA. In optimizations of the complex using the 'water soak' option of MOE, 339 water molecules in the default layer width and box metric were used and PEOE (partial equalization of orbital electronegativities) electrostatic charges were computed for all atoms and included.

3.4. RESULTS AND DISCUSSION

3.4.1. DSC Studies on Dry Mixtures of NMEA and Cholesterol

Heating thermograms of dry samples of NMEA, cholesterol and their mixtures are shown in Figure 3.1. Consistent with earlier results, dry NMEA shows a reversible, highly cooperative gel-fluid chain-melting phase transition centered at 95°C, which is in good agreement with the literature value of 93.9°C (Ramakrishnan et al., 1997). Addition of cholesterol at low mole fractions results in two distinct changes in the thermograms. First, intensity of the peak corresponding to the chain-melting transition decreases, becomes somewhat broader and also shifts to a slightly lower temperature. In addition, a second peak appears around 86.5°C, indicating a new phase transition, the relative intensity of which increases with increasing NMEA:cholesterol ratio up to 1:1 (mol/mol). The two peaks partially overlap and the overlap increases with increasing cholesterol content because the shift in the peak corresponding to NMEA alone becomes larger with increasing cholesterol content. For the sample with 40 mol% cholesterol, the thermogram appears to consist of two overlapping peaks – one broad and the other one sharp – indicating

that the two transitions occur at the same temperature. Cooling scans indicate that both the transitions are reversible (not shown). Cholesterol alone did not show any phase transition between 35 and 100°C (not shown).

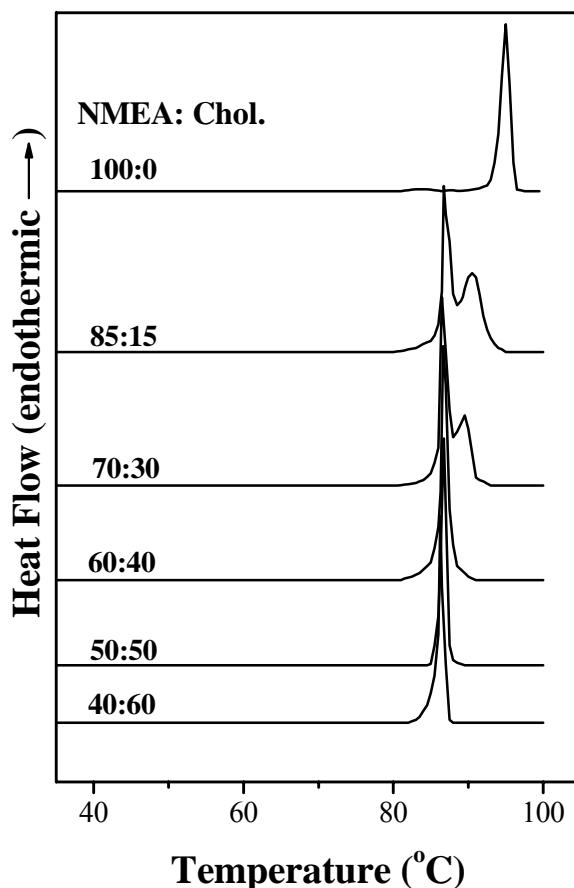


Fig. 3.1: Heating thermograms of NMEA, cholesterol and their mixtures. The composition of the lipid mixture (in mol ratio) is indicated. Scan rate is 2.5°/min. The Y-scale is not the same for all the scans shown.

In view of the overlapping transitions it was not possible to obtain reliable quantitative information on the enthalpies of the two transitions as a function of the cholesterol content. However, the above observations are qualitatively similar to the results obtained earlier in this laboratory with hydrated mixtures of NMEA and

cholesterol (Ramakrishnan, 2001) and suggest that NMEA and cholesterol form a 1:1 (mol/mol) complex in the solid state also.

3.4.2. Molecular Modeling Studies on NMEA-Cholesterol Interaction

In order to investigate the interaction between NMEA and cholesterol further, computational modeling studies were carried out. Molecular modeling combining empirical force field and semiempirical quantum chemical AM1 computations strongly support the conclusions arrived at from earlier DSC and FAB-MS studies on the hydrated mixtures and the above results on the dry mixtures of NMEA and cholesterol indicating the formation of a 1:1 stoichiometric complex between NMEA and cholesterol and provide a plausible structural model for it. Geometries of NMEA and cholesterol were optimized using empirical potentials; the NMEA structure obtained through a stochastic followed by systematic conformational search agrees well with the one obtained from the crystal structure analysis (Ramakrishnan and Swamy, 1999). The two molecules were oriented appropriately to facilitate H-bond interaction between their hydrophilic groups; suitable and minimal bond rotations in the hydrophilic regions of the two molecules were effected for this purpose. An extensive set of initial geometries of the complex was then examined through full geometry optimization using the AM1 method employing the PRECISE conditions.

Alternately the initial geometries were optimized under the 'water soak' option of MOE followed by AM1 optimization. The low energy optimized structures of the complex showed significant H-bond interactions between the hydroxy group of cholesterol and the hydroxy and carbonyl groups of NMEA. The lowest energy structure obtained in our computations is shown in Figure 3.2. Two prominent H-bond interactions, one between the hydroxyl group of cholesterol and

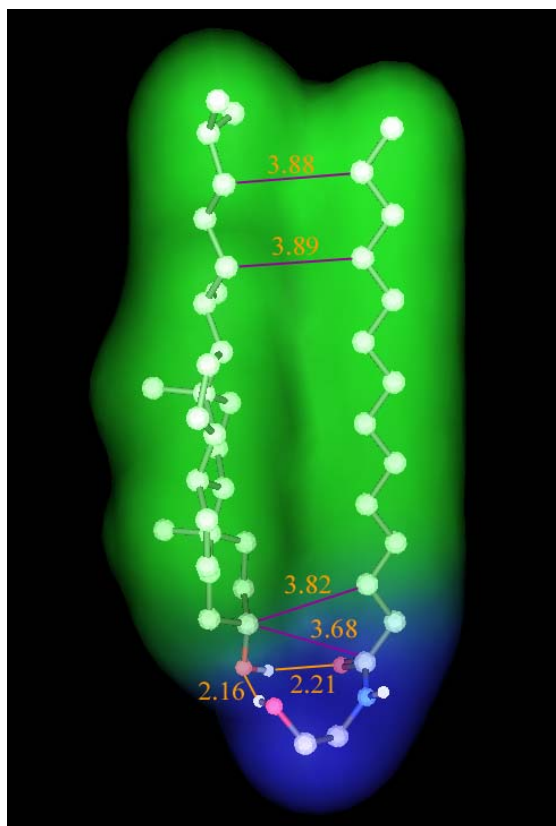


Fig. 3.2: AM1 optimized structure of the NMEA-cholesterol complex. Non-polar H atoms were omitted for clarity. The hydrophilic (blue) and hydrophobic (green) regions are represented using the Gauss-Connolly molecular surface computed using the default options in MOE. Orange lines represent short intermolecular H-bonds and violet lines indicate the non-bonded C-C contacts; the distances shown are in Å.

the carbonyl group of NMEA ($r_{\text{H}\cdots\text{O}} = 2.21$ Å, $\theta_{\text{O-H}\cdots\text{O}} = 135.0^\circ$) and the other formed by the hydroxy groups of NMEA and cholesterol ($r_{\text{H}\cdots\text{O}} = 2.16$ Å, $\theta_{\text{O-H}\cdots\text{O}} = 157.5^\circ$) lead to the cyclic formation, which can be represented as $r_2^2(9)$, in graph set notation (Etter, 1990). Interestingly, the optimized geometry of the complex also reveals appreciable dispersion interaction between the hydrocarbon domains of the two molecules as seen from several close C \cdots C contacts, the lowest ones ranging from 3.68 Å to 3.89 Å. Figure 3.2 emphasizes the hydrophobic and hydrophilic regions of the complex resulting from the various intermolecular interactions. The

model structure of the complex illustrates a close matching of the size and hydrophilic/hydrophobic regions of the partner molecules leading to a compact pairing. The enthalpies of formation of the fully AM1 optimized geometries of the complex, NMEA and cholesterol indicate an appreciable stabilization of 5.3 kcal/mol for the complex. If the nearest local minima of cholesterol and NMEA, obtained by optimization starting from their respective geometries in the complex are used, the stabilization of the complex increases to 6.9 kcal/mol.

3.4.3. DSC Studies on Hydrated Mixtures of NPEA and NSEA with Cholesterol

The above results taken together with the results obtained earlier have clearly demonstrated that NMEA and cholesterol form a 1:1 (mol/mol) complex and suggested that other NAEs may also form similar complexes with cholesterol, in their parent organisms. In order to characterize the interaction of NPEA and NSEA, which are the major NAEs found in various living systems, DSC studies were carried out on mixtures of these two compounds with cholesterol.

Heating thermograms of hydrated samples of NPEA and NPEA/cholesterol mixtures are shown in Figure 3.3A and thermograms corresponding to hydrated samples of NSEA and NSEA/cholesterol mixtures are shown in Figure 3.3B. Overall the results obtained with these two systems are qualitatively rather similar and also parallel those obtained earlier with hydrated mixtures of NMEA and cholesterol (Ramakrishnan, 2001; Ramakrishnan et al., 2002). Therefore, results obtained with NPEA/cholesterol and NSEA/cholesterol mixtures are discussed together here.

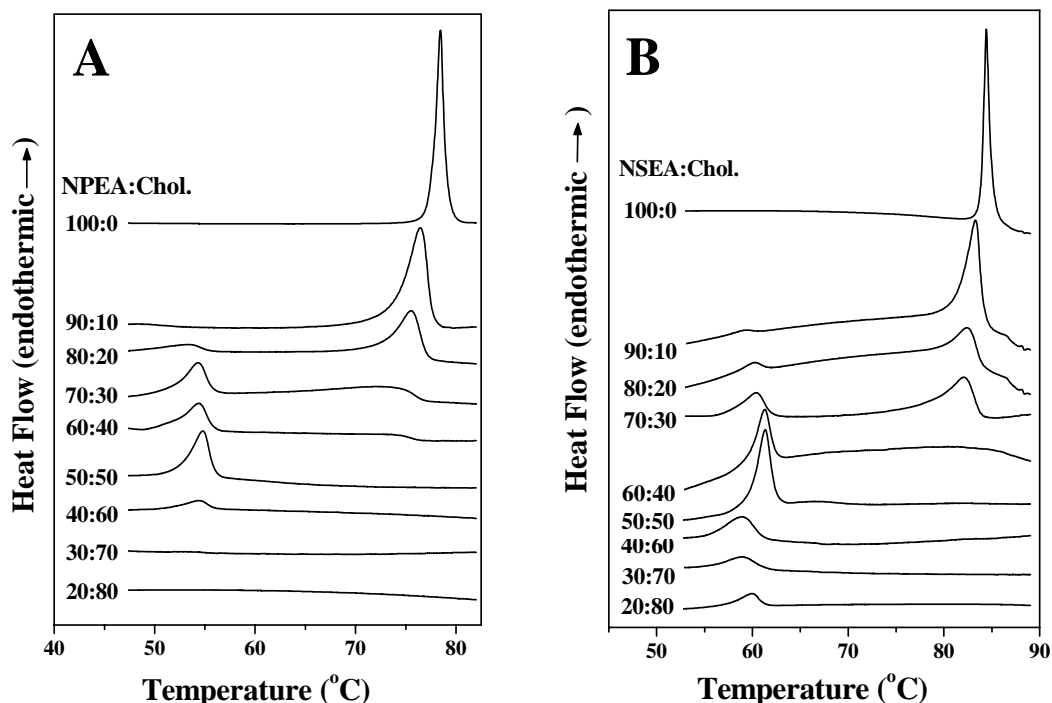


Fig. 3.3: Heating thermograms of aqueous dispersions of A) NPEA/cholesterol and B) NSEA/cholesterol mixtures. The composition of the lipid mixture (in mol ratio) is indicated. Scan rate is 2.5°/min. The Y-scale is not the same for all the scans shown.

From the thermograms shown in Figures 3.3A and 3.3B it can be seen that hydrated samples of NPEA and NSEA show reversible, highly cooperative gel-fluid chain-melting phase transitions centered at 78.4°C and 84.4°C, respectively. These values are in good agreement with the results published earlier (Ramakrishnan et al., 1997). Addition of cholesterol at low mole fractions results in two distinct changes in the thermograms. First, the intensity of the peak corresponding to the chain-melting transition decreases with slight broadening and a shift to lower temperature. In addition, a second peak appears around 53-55°C for the NPEA/cholesterol mixtures and 59-61°C for the NSEA/cholesterol

mixtures, indicating a new phase transition in each case. In both cases, intensity of this new peak increases with increasing cholesterol content up to 1:1 mol ratio of the two components in the mixture, whereas the intensity of the peak corresponding to the chain melting of the NAE decreases steadily and disappears completely at the same ratio. These observations are similar to the results obtained with the NMEA/cholesterol system and suggest the formation of 1:1 (mol/mol) complexes of both NPEA and NSEA with cholesterol and hence this new peak will be referred to as the complex peak. Intensity of the complex peak also decreases with increasing cholesterol content and becomes nearly zero at ca. 0.7 mole fraction of the sterol (for the NPEA/cholesterol mixture), whereas for the NSEA/cholesterol mixture even at 0.8 mole fraction of the sterol the complex peak has some intensity. Cooling scans with both sets of mixtures indicate that both the transitions are reversible. Cholesterol alone did not show any phase transition between 35 and 90°C (Ramakrishnan et al., 2002).

A plot depicting the variation of the change in enthalpy (ΔH_t) of the two transitions as a function of the cholesterol content in NPEA/cholesterol and NSEA/cholesterol mixtures is given in Figure 3.4. For the sake of comparison, the corresponding data for the NMEA/cholesterol system, taken from Ramakrishnan et al. (2002), is also shown in this Figure. In each case, ΔH_t for the transition corresponding to the NAE/cholesterol complex increases gradually up to 50 mol% cholesterol and then decreases steadily, becoming negligible around 70-80 mol% cholesterol for NMEA and NPEA, whereas for NSEA the decrease is more gradual with some intensity remaining even at 80 mol% cholesterol. ΔH_t values corresponding to the chain-melting transition of each NAE decrease monotonically with increasing cholesterol content and approach zero at 50 mol% cholesterol. These results suggest the formation of a 1:1 complex between the different NAEs investigated and cholesterol. The thermograms suggest the coexistence of the

complex and NAE in the mixtures containing <50 mol% cholesterol, and the complex and cholesterol in the mixtures containing >50 mol% cholesterol. The mixture having 50 mol% cholesterol appears to contain the complex exclusively.

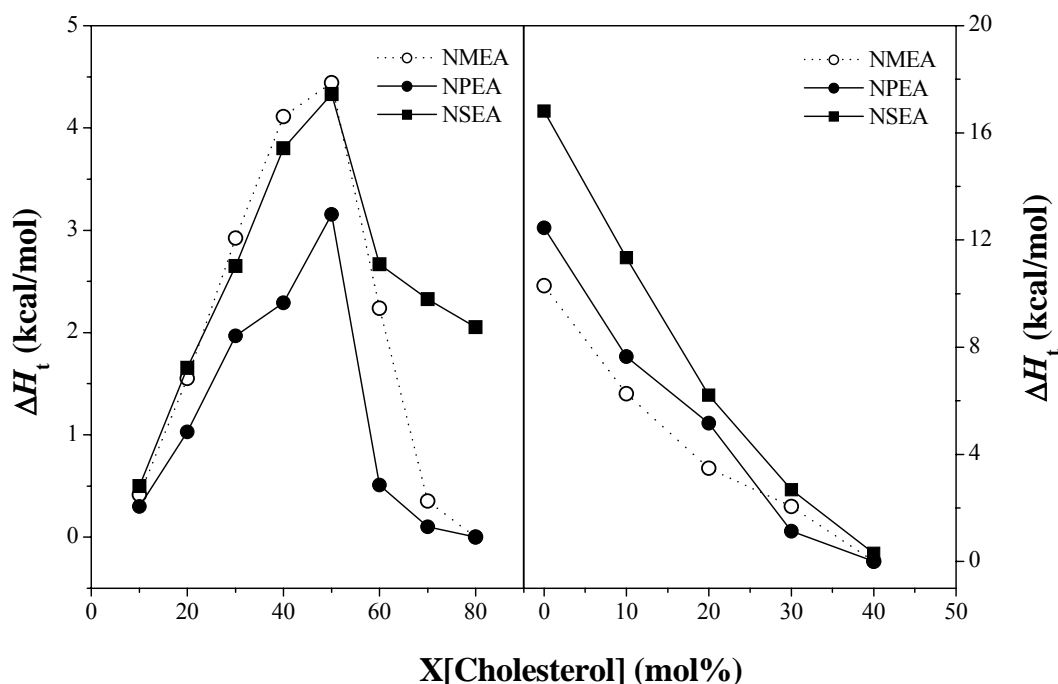


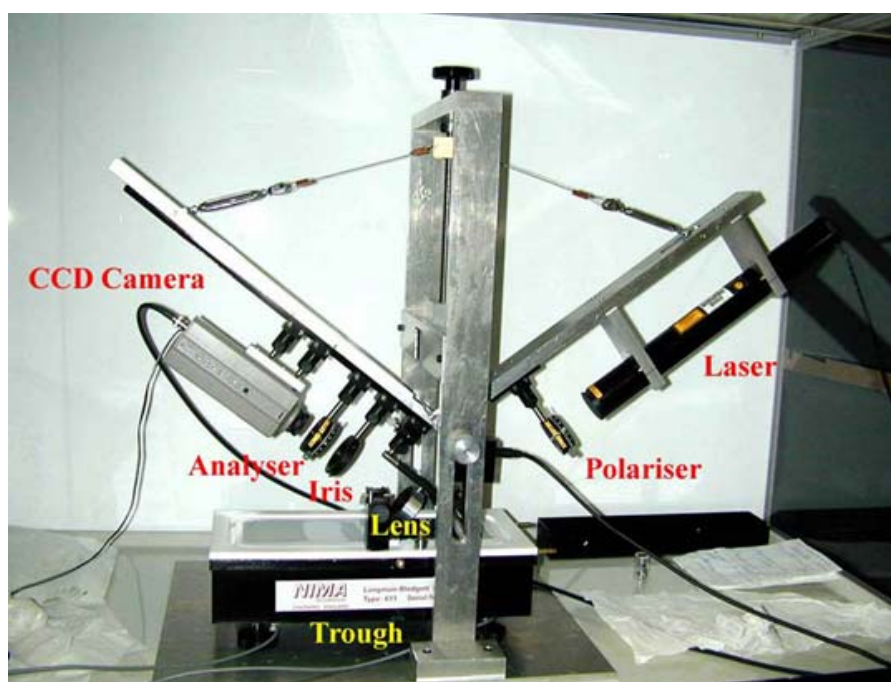
Fig. 3.4. Plot of the change in transition enthalpy (ΔH_t) as a function of cholesterol composition for hydrated mixtures of cholesterol with NMEA, NPEA and NSEA. A) Transition corresponding to the 1:1 complex. B) Transition corresponding to the chain-melting of the NAEs. Transition enthalpies in A were calculated using the weighted average of the molecular weights of NMEA and cholesterol, whereas those in B were calculated based on the molecular weight of NAE alone.

3.4.4. Functional Implications

Due to the ubiquitous presence of cholesterol in animal plasma membranes its interaction with different phospholipids and sphingolipids has been investigated in great detail (Feingold, 1993; Ohvo-Rekilä et al., 2002). Studies on the interaction of cholesterol with other lipids have received a new impetus during the last decade

in view of its presence in membrane *rafts*, which are rich in cholesterol and sphingolipids. Such studies have led to the identification of novel "condensed complexes" between cholesterol and different phospholipids with simple integral stoichiometry (Brown and Rose, 1992; Brown and London, 1998; Simons and Ikonen, 1997; Sheets et al., 1999; Radhakrishnan and McConnell, 1999a, b; Radhakrishnan et al., 2001). These complexes have been implicated in the formation of lipid rafts and are suggested to modulate the chemical activity of cholesterol, which in turn could regulate its biosynthesis (Radhakrishnan and McConnell, 2000; Radhakrishnan et al., 2000). The formation of relatively strong stoichiometric complexes between *N*-acylethanolamines such as NMEA, NPEA and NSEA with cholesterol demonstrated earlier (Ramakrishnan, 2001) and in the present study provides a potential model system for investigating the importance of lipid-lipid interactions in the formation and dynamics of rafts. Such specific complexes could be important in the cytoprotective and stress-combating actions of *N*-acylethanolamines.

Interaction of *N*-Myristoylethanolamine with Cholesterol: Monolayer and Brewster Angle Microscopic Studies



Langmuir film balance with Brewster angle microscope

4.1 SUMMARY

N-acylethanolamines have elicited much interest in recent years due to the dramatic increase in their content in the parent organism under stress, suggesting a putative role in stress-combating response of the organism. Previous studies employing DSC, FAB-MS and computational modeling suggested that *N*-myristoylethanolamine and cholesterol interact to form a 1:1 (mol/mol) complex. In the present study, this interaction has been further characterized by the Langmuir film balance technique and Brewster angle microscopy (BAM). For NMEA-cholesterol mixtures, monolayer experiments have shown that at low fractions of cholesterol, the average area per molecule is lower than that predicted for ideal mixing, whereas at high cholesterol content the experimentally determined molecular area is higher than the ideal value calculated from the molecular areas of NMEA and cholesterol, with a cross-over point at 1:1 (mol/mol) ratio. These observations suggest that addition of small amounts of cholesterol to NMEA leads to stabilization of the intermolecular interactions, leading to the formation of stable and compact monolayer film, whereas at the other end of the composition diagram, addition of small amounts of NMEA to cholesterol results in a tilting of the cholesterol molecules leading to an increase in the average area per molecule. In BAM experiments, a stable and bright homogeneous condensed phase was observed at a relatively low applied pressure of 2 mN.m^{-1} for the NMEA:Chol. (1:1, mol/mol) mixture, whereas all other samples required significantly higher pressures ($> 10 \text{ mN.m}^{-1}$) to form a homogeneous condensed phase. These observations are consistent with the formation of a 1:1 stoichiometric complex between NMEA and cholesterol.

4.1. INTRODUCTION

N-Acylethanolamines and *N*-acyl PEs are widely distributed in nature and appear to be ubiquitous and their content increases dramatically in different organisms when they are subjected to different types of stress, such as an injury in animals or dehydration in plants (Schmid et al., 1990; Schmid et al., 1996; Chapman, 2004; see also Chapter 1). These observations led to the speculation that the increased production of NAEs and NAPEs under stress conditions may form part of the stress-combating response of the parent organism (Schmid et al., 1990, 1996; Chapman et al., 2000).

Interest in NAEs was further enhanced during the 1990s when it was discovered that they exhibit a variety of interesting biological and medicinal properties e.g., the ability of *N*-arachidonylethanolamine (anandamide) and NPEA to bind to type-I and type-II cannabinoid receptors, respectively (Devane et al., 1992; Facci et al., 1995). Anandamide and other ethanolamides of polyunsaturated fatty acids also inhibit adenylyl cyclase and *N*-type calcium channels and produce hypothermia, catalepsy, analgesia and hypoactivity (Pertwee, 1972; Janusz et al., 1993; Mackie et al., 1993; Vogel et al., 1993; Romero et al., 1995; Seltzman et al., 1997). NAEs also exhibit anti-inflammatory, antibacterial and antiviral properties, which are of considerable application potential (cf. Schmid et al., 1990). Further, both NAEs and NAPEs are likely to be useful in developing liposomal formulations for drug delivery applications because it has been shown that compounds belonging to both these classes can stabilize the bilayer structure (Ambrosini et al., 1993; Domingo et al., 1993; Mercadal et al., 1995).

In view of the interesting biological and medicinal properties of NAEs and NAPEs, as well as their putative role in combating stress, it is important to investigate their biosynthesis, catabolism and biophysical properties such as 3-

dimensional structure and interaction with membrane lipids and proteins, in order to develop structure-function correlations and to rationalize their role in the parent organisms. As discussed in the Introduction, the metabolism of NAEs and NAEs has been investigated in considerable detail and several of the important enzymes involved in the metabolism of NAEs and NAEs have been purified, characterized and cloned (Okamoto et al., 2004; Sun et al., 2004; Tsuboi et al., 2005).

A number of biophysical studies have also been carried out on NAEs and NAEs (see for a review, Marsh and Swamy, 2000). In studies from this laboratory the phase transitions of a homologous series of NAEs were characterized by DSC, which suggested that they exhibit structural polymorphism in the solid state (Ramakrishnan et al., 1997; Ramakrishnan and Swamy, 1998). The molecular packing and intermolecular interactions of one polymorph of NMEA was studied by single-crystal X-ray diffraction (Ramakrishnan and Swamy, 1999). Very recently we reported the crystal structures of two different polymorphs of NPEA – which firmly established structural polymorphism in NAEs in the solid state – and provided a possible mechanism for the interconversion between them (Chapter 2; Kamlekar and Swamy, 2006). In all these structures NAE molecules pack in a bilayer format, analogous to that found in phospholipid membranes (Ramakrishnan and Swamy, 1999; Kamlekar and Swamy, 2006).

At least some of the biological and pharmacological effects of NAEs are expected to be mediated by their interaction with other membrane constituents, or will be affected by such interactions. Therefore, it is essential to investigate the interaction of NAEs with major membrane lipids such as phospholipids and cholesterol. In one study, the interaction of NPEA with DPPC was investigated by DSC, ³¹P-NMR and small-angle X-ray scattering experiments (Swamy et al., 2003). In another study, DSC and FAB-MS experiments, complemented by computational modeling studies have provided a strong evidence for the formation of a 1:1

(mol/mol) complex between NMEA and cholesterol (Ramakrishnan et al., 2002). In the present study we have investigated this interaction further using the monolayer approach. The interfacial packing properties of NMEA and its mixtures with cholesterol at different compositions have been characterized by using Langmuir-type film balance technique and Brewster angle microscopy.

4.2. MATERIALS AND METHODS

4.2.1. Materials

N-Myristoylethanolamine was synthesized and characterized as described earlier (Ramakrishnan et al., 1997). Cholesterol was purchased from Avanti Polar Lipids (Alabaster, AL, USA).

4.2.2. Langmuir Film Balance Measurements

Pressure-area (π -A) isotherms were investigated on a Nima Model 611M Langmuir-Blodgett trough using a Wilhelmy plate for pressure sensing. All experiments have been done at 25 (\pm 1) °C. Water for the sub-phase has been purified by double distillation and then passed through Milli-Q UV plus system (Millipore, Bedford, MA). After spreading the amphiphile solution, a 15-minute wait period was given before recording the π -A isotherm. The π -A isotherms were recorded using a barrier speed of 50 cm²/min. All π -A isotherm experiments were repeated on fresh subphases 3 times to ensure reproducibility.

4.2.3. Brewster Angle Microscopy

Morphology of the Langmuir films at air-water interface was observed by a Brewster angle microscope. BAM images of the monolayers were recorded using a Nanofilm Model BAM2Plus microscope equipped with a frequency doubled

Nd:YAG laser (20mW power) at a wavelength of 520 nm. The air-water interface was illuminated at the Brewster incidence angle ($\sim 53^\circ$) and the monolayer film was examined at different stages of compression. The reflected beam was received by a microscope and analyzed by a polarization analyzer, and the signal was recorded by a CCD video camera with a 20 X-magnification lens to develop an image of the monolayer. The image size collected from BAM experiment was $220 \times 273 \mu\text{m}$. Length scales of the images were corrected for the angle of incidence of the beam.

4.2.4. Sample Preparation for Monolayer and BAM Studies

Stock solutions of NMEA and cholesterol were prepared in chloroform (Uvasol grade, E. Merck). Appropriate volumes of the stock solutions were mixed to yield desired mol ratio of the two components. The mixed solutions were then sprayed gently drop by drop on the surface of water in the Langmuir trough so that it will form a thin monolayer on the surface of water after evaporation of the solvent.

4.3. RESULTS AND DISCUSSION

A considerable body of evidence has accumulated indicating that the content of *N*-acylethanolamines in a variety of organism increases dramatically in response to membrane stress, leading to the hypothesis that such increase is due to a stress-fighting response of the parent organism. In such a case, the mechanism of such a stress-combating action would involve, at least in part, the interaction of NAEs with other membrane constituents, or such interactions would have some affect on the role of the NAEs. In this regard, studies aimed at understanding the interaction of NAEs with the major membrane lipids such as phosphatidylcholine and cholesterol are expected to help us define the molecular features of such interactions and thus help in unraveling the mode of action of *N*-acylethanolamines in their various putative functions. In an earlier study, we have investigated the interaction of

NPEA, an endogenous ligand for the type-II cannabinoid receptor, with dipalmitoylphosphatidylcholine (Swamy et al., 2003). In another study, it has been shown that NMEA and cholesterol most likely form a 1:1 (mol/mol) mixture (Ramakrishnan et al., 2002). In this study this interaction has been further investigated in monolayers by Langmuir type film balance and Brewster-angle microscopy and the results obtained are discussed below.

4.3.1. Monolayer Studies of *N*-Myristoylethanolamine - Cholesterol Mixtures

Pressure-area isotherms of NMEA, cholesterol and their mixtures of various compositions are shown in Fig. 4.1. The monolayer formed at the air-water

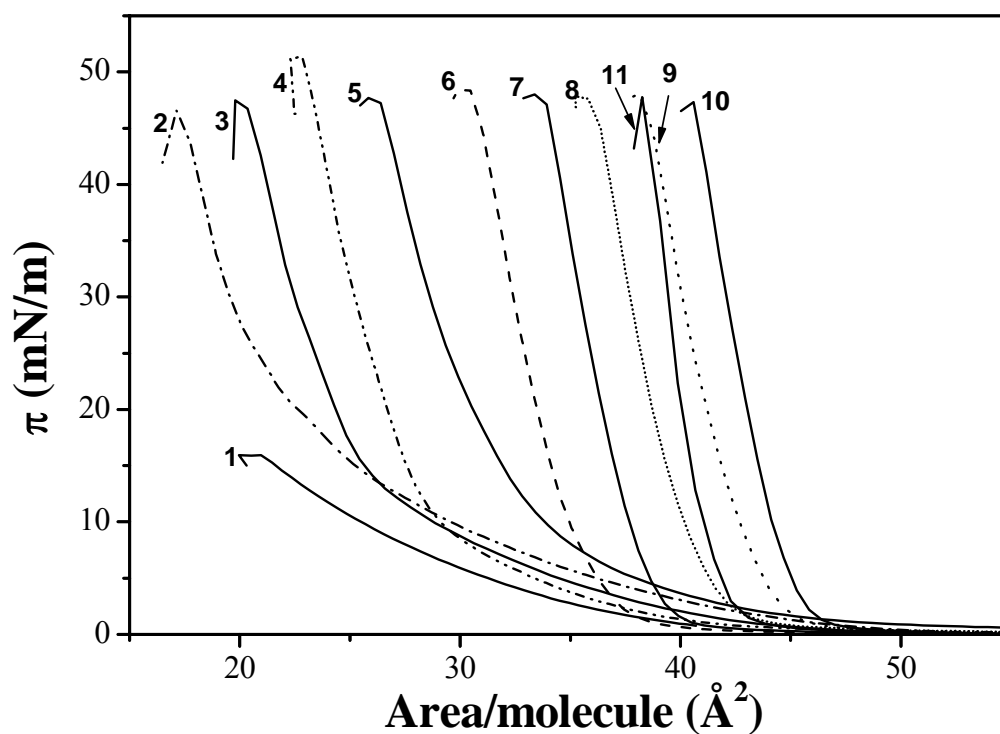


Fig. 4.1: π -A isotherms of NMEA-cholesterol mixtures. The different isotherms shown correspond to 1) NMEA alone, 11) cholesterol alone and mixtures of NMEA and cholesterol at the ratios indicated: 2) 9:1, 3) 8:2, 4) 7:3, 5) 6:4, 6) 5:5, 7) 4:6, 8) 3:7, 9) 2:8, 10) 1:9.

interface by NMEA alone is not stable and collapses at a surface pressure of ca. 16 mN.m⁻¹ with the corresponding molecular area being 21 Å² (curve 1), whereas cholesterol forms a rather stable monolayer which does not collapse at least up to 47.5 mN.m⁻¹ (curve 11). However, addition of cholesterol to NMEA even at relatively low proportions has a marked effect on the properties of the isotherm; addition of as little as 5 mol% of cholesterol resulted in a significant stabilization of the monolayer formed by NMEA and at 10 mol% of the sterol the collapse pressure increased to about 45.5 mN.m⁻¹ (curve 2). All the remaining mixtures up to 90 mol% cholesterol yielded rather stable monolayers with collapse pressure being rather constant around 50 mN.m⁻¹ (Fig. 4.1).

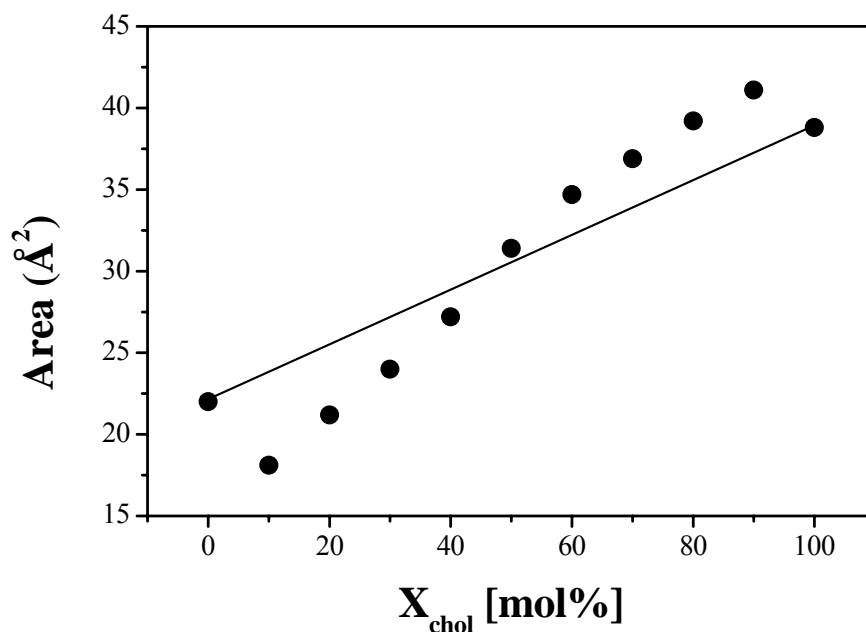


Fig. 4.2: Dependence of area/molecule on the mol fraction of cholesterol in NMEA-cholesterol mixtures. The straight line indicates the area for ideal mixing.

In order to investigate the effect of cholesterol on the chain ordering, the mean molecular area at 40 mN.m⁻¹ was plotted as a function of cholesterol fraction

in the mixture (Fig. 4.2). Because NMEA alone did not form a stable monolayer, it was not possible to compare the results obtained at different surface pressures. Therefore, for NMEA the molecular area determined from its crystal structure (Ramakrishnan and Swamy, 1999) was used and for all the other samples the molecular area determined at 40 mN.m^{-1} was used. Since this value is close to the collapse pressure for all the other samples, the molecules would be rather tightly packed and the molecular areas obtained at this surface pressure are expected to be a good approximation for the close packing expected in the solid state and hence using this data together with the molecular area of NMEA obtained from its crystal structure seems reasonable. The solid line in Fig. 4.2 represents ideal additivity calculated from the molecular areas of pure NMEA from the crystal structure and that of cholesterol at 40 mN.m^{-1} . Interestingly, the area/molecule for mixtures with cholesterol contents below 50 mol% is lower than that expected from ideal mixing, whereas above 50 mol% cholesterol, the average molecular area is larger than the value expected from ideal mixing (Fig. 4.2).

The above observations are quite interesting and although it is not possible to rationalize them in a definitive manner, a plausible explanation is given below. The NMEA molecules are tilted in the crystal structure due to a gauche conformation at the C4–C5 bond and if it is assumed that in the monolayer also they are tilted in pure NMEA, then the molecular area in the monolayer at collapse pressure should be comparable to that observed in the crystal. The area per molecule of 21 \AA^2 obtained from the monolayer measurements is rather close to the value of 21.95 \AA^2 determined from the crystal structure of NMEA and supports the above interpretation. Addition of cholesterol at small proportions decreases the area per molecule, despite the fact that the area per molecule for cholesterol alone is significantly higher than that of NMEA. This can be interpreted as being due to straightening of the tilted acyl chains of NMEA molecules. At the other end of the

composition range, addition of NMEA to cholesterol appears to lead to the tilting of the orientation of the cholesterol molecules resulting in an increase in the area/molecule, as compared to that of pure cholesterol. The two effects observed at either end of the composition range apparently cancel towards the middle causing a coincidental ideal area/molecule near 1:1 composition. Comparison of the theoretical area/molecule with the experimental values (taken at 40mN.m^{-1} pressure) reveals a crossover at 1:1 composition.

The change occurring at the equimolar composition is also reflected in the shape of the π -A isotherms (Fig. 4.1). As long as free NMEA is present, the isotherms show a slow rise with compression indicative of a liquid-like regime. However, once all the NMEA are in the complexed state, *i.e.* from the 1:1 composition onwards, there is a drastic change in the shape of the isotherm indicating transition to a solid condensed phase at lower areas. This suggests that NMEA interacts strongly in a 1:1 ratio with cholesterol. After the 1:1 composition the isotherms continue to behave similarly because of the higher percentage of cholesterol. These observations are consistent with previous studies using mass spectrometry, calorimetry and computational modeling, which showed that NMEA and cholesterol form a 1:1 (mol/mol) complex (Ramakrishnan et al., 2002).

4.3.2. Brewster Angle Microscopy

Brewster angle microscopy (BAM) is a technique that can be used for investigating the morphology of surfaces of thin films. It is based on the principle that when light is illuminated on the interface between two phases at the Brewster angle (53° for air-water interface), there will be no reflection, but when a thin film is introduced between the two phases, a fraction of the incident light is reflected (Hönig and Möbius, 1992). The reflected light can be captured by a device such as a CCD camera and recorded. To study monolayers formed in a Langmuir trough,

BAM pictures can be collected at different surface pressures in order to characterize the changes in the surface topography and morphology as a function of the applied pressure. Local differences in the monolayer refractive index due to differences in molecular density or packing result in differences in the brightness in BAM images (Romão and da Silva, 2004). A dark image is ascribed to a low density monolayer, as in liquid expanded (LE) phase, while a bright image is attributed to a high density of molecules at the interface e.g., a liquid condensed (LC) or a solid phase.

As the monolayer experiments showed interesting trends in the behavior of the various compositions of NMEA and cholesterol in the mixture (Fig. 4.1), we performed BAM experiments to investigate changes in the surface morphology of the monolayers formed by the mixtures as a function of the applied pressure. BAM images of NMEA at 13.5 mN.m^{-1} and cholesterol at different applied pressures are given in Fig. 4.3. The image shown in Fig. 4.3A corresponding to NMEA alone has been collected at a pressure close to its collapse pressure; however, the image shows a relatively low brightness, implying that the molecules are not closely packed. This is consistent with the results obtained from its π -A isotherm, where NMEA did not form a stable monolayer.

In contrast to NMEA, cholesterol forms a rather stable monolayer. BAM images of cholesterol shown in Fig. 4.3 (images B-G) show a clear progression from a predominantly liquid expanded phase to a solid condensed phase. Image B ($\pi = 0 \text{ mN.m}^{-1}$) contains mostly small, bright domains of LC phase in a rather dark LE background. Increasing the pressure to 0.4 mN.m^{-1} leads to the formation of larger domains of LC phase (image C). At 5 mN.m^{-1} , the domains become still larger (image D). At higher applied pressures the monolayer consists of an essentially homogenous condensed phase, with gradually increasing brightness (images E, F and G).

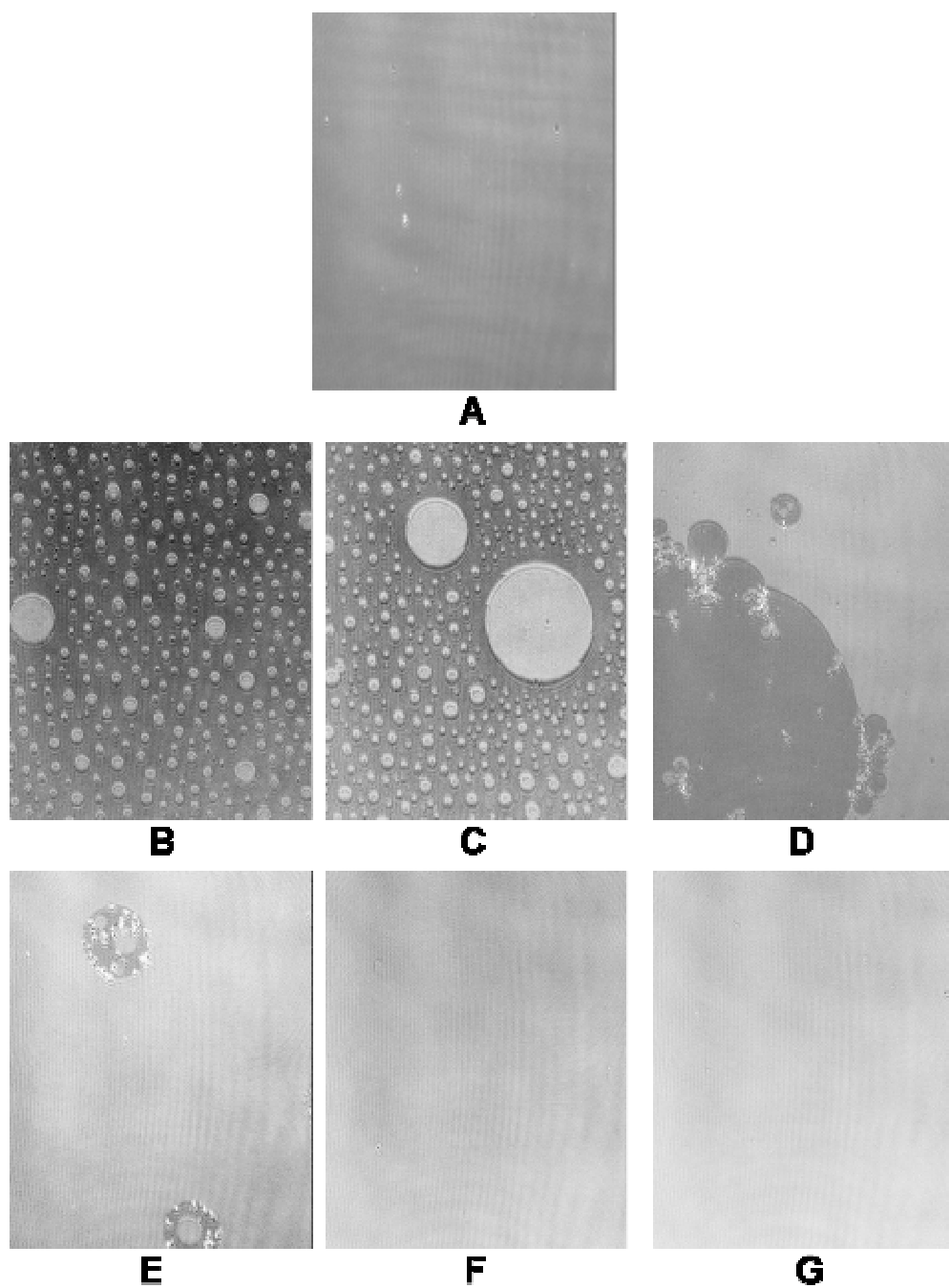


Fig. 4.3: BAM images of NMEA (A) and cholesterol (B-G). The surface pressures at which the pictures were taken are: A) 13.5, (B) 0, (C) 0.4, (D) 5, (E) 10, (F) 15, and (G) 40 $\text{mN}\cdot\text{m}^{-1}$.

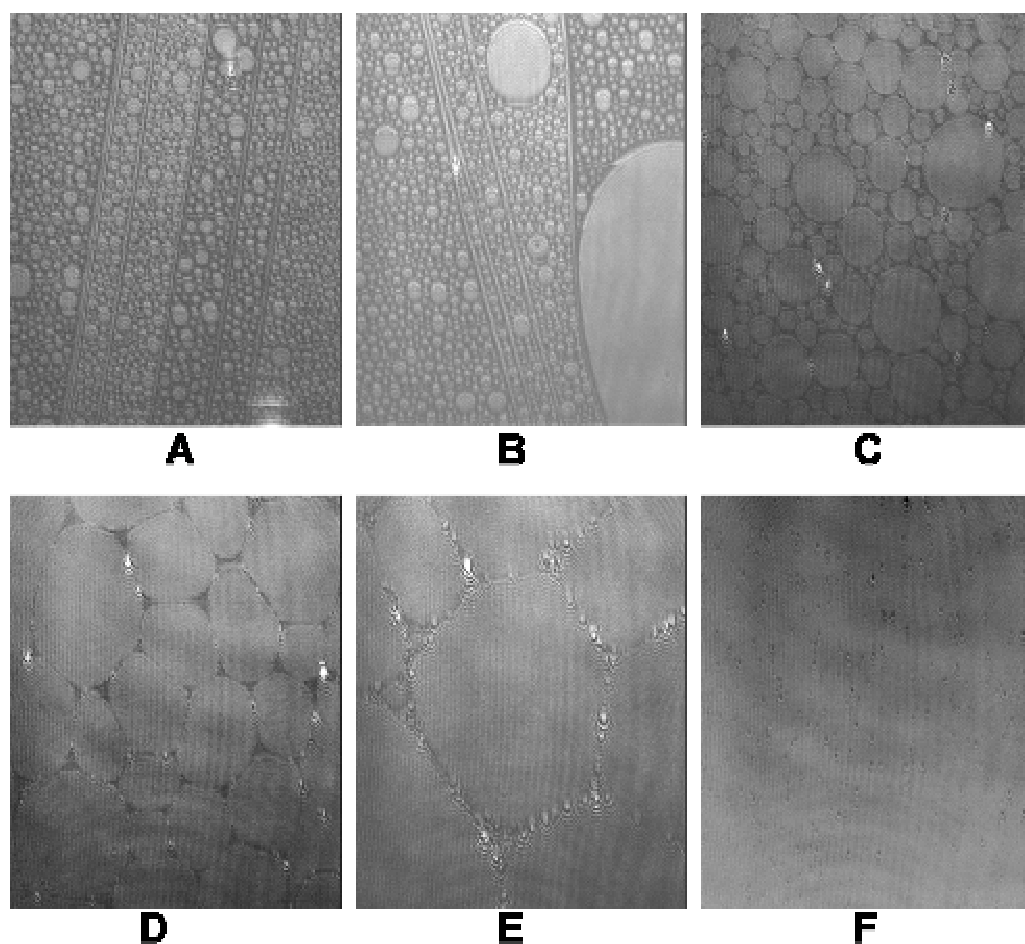


Fig. 4.4: BAM images of NMEA:Chol (7:3, mol/mol). (A) 0, (B) 1, (C) 10, (D) 15, (E) 20, and (F) 25 mN.m^{-1} .

BAM images corresponding to NMEA:Chol. (7:3, mol/mol) mixture are shown in Fig. 4.4. Even in the absence of any applied pressure (0 mN.m^{-1} , image A) the monolayer shows small domains of intermediate brightness in a continuous dark background. At 1 mN.m^{-1} some of the smaller domains coalesce resulting in the coexistence of small and large domains in a dark background (image B). Increasing the surface pressure to 10 mN.m^{-1} results in a closer packing of small and large domains (image C), while further increase to 15 and 20 mN.m^{-1} led to an increase in the average size of the domains which are rather closely packed (images

D and E). At 25 mN.m^{-1} the domains (image F) coalesce to form a nearly continuous liquid condensed phase of intermediate brightness.

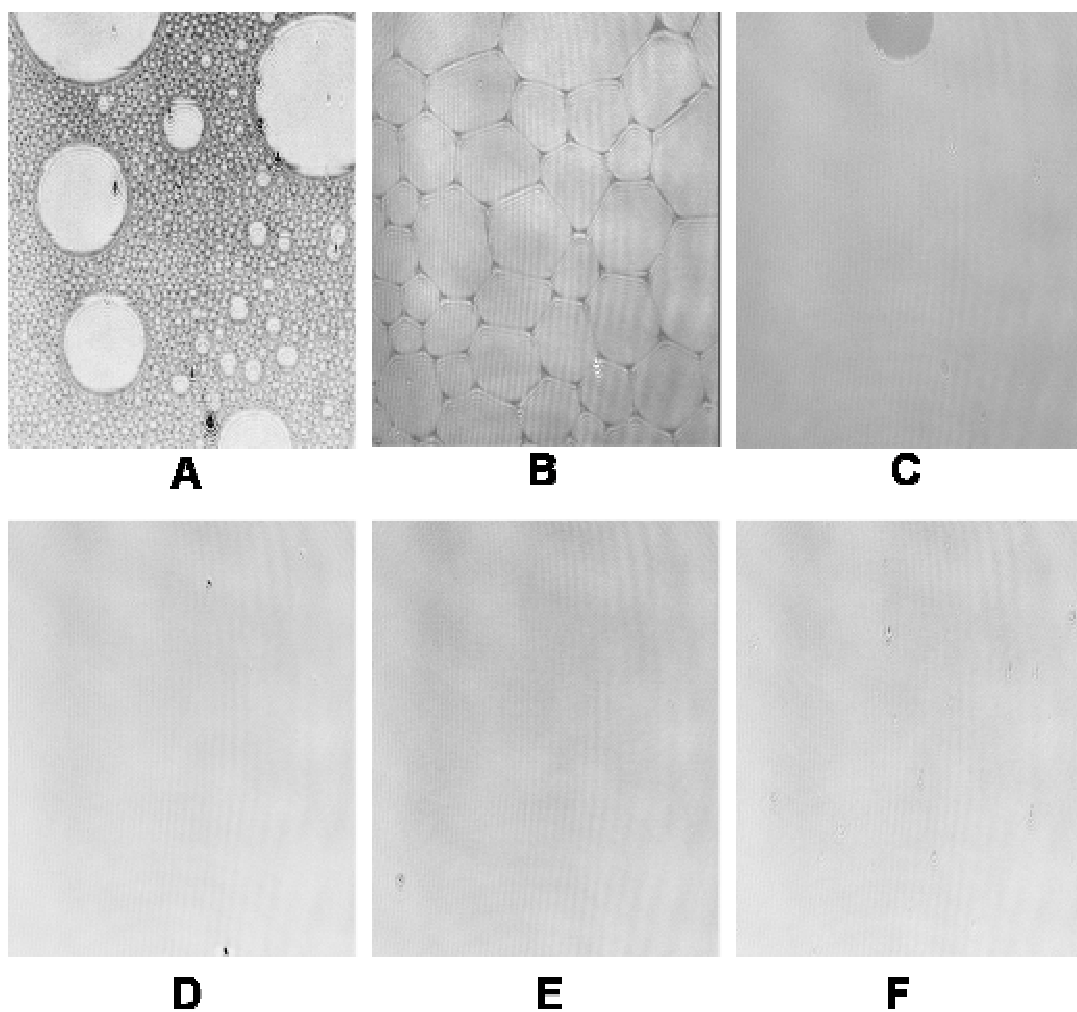


Fig. 4.5: BAM images of NMEA:Chol (1:1, mol/mol). The surface pressures at which the images were taken are: (A) 0, (B) 1, (C) 2, (D) 4, (E) 20, and (F) 39 mN.m^{-1} .

Figure 4.5 shows BAM images of monolayers formed by NMEA:Chol. (1:1, mol/mol) mixture at different applied pressures. Interestingly, even in the absence of any applied pressure, the monolayer shows several bright and relatively large

domains, in addition to smaller domains (image A). Even a small applied pressure of 1 mN.m^{-1} leads to the formation of rather tightly packed bright domains, with very little space around them. When the applied pressure is increased to 2 mN.m^{-1} , the domains coalesce to form a stable monolayer (image C), the brightness of which increases with further increase in applied pressure (images D-F).

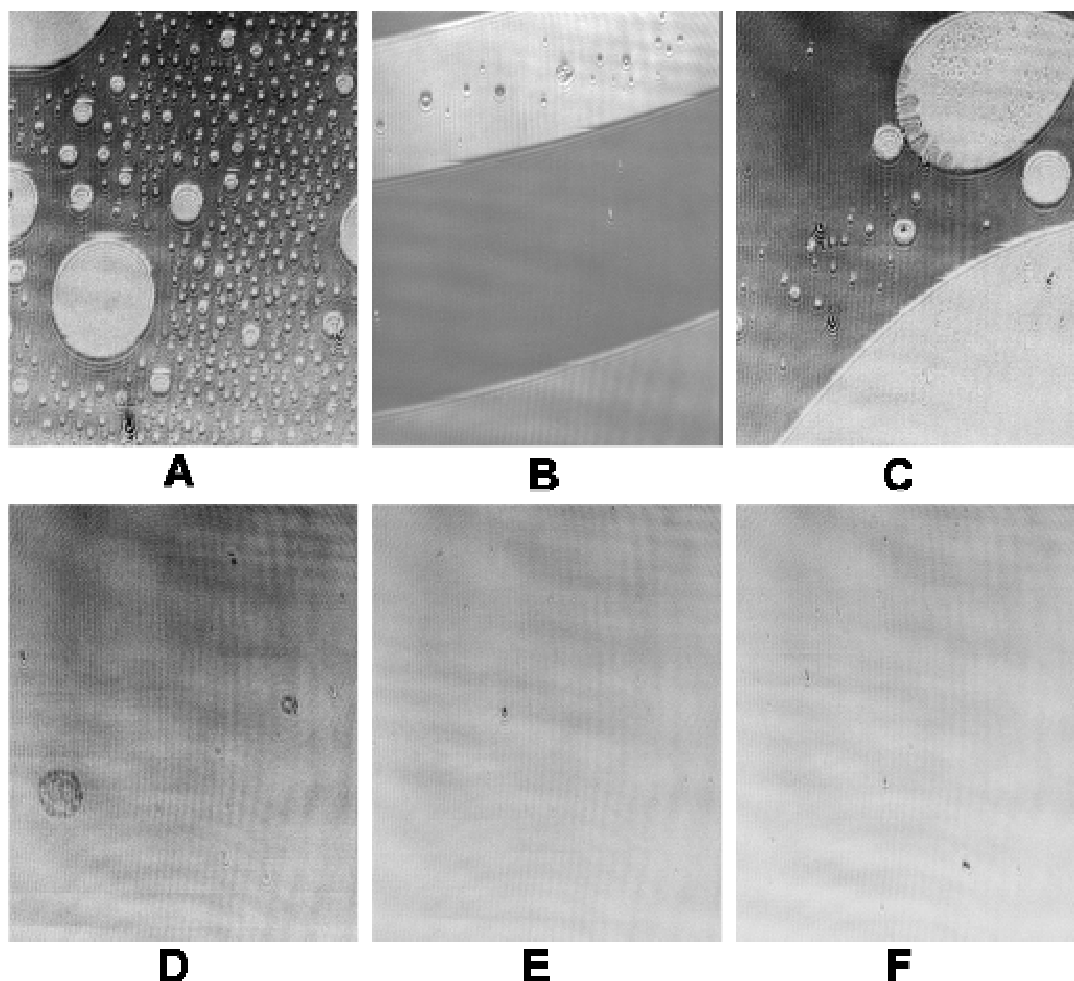


Fig. 4.6: BAM images of NMEA:Chol (3:7, mol/mol). (A) 0, (B) 1, (C) 5, (D) 10, (E) 20, and (F) 35 mN.m^{-1} .

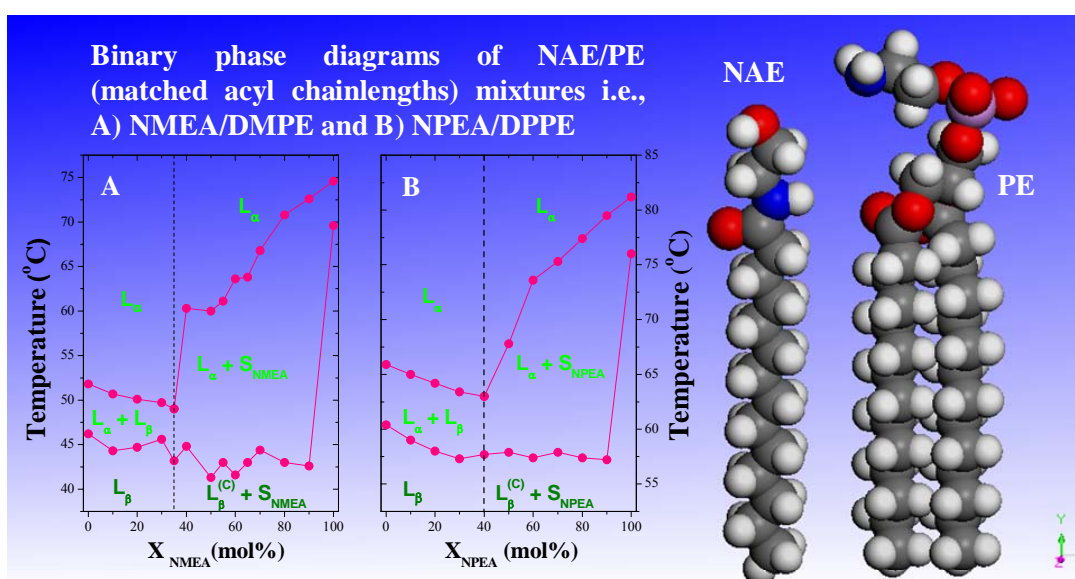
The BAM images shown in Figure 4.6 correspond to NMEA:Chol. (3:7, mol/mol) mixture where cholesterol is the excess component. At zero applied

pressure (image A) rather bright domains of different size are seen in coexistence against a dark background. Increase in the applied pressure to 5 mN.m^{-1} results in the coalescence of the domains forming larger regions of brightness against a darker background (images B and C). Further increase in pressure leads to a complete coalescence of the domains, forming a stable monolayer and its brightness increases with increasing applied pressure (images D-F), indicating the formation of a homogeneous condensed phase. However, the brightness of the homogeneous phase is significantly lower than that obtained with the NMEA:cholesterol (1:1, mol/mol) sample (see Fig. 4.5).

The above observations from Brewster angle microscopy are consistent with the formation of a 1:1 (mol/mol) complex between NMEA and cholesterol. Most interestingly, the NMEA:cholesterol (1:1, mol/mol) sample forms a homogeneous liquid condensed monolayer at a surface pressure of 1 mN.m^{-1} , whereas all other samples require considerably higher pressures (ca 10 mN.m^{-1} or higher) to form similar uniform LC phases. This shows that NMEA and cholesterol have the tendency to interact and form a 1:1 (mol/mol) complex and the heterodimers, thus formed also interact, resulting in relatively tightly packed assemblies. These results are in complete agreement with the previous observations regarding the formation of a 1:1 stoichiometric complex between NMEA and cholesterol, made from DSC, FAB-MS and computational modeling studies.

Chapter 5

Miscibility and phase behavior of *N*-acylethanolamine/diacylphosphatidylethanolamine binary mixtures of matched acyl chainlengths ($n = 14, 16$)



Miscibility and Phase Behavior of *N*-Acylethanolamine/ Diacylphosphatidylethanolamine Binary Mixtures of Matched Acyl Chainlengths ($n = 14, 16$).

Kamlekar, R.K., Satyanarayana, S., Marsh, D. and Swamy, M.J. 2006. (Communicated to *Biophys. J.*).

5.1. SUMMARY

The miscibility and phase behavior of hydrated binary mixtures of two *N*-acylethanolamines, *N*-myristoylethanolamine and *N*-palmitoylethanolamine, with the corresponding diacyl PEs, dimyristoylphosphatidylethanolamine (DMPE) and dipalmitoylphosphatidylethanolamine (DPPE), respectively, have been investigated by differential scanning calorimetry, spin-label ESR and ^{31}P -NMR spectroscopy. Temperature-composition phase diagrams for both NMEA/DMPE and NPEA/DPPE binary systems were established from high sensitivity DSC. The structures of the phases involved were determined by ^{31}P -NMR spectroscopy. For both systems, complete miscibility in the fluid and gel phases is indicated by DSC and ESR, up to 35 mol% of NMEA in DMPE and 40 mol% of NPEA in DPPE. At higher contents of the NAEs, extensive solid-fluid phase separation and solid-solid immiscibility occur depending on the temperature. Characterization of the structures of the mixtures formed with ^{31}P -NMR spectroscopy shows that up to 75 mol% of NAE, both DMPE and DPPE form lamellar structures in the gel phase as well as up to at least 65°C in the fluid phase. ESR spectra of phosphatidylcholine spin-labeled at C-5 position in the *sn*-2 acyl chain present at a probe concentration of 1 mol% exhibit strong spin-spin broadening in the low-temperature region for both systems, suggesting that the acyl chains pack very tightly and exclude the spin label. However, spectra recorded in the fluid phase do not exhibit any spin-spin broadening, and indicate complete miscibility of the two components. The miscibility of NAE and diacyl PE of matched chainlengths is significantly less than that found earlier for NPEA and dipalmitoylphosphatidylcholine, an observation that is consistent with the notion that the NAEs are most likely stored as their precursor lipids (*N*-acyl PEs) and are generated only when the system is subjected to membrane stress.

5.2. INTRODUCTION

From the Introduction and from the previous Chapters, it is clear that the content of *N*-acylethanolamines and *N*-acyl PEs increases quite dramatically in a wide variety of animals, plants and microbes under various types of stress or under disease conditions. It appears, therefore, that the increase in the levels of NAEs and NAEs may be due to a stress/disease-fighting response of the parent organisms. In addition, NAEs also exhibit a number of other interesting biological properties such as the interaction of *N*-arachidonylethanolamine (anandamide) and *N*-palmitoylethanolamine with the type-I and type-II cannabinoid receptor (CB-1), respectively, as endogenous ligands (see, for more details, Chapter 1, section 1.4.2). NAEs have also been shown to exhibit anti-inflammatory, antibacterial and antiviral properties, which may have considerable therapeutic potential (Schmid et al., 1990).

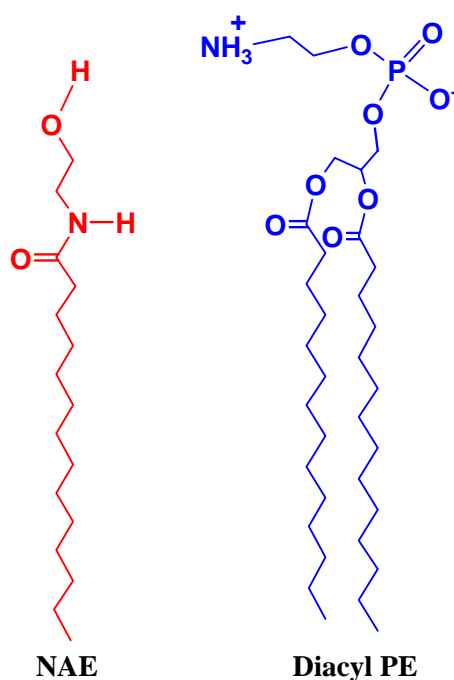


Fig. 5.1: The structures of NAE and diacyl PE. The acyl chainlength in NMEA and DMPE is 14 C-atoms, where as NPEA and DPPE contains the acyl chain in 16 C-atoms.

In view of their possible role in the stress-combating response of organisms, and potential applications in developing liposomal drug delivery systems and as therapeutic agents, it is important to investigate NAEs with respect to their metabolism, physicochemical properties (e.g., phase transitions and supramolecular structure), as well as their interaction with other membrane lipids and proteins. Metabolic studies have shown that NAEs are synthesized by hydrolysis of NAPEs by a phospholipase D-type enzyme; the NAEs thus produced are further degraded by fatty acid amidohydrolase (Schmid et al., 1996; Cravatt and Lichtman, 2003). More recent studies indicate that NAEs can also be synthesized by the sequential action of phospholipase A₂ and lysophospholipase D on NAPE (Sun et al., 2004).

While a number of studies have been carried out to characterize the accumulation of NAEs and NAPEs in various species under stress and to understand their metabolism as described above, studies aimed at understanding the phase behavior and membrane interactions of these molecules are relatively fewer. Initial studies on the interaction of several NAEs with dipalmitoylphosphatidylcholine (DPPC) multilamellar vesicles have shown that NAEs modulate the phase transition characteristics of DPPC in different ways depending on the acyl chain length and unsaturation (Ambrosini et al., 1993). In earlier work from this laboratory the chain-melting phase transitions of homologous series of these two classes of compounds were investigated by DSC and the crystal structure of NMEA has been determined (Marsh and Swamy, 2000; Ramakrishnan and Swamy, 1998, 1999; Ramakrishnan et al., 1997; Swamy et al., 1997). In Chapter 2 the crystal structures of two polymorphs of NPEA have been reported and the molecular packing and intermolecular interactions have been analyzed (See also Kamlekar and Swamy, 2006). Studies employing DSC, fast-atom-bombardment mass spectrometry and computational modeling have indicated that NMEA forms a 1:1 (mol/mol) complex with cholesterol (Ramakrishnan et al.,

2002). Studies reported in Chapter 3 show that NPEA and NSEA also form complexes with cholesterol with 1:1 (mol/mol) stoichiometry. In another study, the interaction of *N*-palmitoylethanolamine (NPEA) with DPPC was investigated by DSC, ^{31}P -NMR and small-angle X-ray scattering (Swamy et al., 2003).

In the present study, we have investigated the interaction of two NAEs, namely *N*-myristoylethanolamine and *N*-palmitoylethanolamine with diacyl phosphatidylethanolamines (PEs) of matched acyl chainlengths, i.e., with dimyristoyl (DMPE) and dipalmitoyl (DPPE) PEs (Fig. 5.1). The phase properties of binary NAE/PE mixtures were characterized at various compositions, temperature-composition phase diagrams constructed from DSC data, and the structures of the phases delineated from ^{31}P NMR spectroscopic data.

5.3. MATERIALS AND METHODS

5.3.1. Materials

1,2-dimyristoyl-*sn*-glycero-3-phosphoethanolamine (DMPE) and 1,2-dipalmitoyl-*sn*-glycero-3-phosphoethanolamine (DPPE) were purchased from Avanti Polar Lipids (Alabaster, AL, USA). Myristic acid and palmitic acid were obtained from Sigma (St. Louis, MO, USA) and oxalyl chloride was a product of Fluka (Buchs, Switzerland). Ethanolamine was obtained from Ranbaxy (Mumbai, India). All solvents were distilled and dried prior to use. The 5-PCSL phosphatidylcholine spin label bearing the nitroxide oxazolidine ring on the 5 C-atom of the *sn*-2 chain was synthesized as described in Marsh and Watts (1982).

5.3.2. Synthesis of *N*-Myristoylethanolamine and *N*-Palmitoylethanolamine

Myristic acid and palmitic acid were converted to the corresponding acid chlorides by treating with 4 mole equivalents of oxalyl chloride according to the procedure

described in Akoka et al. (1988). *N*-Myristylethanolamine and *N*-palmitylethanolamine were synthesized by the reaction of myristoyl chloride and palmitoyl chloride, respectively, with ethanolamine and the products were characterised by thin layer chromatography (TLC) and infrared spectroscopy as reported earlier (Ramakrishnan et al., 1997).

5.3.3. Sample Preparation

Samples for DSC experiments were prepared in the following way. Stock solutions of the two lipids were prepared in dichloromethane/methanol (1:1, v/v) and appropriate volumes were aliquoted into glass test tubes to yield the desired mole ratio. The lipid mixture was then vortexed thoroughly and the organic solvent was removed under a stream of dry nitrogen gas. The resulting lipid film was vacuum desiccated overnight in order to remove residual traces of the solvent. About 3 – 6 mg of the lipid was weighed and placed into 1.5 ml Hastelloy ampoules and then 500 μ L of 10 mM HEPES buffer, pH 7.4, containing 1 mM EDTA and 1 M NaCl (HBS) was added. The ampoules were then tightly sealed with screw caps and placed in the calorimeter. The reference ampoule contained an equal volume of the buffer alone.

Samples for ESR spectroscopy were prepared by co-dissolving 1 mg of the lipid and 1 mol % of the spin-label in dichloromethane/methanol (1:1, v/v) in a dry glass test tube. The solvent was then evaporated with a gentle stream of dry nitrogen gas and the residual solvent was removed by subjecting the sample to vacuum desiccation overnight. The sample was then hydrated with 100 μ L of HBS by heating it above the phase transition temperature with intermittent vortexing and finally transferred to a 100 μ L glass capillary. The hydrated lipid was pelleted by centrifuging at 10,000 rpm in a Biofuge (Heraeus), excess supernatant was removed with the aid of a drawn-out Pasteur pipette and the capillary was flame-sealed.

Samples for phosphorus-31 nuclear magnetic resonance (^{31}P -NMR) spectroscopy were prepared by codissolving 20-40 mg of the required lipid mixture (NMEA + DMPE or NPEA + DPPE) in dichloromethane/methanol (1:1, v/v). The solvent was then evaporated by blowing dry nitrogen gas gently over the sample and the final traces were completely removed by vacuum desiccation for 5-6 hours. The dry lipid was hydrated with 0.5 ml of HBS at approximately 10° above the chain-melting temperature of NMEA or NPEA for the mixtures with DMPE or DPPE, respectively, and transferred to a 5 mm-diameter NMR tube. Samples were freeze-thawed five times, then pelleted in a bench-top centrifuge, and excess buffer was removed prior to measurement.

5.3.4. Differential Scanning Calorimetry

DSC experiments were performed on a Hart Scientific 4207 heat-flow differential scanning calorimeter. Samples, prepared as described above, were subjected to heating and cooling scans at a scan rate of $10^\circ/\text{hour}$. Hydration of the lipid was achieved by first heating the samples in the calorimeter to a temperature that is above the lipid chain-melting phase transition.

5.3.5. Electron Spin Resonance Spectroscopy

ESR spectra were recorded on a 9-GHz Bruker-EMX-EPR spectrometer with model ER 041 XK-D Microwave Bridge and equipped with nitrogen gas-flow temperature regulation. Samples in 1 mm ID glass capillaries were placed in a standard quartz ESR tube containing light silicone oil for thermal stability. Temperature was measured with a fine-wire thermocouple positioned in the silicone oil just above the ESR cavity.

5.3.6. ³¹P-NMR Spectroscopy

³¹P-NMR spectra were recorded at a frequency of 162 MHz on a Bruker Avance 400 FT-NMR spectrometer. Spectra were recorded using the zgpg30 pulse program provided by Bruker with ¹H decoupling with a decoupling power of 14db. The $\pi/2$ pulse width used was 9.5 μ s for ³¹P and the recycle delay was 1 sec. About 2048 to 16384 scans were accumulated for each spectrum and the free induction decay was processed using 100 Hz of line broadening in order to improve s/n ratio. Temperature was regulated by a thermostatted air-flow system. The spectral width was set to 400 ppm.

5.4. RESULTS

The interaction of *N*-myristoylethanolamine and *N*-palmitoylethanolamine with diacylphosphatidylethanolamines of matched acyl chainlengths, namely DMPE and DPPE, has been investigated in this study by biophysical approaches. Binary temperature-composition phase diagrams have been established from the DSC thermograms and the structures of the different phases have been assigned by ³¹P-NMR spectroscopy. In addition, the lipid mixing behavior and chain dynamics have been investigated by spin-label ESR spectroscopy.

5.4.1. Differential Scanning Calorimetry

Thermograms of the heating scans of DMPE, NMEA and their mixtures of various compositions are given in Fig. 5.2 and the corresponding cooling scans are given in Fig. 5.3. Similarly, heating and cooling thermograms of DPPE, NPEA and their mixtures are given in Fig. 5.4 and Fig. 5.5, respectively. From Fig. 5.2A and Fig. 5.4A it is seen that the chain-melting endothermic transitions of DMPE and DPPE, observed at 49.4°C and 63.6°C, respectively, are consistent with literature reports

(Marsh, 1990). The chain melting phase transitions of NMEA and NPEA, seen at 72.5°C and 79.6°C, in Fig. 5.2B and Fig. 5.4B, respectively, are also consistent with the values reported in the literature (Ramakrishnan et al., 1997). Examination of the thermograms for the NMEA/DMPE and NPEA/DPPE mixtures indicates that the changes occurring in the phase transition behavior with increasing mole fraction of NAE in the diacyl PE are broadly similar for the two systems; therefore, both sets of lipid mixtures are dealt with together in the following discussion.

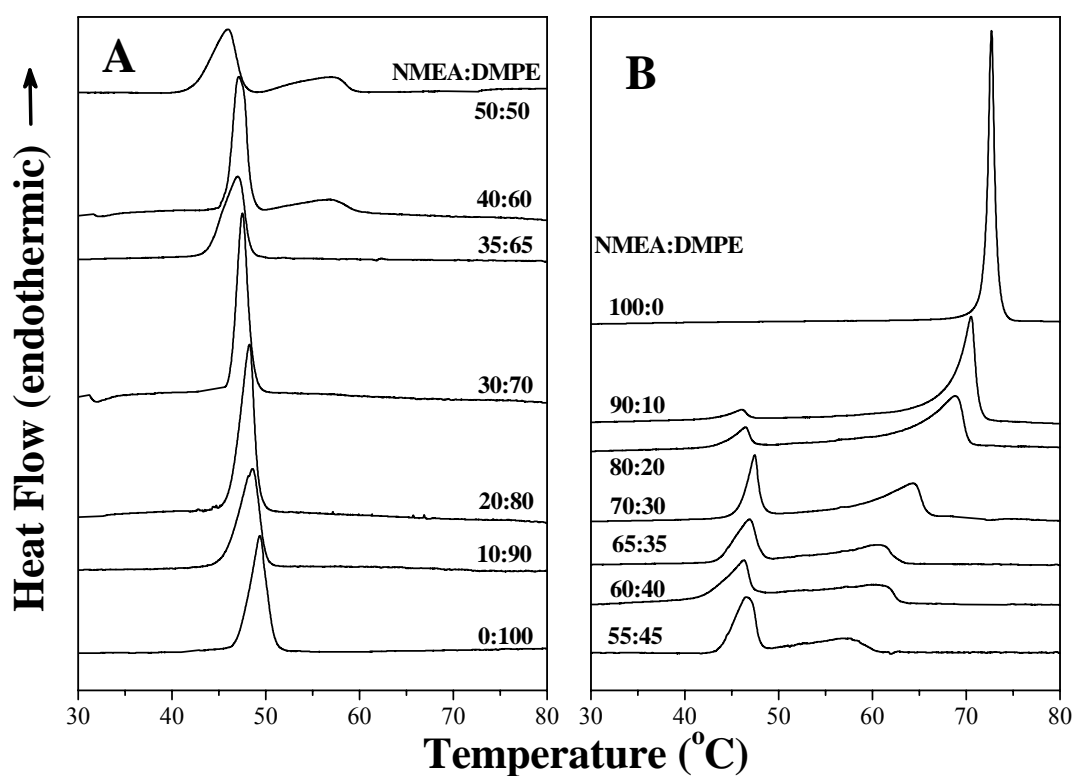


Fig. 5.2: Calorimetric heating scans of NMEA, DMPE and their mixtures of different compositions. Samples were dispersed in 10 mM Hepes buffer containing 1 M NaCl, and 1 mM EDTA, pH 7.4. Thermograms were recorded at a rate of 10°/h (Celsius scale). The molar composition (NMEA/DMPE) for each sample is indicated.

Addition of NMEA to DMPE and NPEA to DPPE at low to moderate mole fractions results in a decrease in the onset temperature of the phase transition temperature of the PE, with a sharpening of the phase transition. The thermograms

become sharper with increasing NMEA fraction up to 30 mol%, whereas the thermogram corresponding to 35 mol% NMEA is somewhat broader than that of DMPE alone. For samples containing 40 – 90 mol% NMEA, the thermograms display two peaks in heat capacity indicating phase separation. The onset temperature of the transition at up to 35 mol% NMEA is in the temperature range between 43.0 and 46.0°C, and the completion temperature of this transition decreases from 51.0°C for DMPE alone to 48.3°C for the sample containing 35 mol% NMEA.

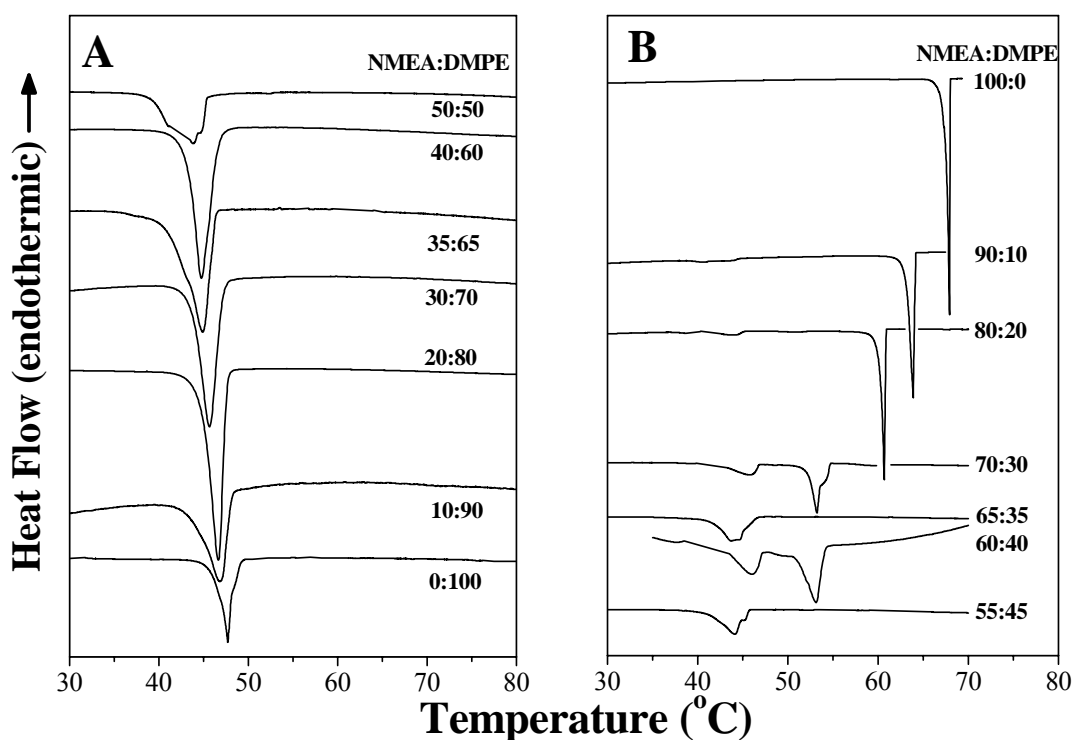


Fig. 5.3: Calorimetric cooling scans of NMEA, DMPE and their mixtures of different compositions. Samples were dispersed in 10 mM Hepes buffer containing 1 M NaCl, and 1 mM EDTA, pH 7.4. Scan rate: 10°/h (Celsius scale). The molar composition (NMEA/DMPE) for each sample is indicated.

In samples containing 40 – 90 mol% NMEA, which exhibit two heat-capacity maxima, the position of the first peak is more or less constant and the onset temperature occurs at around 43 – 46°C. However, the position of the second peak

shifts quite sharply to higher temperature with increasing NMEA content up to the mixture containing 90 mol% NMEA. The completion temperature increases in parallel from 60.3°C for the sample with 40 mol% NMEA to 72.6°C for the mixture containing 90 mol% NMEA.

Several observations can be made from an analysis of the cooling scans shown in Fig. 5.3. First, while the phase transitions corresponding to the samples with NMEA content up to 35 mol% are completely reversible with a small hysteresis, cooling thermograms corresponding to the samples containing 40 – 55 mol% NMEA exhibit a broad single exotherm, which possibly contains more than one underlying peak, with significant hysteresis (the corresponding heating transitions show two peaks). The cooling thermograms corresponding to samples with 70 – 90 mol% NMEA exhibit multiple peaks, with a major peak followed by two or three minor, overlapping peaks. These thermograms also exhibit considerable hysteresis.

The thermograms obtained for the DPPE/NPEA mixtures (shown in Fig. 5.4) are qualitatively very similar to those obtained with the DMPE/NMEA samples. The thermograms become slightly broader for the samples with 10 – 30 mol% NPEA, but the thermogram for the sample with 40 mol% NPEA becomes sharper indicating the formation of an isothermally melting complex between the two components. In addition, the onset temperature decreases steadily from 60.4°C for DPPE alone to 57.7°C for the sample with 40 mol% NPEA, which is also consistent with complex formation between NPEA and DPPE. For samples with 50 – 90 mol% NPEA, the thermograms exhibit two heat-capacity maxima, which is consistent with phase separation. The intensity of the second heat-capacity maximum increases with increasing mole fraction of NPEA, whereas the intensity of the first heat-capacity maximum decreases. Again, the onset temperature remains approximately constant on increasing the content of NPEA from 50 to 90

mol%, whereas the completion temperature increases steeply with increasing NPEA content.

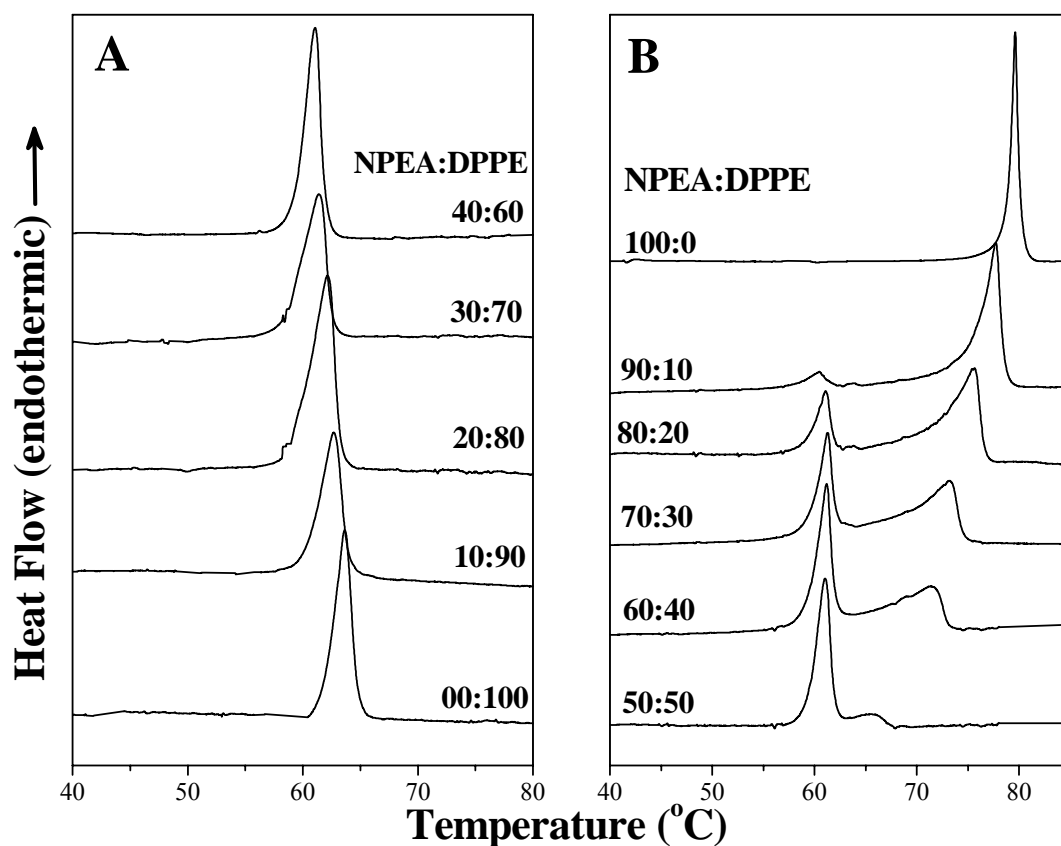


Fig. 5.4: Calorimetric heating scans of NPEA, DPPE and their mixtures of different compositions. Samples were dispersed in 10 mM Hepes buffer containing 1 M NaCl, and 1 mM EDTA, pH 7.4. Thermograms were recorded at a rate of 10°/h (Celsius scale). The molar composition (NPEA/DPPE) for each sample is indicated.

From the cooling thermograms shown in Fig. 5.5 it is seen that the chain melting of DPPE/NPEA mixtures with up to 40 mol% NPEA is essentially reversible with a small hysteresis, whereas the thermograms corresponding to 50 and 60 mol% NPEA exhibit a single peak with significant hysteresis, although the corresponding heating thermograms contain two peaks. The cooling thermograms corresponding to 70 – 90 mol% NPEA display essentially the same peaks as seen in

the corresponding heating thermograms; however, they exhibit considerable hysteresis. Part of the reason for the hysteresis could be the long time that is required to achieve compositional equilibrium between the coexisting phases in the region of lateral phase separation, when one of these two phases is solid NAE.

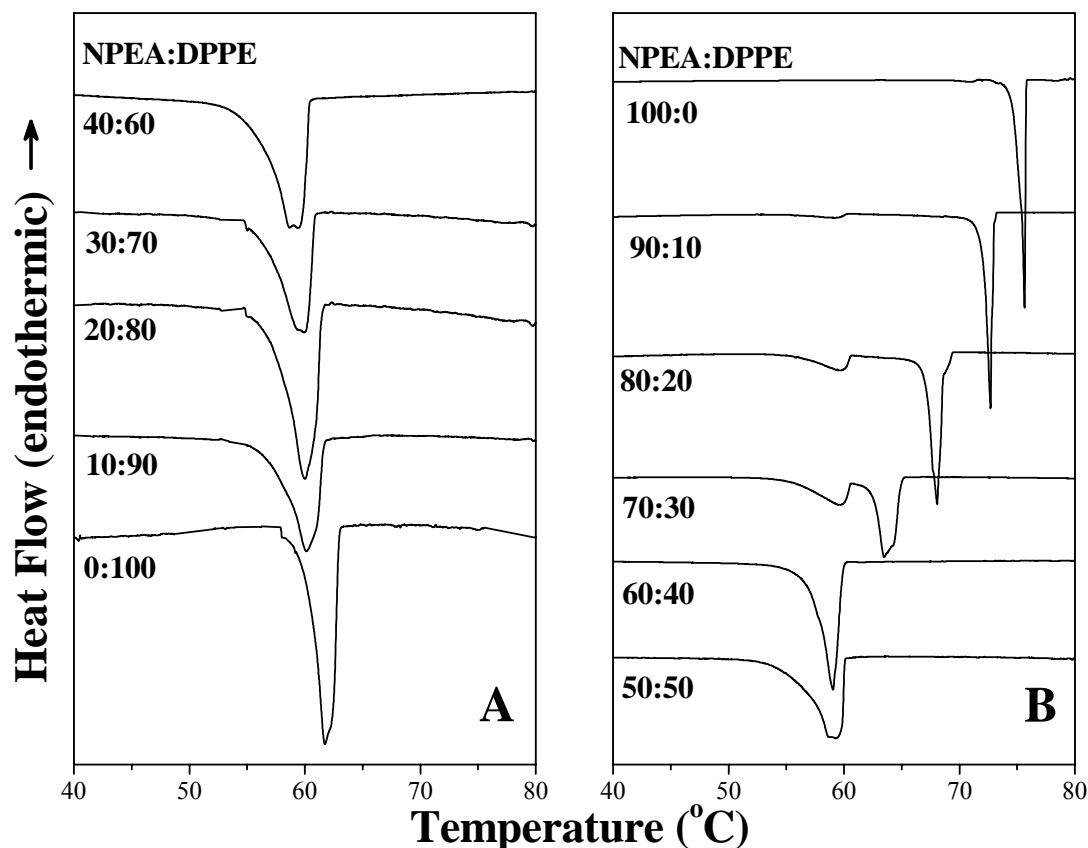


Fig. 5.5: Calorimetric cooling scans of NPEA, DPPE and their mixtures of different compositions. Samples were dispersed in 10 mM Hepes buffer containing 1 M NaCl, and 1 mM EDTA, pH 7.4. Scan rate: 10°/h (Celsius scale). The molar composition (NMEA/DMPE) for each sample is indicated.

5.4.2. Binary Phase Diagrams

Temperature-composition binary phase diagrams of the NMEA/DMPE and NPEA/DPPE mixtures, derived from the temperature boundaries of the heating thermograms shown in Fig. 5.2 and Fig. 5.4, are given in Fig. 5.6A and 5.6B,

respectively. Solid symbols indicate the onset and completion temperatures of the entire endotherm.

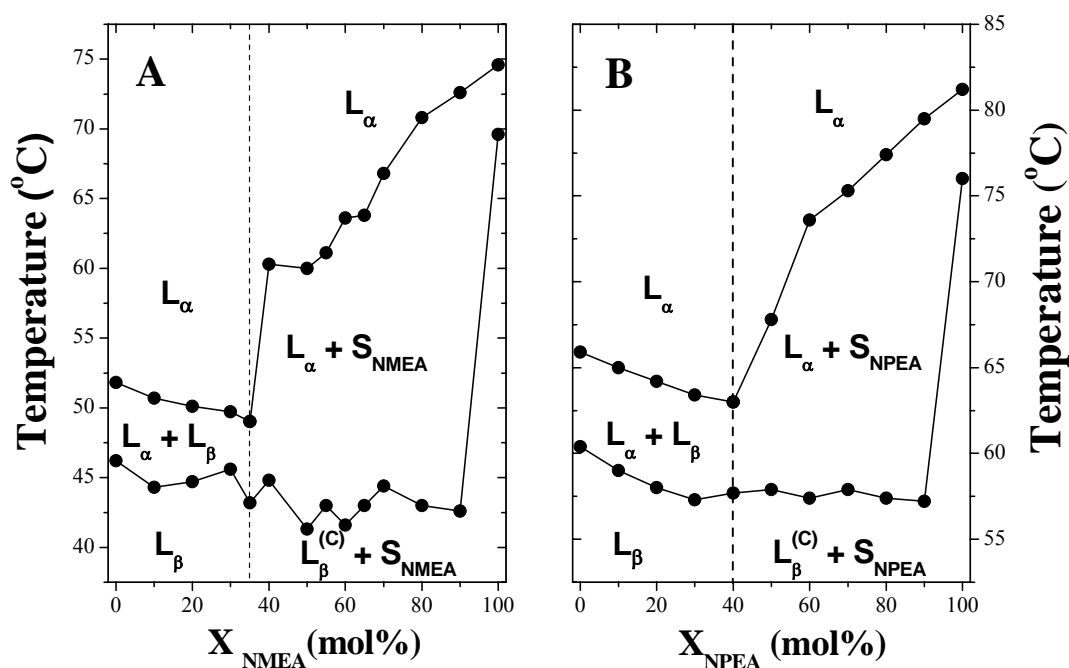


Fig. 5.6: Binary phase diagrams of A) NMEA/DMPE and B) NPEA/DPPE mixtures dispersed in 10 mM Hepes containing 1M NaCl and 1 mM EDTA, pH 7.4. The phase diagrams have been deduced from the phase boundaries established from DSC endotherms shown in Figure 5.2 (for NMEA/DMPE mixture) and Figure 5.4 (for NPEA/DPPE mixture). Phase designations are indicated: L_β and L_α are lamellar gel and fluid phases, respectively; $L_\beta^{(C)}$ is the gel phase of compound C; and S_{NMEA} and S_{NPEA} are solid NMEA and NPEA, respectively.

The overall phase diagram is rather similar in the two cases and contains two distinct regions. In the first region, which spans between 0% NAE and 35 – 40% NAE, the two components mix rather well and the corresponding thermograms contain a single, relatively sharp endothermic peak. Above 35 mol% for NMEA and above 40 mol% for NPEA, the thermograms become more complex with the appearance of a second endothermic peak, which shifts progressively to higher temperature with the increase in content of NAE. This is indicative of extensive

regions of solid-fluid phase separation. Binary phase diagrams constructed from the DSC cooling scans (not shown) are qualitatively similar to those obtained from the heating scans. Only the positions of the *solidus* and *fluidus* lines are somewhat displaced in temperature (cf. Figs. 5.2, 5.3 and 5.4, 5.5).

5.4.3. ^{31}P -NMR Spectroscopy

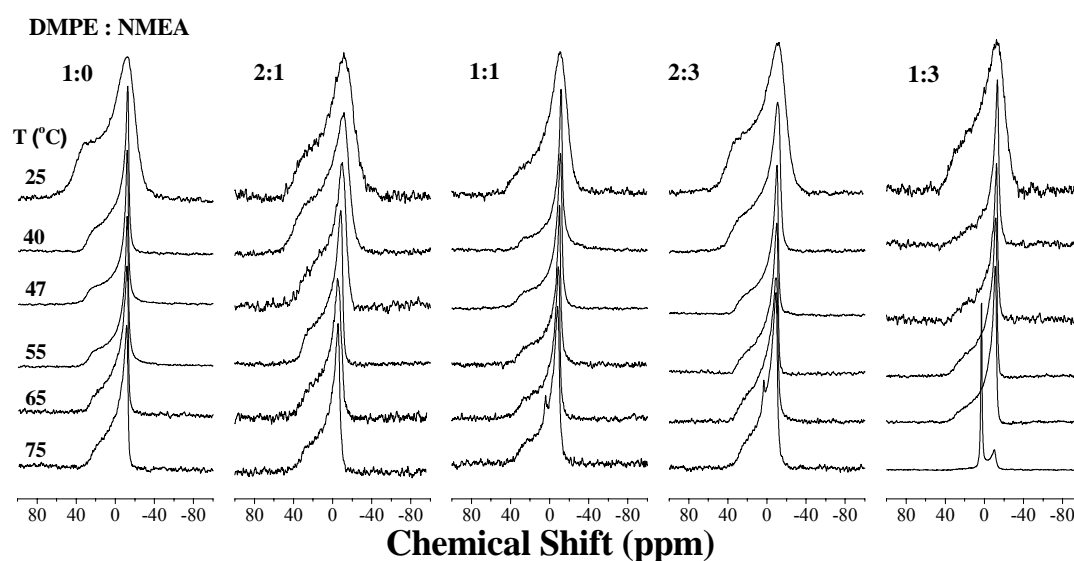


Fig. 5.7: Proton-dipolar decoupled 162 MHz ^{31}P -NMR spectra of DMPE and NMEA/DMPE binary mixtures of different compositions. Samples were hydrated with 10 mM Hepes containing 1M NaCl and 1 mM EDTA, pH 7.4. The lipid composition of the samples and the temperature at which each spectrum was recorded are indicated in the figure. Chemical shifts are referenced to external phosphoric acid.

The structures of the phases for the NMEA/DMPE and NPEA/DPPE mixtures at different compositions were investigated by broad-line ^{31}P -NMR spectroscopy. Spectra of NMEA/DMPE mixtures are shown in Fig. 5.7, and the spectra of NPEA/DPPE mixtures are shown in Fig. 5.8. For both systems, spectra were recorded in the temperature range 25 – 75°C and the chemical shift anisotropies determined from these spectra are listed in Table 5.1. The spectra shown in Fig. 5.7 correspond to DMPE alone, and to DMPE:NMEA mixtures with

mole ratios of 2:1, 1:1, 2:3 and 1:3, that is, 33.3 mol%, 50 mol%, 66.7 mol% and 75 mol% NMEA in the mixture. In the gel phase region at 25°C, the spectra of all the mixtures as well as of DMPE alone are broad, axially anisotropic powder patterns with a high-field peak and a low-field shoulder. The effective chemical shift anisotropies are found to be in the range of $\Delta\sigma = -58.7$ to -63.2 ppm and are typical of a lamellar gel phase. At 47 – 65°C, the spectra for all the samples are considerably sharper, axially anisotropic powder patterns with effective chemical shift anisotropies in the range of $\Delta\sigma = -38.7$ to -48.5 ppm, which are typical of the lamellar fluid phase. At 75°C, the highest temperature at which ^{31}P -NMR spectra were recorded, the spectra for the samples with DMPE/NMEA ratios of 1:1 and 2:3 (mol/mol) contain a small isotropic peak, whose intensity increases significantly in the sample with DMPE/NMEA mole ratio of 1:3.

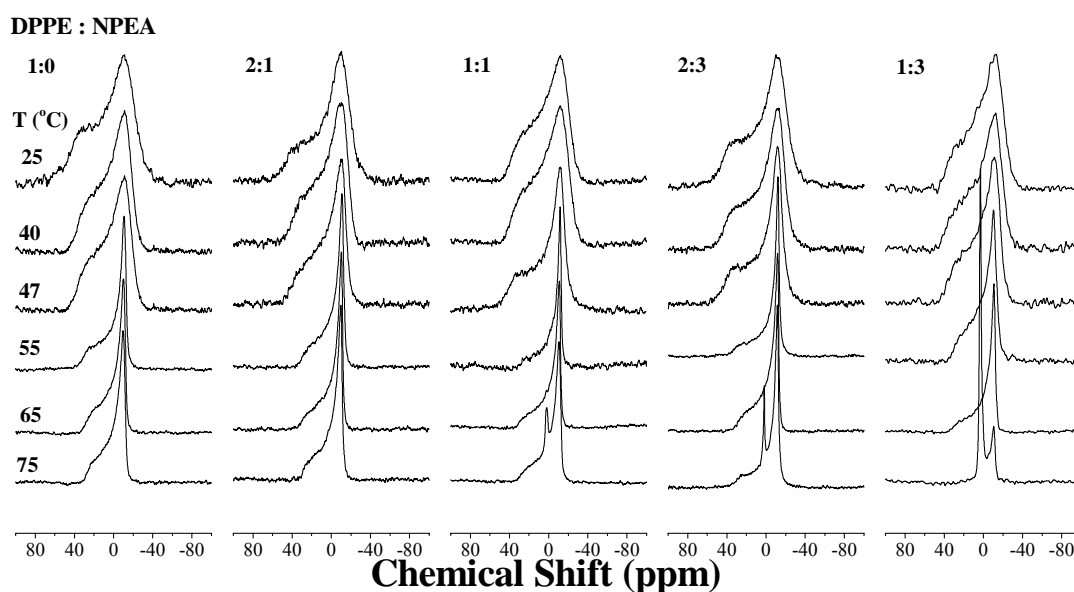


Fig. 5.8: Proton-dipolar decoupled 162 MHz ^{31}P -NMR spectra of DPPE and NPEA/DPPE binary mixtures of different compositions. Samples were hydrated with 10 mM Hepes containing 1M NaCl and 1 mM EDTA, pH 7.4. The lipid composition of the samples and the temperature at which each spectrum was recorded are indicated in the figure. Chemical shifts are referenced to external phosphoric acid.

Table 5.1: Values of effective chemical shift anisotropy (CSA), obtained from the ^{31}P -NMR spectra of hydrated samples of DMPE and DMPE/NMEA mixtures at different temperatures. Buffer: 10 mM HEPES buffer, pH 7.4, containing 1 mM EDTA and 1 M NaCl.

Diacyl PE/NAE ratio (mol/mol)	T (°C)	CSA (ppm) for	
		DMPE/NMEA	DPPE/NPEA
1:0	25	-63.8	-69.0
	40	-41.7	-56.1
	47	-42.4	-56.7
	55	-41.7	-45.5
	65	-38.7	-40.7
	75	-38.8	-38.4
2:1	25	-62.7	-66.6
	40	-58.1	-58.0
	47	-48.5	-56.2
	55	-41.4	-42.6
	65	-40.2	-41.7
	75	-40.0	-40.6
1:1	25	-59.5	-60.5
	40	-45.1	-60.4
	47	-47.1	-59.8
	55	-42.4	-40.5
	65	-42.6	-43.1
	75	-42.2	-41.5
2:3	25	-62.0	-68.6
	40	-52.2	-64.1
	47	-42.1	-61.8
	55	-41.1	-47.2
	65	-40.3	-42.2
	75	-39.9	-43.2
1:3	25	-58.7	-59.6
	40	-46.9	-59.9
	47	-44.7	-56.3
	55	-43.6	-44.5
	65	-43.1	-43.4
	75	-43.5

^{31}P -NMR spectra of DPPE/NPEA mixtures shown in Fig. 5.8 are qualitatively very similar to those of DMPE/NMEA mixtures discussed above. All the spectra recorded at 25, 40 and 47°C, which are in a temperature region corresponding to the gel phase of DPPE, are broad, axially anisotropic powder patterns with effective CSA values ranging between -56.2 to -69.0 ppm that are characteristic of a lamellar gel phase. The spectra recorded at 55 and 65°C are significantly sharper, axially anisotropic powder patterns that are consistent with a lamellar liquid crystalline phase. Interestingly, the spectra recorded at 75°C for the samples with DPPE/NPEA (mol/mol) ratios of 1:1, 2:3 and 1:3 all contain an isotropic peak. The intensity of this isotropic component is considerably higher for all three samples than it is in the DMPE/NMEA mixtures with corresponding diacyl PE/NAE ratios at 75°C.

5.4.4. Spin-Label ESR Spectroscopy

DMPE/NMEA System: The temperature dependences of the ESR spectra of 5-PCSL phosphatidylcholine spin label in DMPE, NMEA and their mixtures with DMPE/NMEA mole ratios of 80:20, 65:35, and 30:70 are shown in Fig. 5.9. The spectra recorded at temperatures below the chain-melting transition of DMPE (30 and 40°C) in DMPE alone, and in DMPE/NMEA (80:20 mol/mol), are in the slow motional regime. They contain a single component and the hyperfine splitting constants are close to those expected for rigid limit spectra. The spectra recorded close to the phase transition temperature (at 48 and 52°C) consist of two components – one component is similar to that seen at lower temperatures and the second corresponds to a lipid fraction that is more mobile and is strongly spin-spin broadened. These two components can be explained as arising from the coexistence of a large fraction of gel-phase lipid with a small fraction of liquid-crystalline lipid into which a major fraction of the spin label partitions, resulting in

strong spin-spin interaction that yields the broad component in the ESR spectrum. Spectra recorded at higher temperatures display features that are characteristic of a fluid liquid crystalline phase with partially motionally averaged, axial hyperfine anisotropy.

DMPE: NMEA

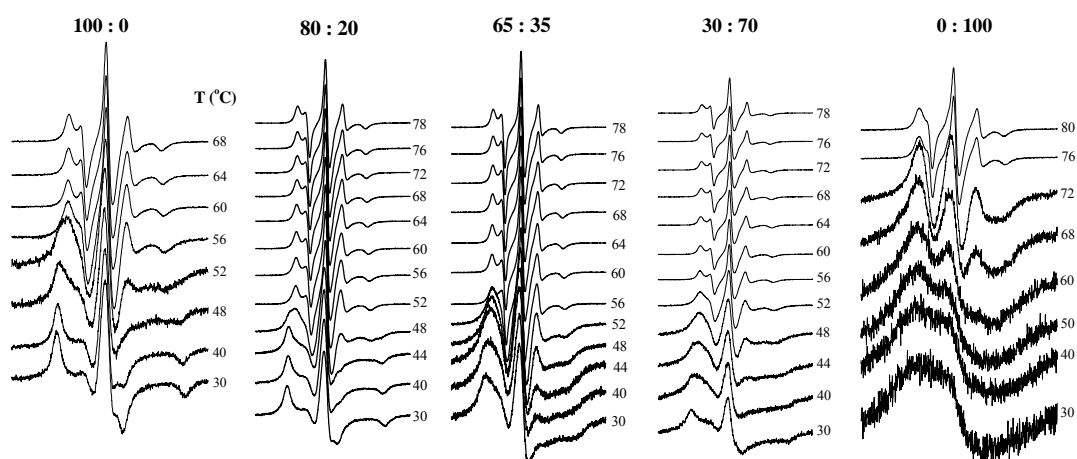


Fig. 5.9: ESR spectra of 5-PCSL spin label in DMPE, NMEA and DMPE/NMEA mixtures of the mole ratios indicated. Samples were hydrated with 10 mM Hepes containing 1 M NaCl and 1 mM EDTA, pH 7.4. The temperature at which each spectrum is recorded is indicated in the figure. Total scan width = 100 G.

In contrast to the above, ESR spectra of 5-PCSL in mixtures with DMPE/NMEA mole ratios of 65:35 and 30:70, recorded in the low-temperature region (30 and 40°C) evidence strong spin-spin broadening. Because the DSC data suggest that the 65:35 mol/mol mixture corresponds to a complex between the two components, it is likely that the solubility of the spin label in the complex is rather low, resulting in its partial exclusion from the tightly packed lipid in the gel phase. The spectra of the DMPE/NMEA (65:35 mol/mol) mixture recorded at 56°C and above are sharp, partially motionally averaged, and contain a single component. This is consistent with the fluid liquid-crystalline nature of this mixture at these temperatures. For the DMPE/NMEA (30:70 mol/mol) mixture, the ESR spectra

recorded at 56°C and above are also characteristic of the spin label in a liquid crystalline phase, although the DSC data and the phase diagram obtained from them indicate that the sample should be a mixture of solid and fluid phases at this temperature. It therefore appears that the spin label is predominantly partitioned into the fluid phase and thus seems to consist of only a single component. This is consistent with the very poor solubility of the spin label in the solid phase of NMEA alone as seen from the spectra shown in the extreme right panel of Fig. 5.9. The spectra of 5-PCSL in NMEA alone recorded at temperatures below 70°C are all highly spin-spin broadened, clearly indicating that in the crystalline phase the acyl chains of this single-chain lipid are very tightly packed. Even at 72°C, which is near the phase transition, the spectra are strongly broadened. However, above the phase transition temperature, the spectra are characteristic of a liquid crystalline phase with sharp, only partially motionally averaged, spectral lines.

Although there is considerable spin-spin broadening in the low-temperature spectra from some of the mixtures of NMEA and DMPE, the outer wings of the spectra could be analysed unambiguously to obtain the outer hyperfine splitting, $2A_{\max}$, for all mixtures, both in the gel phase and in the liquid crystalline phase with the exception of the spectra of 5-PCSL in NMEA alone in the solid phase. A plot giving the values of $2A_{\max}$ at 30°C in the gel phase (●) and at 76°C in the liquid crystalline phase (■), as a function of mole fraction, X_{NMEA} , of NMEA is given in Fig. 5.10. From this figure it is seen that the values of $2A_{\max}$ range between 63.3 and 65.3 G in the gel phase and between 44.5 and 45.5 G in the fluid phase for the different mixtures of DMPE and NMEA. The hyperfine anisotropy for DMPE alone is similar with values of $2A_{\max}$ of 65.5 and 45.7 G at 30°C and 76°C in the gel and fluid phases, respectively. These values indicate that the lipid acyl chain packing does not change much with change in the lipid composition, which suggests that the bilayer structure is preserved at compositions up to 90 mol% NMEA and that there

is good hydrophobic matching between NMEA and DMPE. For 100% NMEA, the ESR spectra at low temperature are indicative of a crystalline phase because they are almost completely spin-spin broadened, as a result of exclusion of the spin label from the very tightly packed chains of the host lipid. However, in the fluid phase of NMEA, the value of $2A_{\max}$ for 5-PCSL is 44.0 G, which is in the range expected for the liquid-crystalline phase of a bilayer membrane.

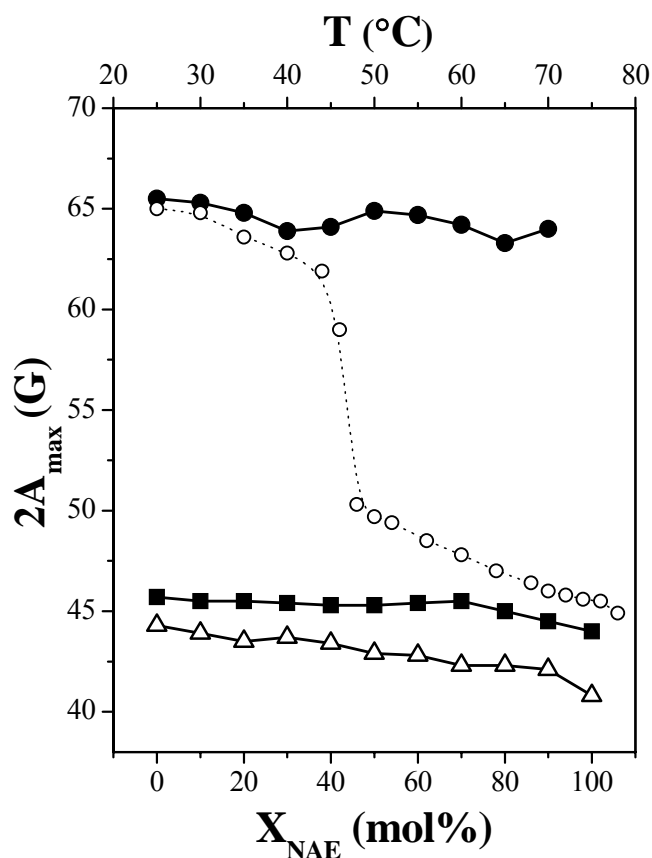


Fig. 5.10: Plot of $2A_{\max}$ vs. mole% of NAE, X_{NAE} , for the 5-PCSL spin label in various NAE/diacyl PE mixtures. The values of $2A_{\max}$ obtained for 5-PCSL in mixtures of NMEA and DMPE in the gel phase at 30°C (●) and in the liquid crystalline phase at 76°C (■) are shown along with the corresponding values obtained for 5-PCSL in mixtures of NPEA and DPPE in the liquid crystalline phase at 83°C (Δ). The curve shown as a dotted line indicates the sharp decline in the $2A_{\max}$ values during the gel-fluid phase transition of 20% NMEA in DMPE sample (upper ordinate).

DPPE/NPEA System: The ESR spectra of 5-PCSL in pure DPPE and in pure NPEA are very strongly spin-spin broadened in the low-temperature region (Fig. 5.11), suggesting that the spin label is strongly excluded from the tightly packed lipid chains in the gel or crystalline phase. Although somewhat less pronounced, in the three mixtures with DMPE/NPEA molar ratios of 80:20, 60:40 and 30:70, the spectra in the region below ca. 60°C are all strongly spin-spin broadened, suggesting that the lipid acyl chains are rather tightly packed in the low-temperature phase, resulting in an exclusion of the spin labeled probe (Fig. 5.11). Above the phase transition temperature of pure DPPE, the spectra become sharper and are composed of a single component. The liquid crystalline phase in all the mixtures appears to be homogeneous because the spin-labeled probe reports a single, anisotropically averaged, axial component.

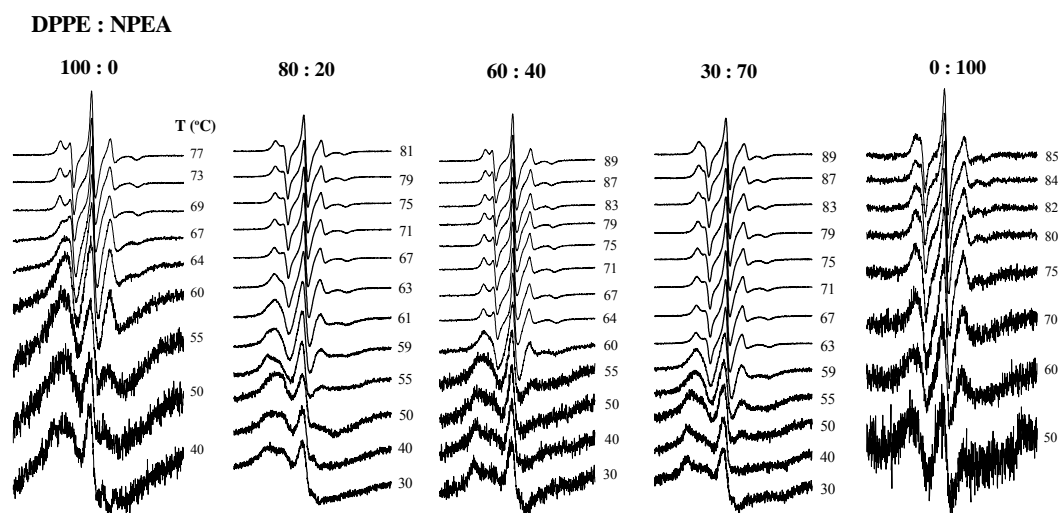


Fig. 5.11: ESR spectra of 5-PCSL spin label in DPPE, NPEA and DPPE/NPEA mixtures of the mole ratios indicated. Samples were hydrated with 10 mM Hepes containing 1 M NaCl and 1 mM EDTA, pH 7.4. The temperature at which each spectrum is recorded is indicated in the figure. Total scan width = 100 G.

The strong spin-spin broadening in the ESR spectra in the low-temperature region precludes analysis of the spectra to obtain values of $2A_{\max}$ for most of the

samples. However, the values of $2A_{\max}$ could be determined for all the mixtures of NPEA and DPPE in the fluid phase and these were found to range between 42.1 and 43.9 G at 83°C for the different mixtures with NPEA mole fractions ranging between 0.1 and 0.9. The value of $2A_{\max}$ for 5-PCSL in DPPE alone is similar at 44.3 G. These values for DPPE/NPEA mixtures in the fluid phase are also shown in Fig. 5.10 (Δ). Again, the relatively constant values of $2A_{\max}$ suggest preservation of the bilayer structure and good hydrophobic matching between the two lipid components.

5.5. DISCUSSION

In view of the potential role of NAEs in combating membrane stress, it is of interest to investigate the interaction of various NAEs with other membrane components, especially with the major membrane lipids such as phosphatidylcholine, phosphatidylethanolamine and cholesterol. The mixing behavior of NMEA with cholesterol and that of NPEA with dipalmitoylphosphatidylcholine have been investigated in earlier studies (Ramakrishnan et al., 2002; Swamy et al., 2003). In the present study we report DSC, spin-label ESR and ^{31}P -NMR studies on the interaction of NMEA with DMPE and of NPEA with DPPE. The structures of the various phases of the hydrated mixtures for the two systems are discussed first. This is followed by a discussion of the phase diagrams and phase coexistence. Then the biological/functional implications of the mixing properties of NAEs with other membrane lipids are considered.

5.5.1. Structures of Phases and Lipid Miscibility

The structures of the phases have been examined by ^{31}P -NMR spectroscopy, which can distinguish between various types of structures formed by phospholipids (viz., DMPE and DPPE in the mixtures investigated here) but cannot provide direct

information on the structures formed by other non-phosphorus-containing lipids (NMEA and NPEA here). However, if the phase structure of the diacyl PEs is affected by the NAEs, this can be detected by this technique. The ^{31}P -NMR spectra of NMEA/DMPE and NPEA/DPPE mixtures shown in Fig. 5.9 and Fig. 5.11 suggest that in the gel-phase region all the samples examined are in a lamellar state. For both systems, the spectra recorded up to 65°C are also characteristic of a lamellar phase, indicating that the diacyl PEs exist in a bilayer structure up to this temperature. The spectra recorded at 75°C for mixtures of NMEA and DMPE with mole compositions of 1:1 and 2:3 contain a small isotropic component, which increases significantly in the spectrum of the DMPE/NMEA (1:3 mol/mol) sample. This isotropic component may be attributed to the formation of small vesicles, or possibly even of a fluid non-lamellar (cubic) structure. In the DPPE/NPEA system, lamellar structure is also seen for all samples at temperatures up to 65°C, and at 75°C there is a distinct isotropic ^{31}P -NMR component for the samples with DPPE/NPEA mole ratios of 1:1, 2:3 and 1:3. Interestingly, the isotropic content in the samples with DPPE/NPEA mole ratios of 1:1 and 2:3 is relatively larger than in the corresponding samples in the DMPE/NMEA system. Also, the magnitude of the isotropic component increases with increasing NPEA content. These observations are consistent with a model in which the phase structure of the diacyl PE is affected by the NAE at high mole fractions and leads to the formation of highly curved vesicles or a non-lamellar structure. According to the phase diagram presented in Fig. 5.6B (or the equivalent constructed from DSC cooling scans), the sample with DPPE/NPEA 1:3 mole ratio would be in a region of solid-fluid phase separation at 75°C. Under these conditions, coexistence of two fluid phases (i.e., lamellar and non-lamellar) in addition to the solid phase would be forbidden by the Gibbs Phase Rule. Further studies have to be carried out to investigate this aspect in greater detail.

5.5.2. Binary Phase Diagram and Phase Coexistence

The phase diagrams of the two binary systems investigated here, namely those of DMPE/NMEA and DPPE/NPEA, constructed from the DSC *solidus* and *liquidus* data, can be divided broadly into two regions. In the first region, which corresponds to mole fractions up to $X_{\text{NMEA}} = 0.35$ (and $X_{\text{NPEA}} = 0.4$), the phase diagram is of the isomorphous type and the diacyl PE and NAE mix well in both gel and fluid phases. The ^{31}P -NMR results discussed above are fully consistent with this model. At the above stoichiometries the two components form a complex, C, which melts at a lower temperature than the PE component alone. In the low-temperature region, the uncomplexed PE and complex mix well in a uniform gel phase, L_β , and correspondingly form a uniform fluid phase, L_α , in the high-temperature region. In the intermediate chain-melting region, fluid and gel phases coexist, $L_\alpha + L_\beta$.

The second region spans from 35 to 100 mol% NMEA in mixture with DMPE (or 40 to 100 mol% NPEA in mixture with DPPE). In this region, the phase diagram is characteristic of solid phase immiscibility, with a horizontal *solidus* at the melting temperature of the compound C. Below this temperature the compound in the gel-phase, $L_\beta^{(\text{C})}$ coexists with solid NAE, S_{NAE} . Above the *solidus*, there is an extended region, $L_\alpha + S_{\text{NAE}}$, over which a fluid lamellar lipid phase coexists with solid NAE. Above the *fluidus* line, the system is in a liquid crystalline phase at all compositions and is predominantly lamellar, although some non-lamellar cubic phase cannot entirely be excluded on the basis of the ^{31}P -NMR results.

It is pertinent here to compare the two phase diagrams obtained in this study for the interaction of NMEA and NPEA with diacyl PEs of matched chainlengths with the phase diagrams obtained in earlier studies for the interaction of NPEA with DPPC (Swamy et al., 2003), and for the interaction of *N*-myristoyldimyristoyl-

phosphatidylethanolamine (*N*-14 DMPE) with dimyristoylphosphatidylcholine (DMPC) (Ramakrishnan et al., 2001). Whereas NMEA and NPEA mix well with diacyl PEs of matched chainlengths only up to 35-40 mol% in the gel phase, *N*-14 DMPE was found to mix well with DMPC over the entire composition range in both gel and fluid phases. The binary phase diagram of NPEA with DPPC resembles more closely that of the NAE/PE systems. Gel-phase miscibility extends to 60 mol% of NPEA in DPPC, corresponding to the formation of an isothermally melting compound with a higher proportion of NPEA than that which is formed with DPPE. At higher contents of NPEA, the low-temperature behavior of NPEA/DPPC mixtures is complicated by the presence of one or more metastable polymorphs that are absent in the NAE/PE systems. Nonetheless, solid-solid immiscibility is indicated with uncomplexed solid NPEA, as in the NPEA/DPPE system. In view of the lower phase transition temperatures of NAEs as compared with the NAEs of equivalent acyl chainlengths, it appears that the NAEs are the more compatible with the phospholipids present in fluid biological membranes.

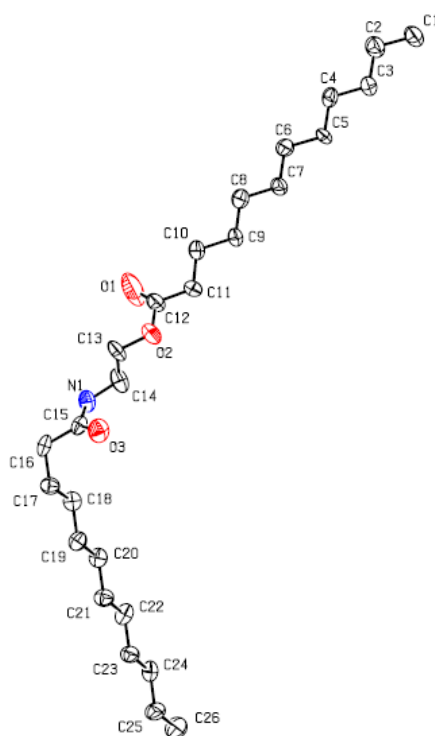
5.5.3. Biological Implications

The two NAEs investigated in this study, namely NMEA and NPEA, exhibit good miscibility with phosphatidylethanolamines of equivalent acyl chainlength at contents up to only 35-40 mol%. This is considerably lower than the miscibility of NPEA and DPPC, which were found to mix well at contents up to 60 mol% of the former (Swamy et al., 2003). It is interesting to note that although the phase transition temperatures of the diacyl PEs are closer to those of the NAEs of corresponding chainlengths, the miscibility of the NAE/diacyl PE systems is less extensive than that of the NAE/diacyl PC system. Overall, these results indicate that the NAEs do not exhibit complete miscibility with either of the two major phospholipids of eukaryotic cell plasma membranes, namely phosphatidylcholine

and phosphatidylethanolamine. Consequently, it appears that the NAEs may be stored in the biological membranes as their precursor lipids, namely NAPEs, which are mobilized when necessary, i.e., when subjected to membrane stress (cf. Ramakrishnan et al., 2001).

Chapter 6

Synthesis, Characterization and Differential Scanning Calorimetry of *N*-, *O*-Diacylethanamines of Matched Acyl Chainlengths ($n = 10$ -20) and Crystal Structure of *N*-, *O*-Dilauroylethanolamine



Synthesis and Characterization of *N*-, *O*-Diacylethanamines of Matched Acyl Chainlengths ($n = 10$ -20) and Crystal Structure and Molecular Packing of *N*-, *O*-Dilauroylethanolamine.
Kamlekar, R.K., Tarafdar, P.K. and Swamy, M.J. 2006. (Manuscript under preparation).

6.1. SUMMARY

Ethanolamine is a key building block in a variety of important membrane lipids and it was recently suggested that *N-, O*-diacylethanolamines (DAEs) may be present in living systems, generating considerable interest in investigating the properties of DAEs. In this study a homologous series of DAEs with matched even and odd acyl chains ($n = 10 - 20$) have been synthesized and characterized. The molecular conformation, packing properties and intermolecular interactions of a representative of this family, namely *N-, O*-dilauroylethanolamine (DLEA), have been determined by single-crystal X-ray diffraction analysis. DLEA crystallized in the orthorhombic space group Pbc_{21} with unit cell dimensions: $a = 4.8756(4)$, $b = 8.7865(8)$, $c = 60.3(5)$ Å with four symmetry related molecules in each unit cell. The DLEA molecules adopt a bent, L-shaped structure in which the conformation of the *N*-acyl chain and the central ethanolamine moiety are essentially identical to that found in the structures of different *N*-acylethanolamines such as NMEA, NPEA and NSEA (discussed in Chapter 2), whereas the *O*-acyl chain is essentially linear with all-*trans* conformation in the hydrocarbon chain region. The molecules are organized in a bilayer-like fashion wherein the *N*-acyl chains from one layer oppose the *O*-acyl chains of the next layer. The *N*- and *O*-acyl chains are tilted by 36.5° and 34.5° , respectively, with respect to the normal to the bilayer plane. The molecular packing is stabilized by hydrogen bonds, with each amide carbonyl forming a strong $N-H\cdots O$ bond with the amide $N-H$ moiety of an adjacent molecule, and a $C-H\cdots O$ hydrogen bond with a neighboring molecule, besides a $C-H\cdots O$ hydrogen bond between the ester carbonyl with the $C-H$ groups of an adjacent molecule. In DSC studies each DAE gave a sharp endothermic phase transition, which coincided with its capillary melting point, indicating that the phase transition corresponds to chain-melting. The transition enthalpies (ΔH_t) and entropies (ΔS_t) obtained from

DSC for DAEs with even and odd acyl chains independently exhibited linear dependence on the chainlength, indicating that ΔH_t and ΔS_t consist of a fixed component from the terminal methyl groups and the central polar region and a varying component contributed by the two polymethylene chains $[(CH_2)_n]$ belonging to the *N*- and *O*-acyl chains, that is linearly dependent on the number of methylene units in the chains (n). Linear least squares analyses yielded incremental values contributed by each methylene group to the transition enthalpy (ΔH_{inc}) and entropy (ΔS_{inc}) as $2.552 (\pm 0.058)$ kcal.mol⁻¹ and $6.551 (\pm 0.157)$ cal.mol⁻¹.K⁻¹ and the end contributions as $\Delta H_o = -9.283 (\pm 0.782)$ kcal.mol⁻¹ and $\Delta S_o = -19.125 (\pm 2.112)$ cal.mol⁻¹.K⁻¹ for the even chainlength series and $\Delta H_{inc} = 2.319 (\pm 0.107)$ kcal.mol⁻¹, $\Delta S_{inc} = 5.955 (\pm 0.295)$ cal.mol⁻¹.K⁻¹, $\Delta H_o = -9.003 (\pm 1.429)$ kcal.mol⁻¹ and $\Delta S_o = -18.557 (\pm 3.924)$ cal.mol⁻¹.K⁻¹ for the odd chainlength series. These results provide a structural and thermodynamic basis for understanding the phase properties of DAEs in lipid membranes.

6.2. INTRODUCTION

Ethanolamine is a central building block in a number of important membrane phospholipids and other amphiphiles. Diacyl phosphatidylethanolamine, dialkyl phosphatidylethanolamine, phosphatidylethanolamine plasmalogen and *N*-acyl phosphatidylethanolamine (NAPE) are some of the membrane lipids that contain ethanolamine. In addition, choline – which is derived from ethanolamine – is present in phosphatidylcholine, sphingomyelin and platelet activating factor (PAF). Besides these membrane phospholipids, ethanolamine is also a building block of *N*-acylethanolamines (NAEs), which are present in wide variety of organisms and whose content increases in the parent organisms when they are subjected to

different types of stress, suggesting that they may be part of stress-fighting responses of the parent organisms (Schmid et al., 1990; Chapman, 2004).

Among the phospholipids containing the ethanolamine moiety, NAEs are probably the most recently discovered, whereas NAEs are derived from NAEs by the action of a phospholipase D-type enzyme (Schmid et al., 1990; Chapman, 2004). Because of this and in view of their putative roles in combating stress and signaling events in animals and plants (Schmid et al., 1996; Chapman, 2004), we as well as other groups have studied the biophysical properties of NAEs and NAEs and investigated their interaction with other membrane lipids (cf. Akoka et al., 1988; LaFrance et al., 1990; Swamy et al., 1997, 2000; Li et al., 2002). These studies have shown that in NAEs where the *N*-acyl chain is long (≥ 10 C-atoms) it folds back and inserts into the hydrophobic core of the membrane and lies parallel to the *O*-acyl chains and is roughly at the same vertical location as the *sn*-2 acyl chain, whereas in NAEs with short *N*-acyl chains (≤ 6 C-atoms), the *N*-acyl chain remains in the aqueous interface region. Consistent with this, cholesterol exhibits a classic 'condensing effect' on the acyl chains of NAEs, including the *N*-acyl chain (Swamy et al., 2000; Li et al., 2002).

In addition to their putative role in combating stress, NAEs also exhibit interesting biological and medicinal properties (see Chapter 1, section 1.4.2), which provided a strong impetus for investigations on the 3-dimensional structure and biophysical properties of NAEs and their interaction with other membrane lipids. Such studies revealed that NAEs form 1:1 complexes with cholesterol and modulate the phase properties of membrane phospholipids such as phosphatidylcholine and ethanolamine and stabilize bilayer structure by inhibiting the formation of inverted hexagonal phase (Ramakrishnan and Swamy, 1999; Marsh and Swamy, 2000; Kamlekar and Swamy, 2006; Ambrosini et al., 1993; Ramakrishnan et al., 2002; Swamy et al., 2003).

Besides *N*-acylation, amphiphiles can also be produced by the *O*-acylation of ethanolamine with a long acyl chain. Recently it has been shown that *O*-acylethanolamines (OAEs) are converted to *N*-acylethanolamines in a facile manner under mildly basic conditions, whereas the reverse reaction, catalyzed by acid is less facile and requires sonication (Markey et al., 2000). These studies suggested that OAEs are likely to be present in biological membranes and might not have been detected so far due to their conversion to NAEs under conditions employed in the extraction, purification or detection (e.g., tlc using solvents containing ammonia). Interestingly, subsequent studies have led to the detection and identification of *O*-arachidonylethanolamine (virodhamine), which is an isomer of anandamide, in mammalian brain and hippocampus (Porter et al., 2002). Virodhamine has been shown to act as an antagonist of the type 1 cannabinoid receptor, CB-1. It has also been reported that rat heart cell-free preparations can catalyze *O*-acylation of NAEs in the presence of fatty acid and acyl-CoA-generating cofactors to produce *N*-, *O*-diacylethanolamines (Schmid et al., 1990). In another study it was shown that lipases can catalyze *O*-acylation of *N*-acylethanolamines (Furutani et al., 1997). These observations point to the possibility that although their presence in biological membranes is not established yet, *N*-, *O*-diacylethanolamines (DAEs) may be present in biological membranes as minor constituents.

In the light of the foregoing, it was considered interesting to characterize the physico-chemical properties of DAEs and to investigate their interaction with membrane lipids. In the present study we report the synthesis of a homologous series of DAEs of matched acyl chainlengths and their characterization by IR and NMR spectroscopy. In addition, the 3-dimensional structure of *N*-, *O*-dilauroylethanolamine (DLEA) has been investigated by single-crystal X-ray diffraction and the molecular packing and intermolecular interactions in the crystal

lattice have been analyzed. Finally, the thermotropic phase transitions of a homologous series of DAEs with matched *N*- and *O*-acyl chainlengths have been characterized by differential scanning calorimetry.

6.3. MATERIALS AND METHODS

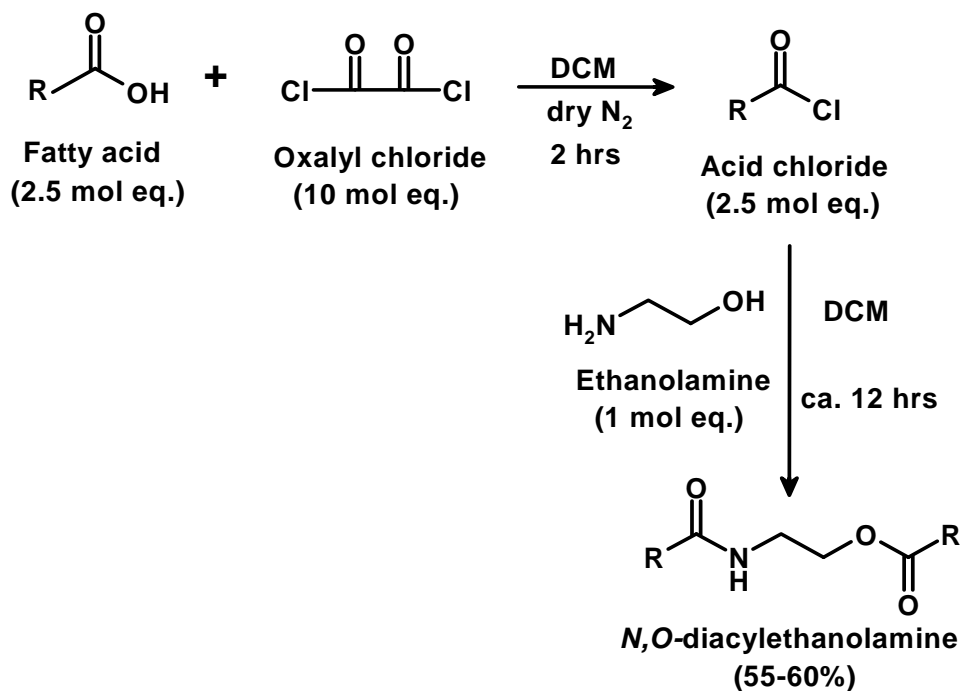
6.3.1. *Materials*

Long chain fatty acids, $\text{CH}_3-(\text{CH}_2)_n-\text{COOH}$, of even and odd chain lengths ($n = 8-18$) were purchased from Aldrich (USA). Oxalyl chloride was obtained from Fluka (Buchs, Switzerland). Ethanolamine and other solvents were purchased locally.

6.3.2. *Synthesis of N, O-Diacylethanolamines*

DAEs of matched acyl chains were synthesized by the reaction of acid chlorides with 2-ethanolamine. For this, long-chain fatty acids were converted into the corresponding acid chlorides by treating with 4 mole equivalents of oxalyl chloride at room temperature for 2 hours under nitrogen atmosphere (Akoka et al., 1988). After completion of the reaction, the excess oxalyl chloride was removed under a stream of dry nitrogen gas. DAEs were synthesized by the drop-wise addition of about 2.5 mole equivalents of the acid chloride in dichloromethane to a solution of 1 mole equivalent of freshly distilled 2-ethanolamine in dichloromethane in an ice-bath, under constant stirring. After all the reagent was added, the reaction was allowed to continue overnight. The reaction mixture was then washed twice with double distilled water and extracted with ether and then the organic solvent was evaporated under a stream of dry nitrogen gas. The crude products were purified by column chromatography on silica gel. Elution was done by using increasing concentration of ethyl acetate in *n*-hexane. The product obtained was concentrated and was dissolved in a small amount of dichloromethane, and about 10 volume of

acetone was added to it and the solution was kept in a freezer (ca. -20°C) overnight. This led to the precipitation of the DAEs, which were recovered by filtration. Yields ranged between 55-60%. The purified products were characterized by IR and ^1H -NMR spectroscopy.



Scheme 6.1: Synthesis of *N*-, *O*-diacylethanolamine (DAE)

6.3.3 Crystallization and X-Ray Diffraction

Thin plate type, colorless crystals of *N*-, *O*-dilauroylethanolamine (DLEA) were grown at room temperature from a 1:1 (vol/vol) mixture of dichloromethane and toluene, containing a trace of ethanol. A crystal of $0.6 \times 0.6 \times 0.16$ mm size was used for data collection in the present study. X-ray diffraction measurements were carried out at room temperature (ca. 25°C) with a Bruker SMART APEX CCD area detector system using a graphite monochromator and Mo- $\text{K}\alpha$ ($\lambda = 0.71073 \text{ \AA}$) radiation obtained from a fine-focus sealed tube.

6.3.4. Structure Solution and Refinement

The data collected in the range of $\theta = 2.03\text{--}25.99^\circ$ were used for structure solution. Data reduction was done using Bruker SAINTPLUS program. Structure solution was carried out in the orthorhombic space group. Absorption correction was applied using SADABS program. The structures were solved successfully by direct methods in the space group Pbc_{21} and refinement was done by full matrix least-squares procedure using the SHELXL-97 program (Sheldrick, 1997). The refinement was carried out using 2455 absorbed [$>2 \sigma(F_o)$] reflections and converged into a final $R_1 = 0.0621$, $wR_2 = 0.1580$ and goodness of fit = 1.175.

The hydrogen atom on the amide group was refined isotropically, whereas all the carbon atoms and heteroatoms (nitrogen and oxygen) were refined anisotropically. All hydrogen atoms on the acyl chains and other carbon atoms were included in the structure factor calculation with fixed thermal parameters at idealized positions but were not refined.

6.3.5. Crystal Parameters of *N-, O-Dilauroylethanolamine*

Molecular formula: $C_{26}H_{51}NO_3$. Molecular formula weight: 425.68; Crystals were thin plate type and colorless. Crystal system, Orthorhombic; Space group, $Sg = Pbc_{21}$; Ambient temperature, $T = 298(2)$ K; Radiation wavelength (λ) = 0.71073 Å; Radiation type, Mo-K α ; Radiation source, Fine-focus sealed tube; Radiation monochromator, graphite; Number of reflections collected, 23103; Unique reflections, 2481; Reflection with $I > 2\sigma(I)$, 2455; Number of parameters, 269.

Unit cell dimensions (with standard deviation in parentheses):

$a = 4.8756(4)$, $b = 8.7865(8)$, $c = 60.3(5)$ Å; Volume of the cell, $V = 2583.2(4)$ Å³ (5); Density, $D_{\text{Calc}} = 1.095$ gm cm⁻³; Number of molecules in the unit cell, $Z = 4$; Angle of tilt of acyl chains, $\theta = 36.5^\circ$ (*N*-acyl chain), 34.5° (*O*-acyl chain); Cross

sectional area of the unit cell, $\Sigma = 43.839 \text{ \AA}^2$; Area per molecule, $S = 21.419 \text{ \AA}^2$; $F_{(000)} = 952$; Absorption Coefficient, $\mu = 0.069 \text{ mm}^{-1}$; $T = 298(2) \text{ K}$.

6.3.6. Differential Scanning Calorimetry

DSC studies were carried out on a TA Instruments Universal V2.6D differential scanning calorimeter. Samples of dry DAEs (1-3 mg) were weighed accurately into aluminium sample pans, covered with an aluminium lid and sealed by crimping. Reference pans were prepared similarly, but without any sample in them. Heating and cooling scans were performed from room temperature (ca. 25°C) to about 120°C at a scan rate of $1.0^\circ/\text{min}$ or $2.0^\circ/\text{min}$ and each sample was subjected to two heating scans and one cooling scan. Transition enthalpies were determined by integrating the peak area under the transition curve. Transition entropies were determined from the transition enthalpies assuming a first order transition according to the expression (Marsh, 1990):

$$\Delta H_t = T \cdot \Delta H_t \quad (1)$$

6.4. RESULTS AND DISCUSSION

In view of reports indicating that DAEs could be present in biological membranes along with NAEs, we have synthesized them in our laboratory in order to investigate their structural and physical properties. In this direction in the present study, the crystal structure of DLEA has been determined and the intermolecular interactions and molecular packing in the crystal are analyzed, and the chain-melting phase transitions have been investigated by differential scanning calorimetry. The results obtained are expected to help in understanding the phase behavior and structure of DAEs better and should also be useful in analyzing their interactions with other membrane lipids.

Table 6.1: Assignment of resonances in the IR spectra of N-, O-diacylethanolamines.

Acyl chain length	Amide (cm ⁻¹)			Ester (cm ⁻¹)		C–H (cm ⁻¹)	
	C=O Amide-1	N–H (def) Amide-2	N–H Strech	C=O	C–O Strech	C–H Strech	C–H (def)
C ₁₀	~1642	~1553	~3302	~1738	~1182	~2920, ~2851	~1471
C ₁₁	~1643	~1557	~3306	~1736	~1188	~2918, ~2851	~1472
C ₁₂	~1642	~1553	~3302	~1738	~1181	~2918, ~2851	~1472
C ₁₃	~1642	~1557	~3306	~1736	~1184	~2918, ~2851	~1470
C ₁₄	~1642	~1553	~3304	~1738	~1181	~2918, ~2851	~1462
C ₁₅	~1642	~1553	~3308	~1736	~1182	~2918, ~2849	~1472
C ₁₆	~1643	~1553	~3306	~1734	~1182	~2918, ~2849	~1472
C ₁₇	~1642	~1551	~3312	~1734	~1182	~2916, ~2849	~1472
C ₁₈	~1642	~1553	~3308	~1738	~1180	~2918, ~2849	~1472
C ₁₉	~1642	~1551	~3308	~1738	~1178	~2918, ~2849	~1472
C ₂₀	~1643	~1549	~3310	~1738	~1178	~2918, ~2849	~1462

6.4.1. Synthesis and Characterization of N-, O-Diacylethanolamines

DAEs of matched acyl chainlengths ($n = 11$ -20) have been synthesized in fair yields by the reaction of the corresponding acid chlorides with 2-ethanolamine. The DAEs, purified by column chromatography and recrystallization, were found to be pure by tlc. IR spectra of all the DAEs contained absorption bands due to the amide linkage at 1643-1642 cm⁻¹ (amide-I) and 1557-1549 cm⁻¹ (amide-II) and at 1738-1734 cm⁻¹ due to the ester carbonyl. The amide N–H stretching is seen at 3312-3302 cm⁻¹, whereas C–O stretching from the ester moiety is observed around 1188-1178 cm⁻¹. The specific band positions for these and other absorptions such as C–H stretching, C–H bending and C–N stretching modes are listed in Table 6.1. A representative ¹H-NMR spectrum corresponding to dipentadecanoylethanolamine (C₁₅ DAE) is shown in Fig. 6.1 and results of ¹H-NMR spectra for the different DAEs investigated in this study together with assignments are given in Table 6.2.

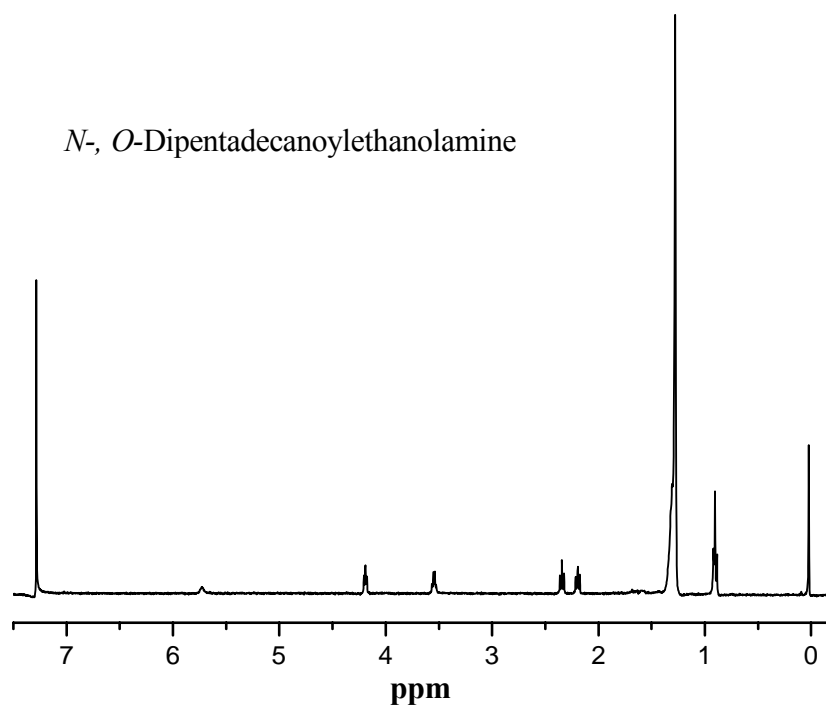


Fig. 6.1: ^1H -NMR spectrum of *N*-, *O*-Dipentadecanoylethanolamine (C_{15} DAE). The resonance at extreme right corresponds to tetramethylsilane (internal reference).

Table 6.2: ^1H -NMR spectral data of *N*-, *O*-diacylethanolamines

Acyl chain length	Amide moiety			Ester group		Acyl chains	
	$\text{CH}_2\text{-CO}$	N-H	$\text{CH}_2\text{-NH}$	$\text{CH}_2\text{-O-CO}$	CH-CO	CH_3	$(\text{CH}_2)_n$
C_{10}	2.19, t	5.75, s	3.53, q	4.19, t	2.34, t	0.90, m	1.28, m
C_{11}	2.19, t	5.75, s	3.53, q	4.19, t	2.34, t	0.90, m	1.28, m
C_{12}	2.17, t	5.75, s	3.53, q	4.18, t	2.34, t	0.90, m	1.28, m
C_{13}	2.19, t	5.75, s	3.53, q	4.19, t	2.34, t	0.90, m	1.28, m
C_{14}	2.19, t	5.75, s	3.55, q	4.19, t	2.34, t	0.90, m	1.28, m
C_{15}	2.19, t	5.75, s	3.55, q	4.19, t	2.34, t	0.90, m	1.28, m
C_{16}	2.23, t	5.75, s	3.56, q	4.20, t	2.46, t	0.90, m	1.29, m
C_{17}	2.19, t	5.75, s	3.56, q	4.19, t	2.34, t	0.90, m	1.28, m
C_{18}	2.19, t	5.75, s	3.53, q	4.19, t	2.34, t	0.90, m	1.28, m
C_{19}	2.19, t	5.75, s	3.53, q	4.19, t	2.34, t	0.90, m	1.28, m
C_{20}	2.20, t	5.75, s	3.53, q	4.19, t	2.34, t	0.90, m	1.28, m

6.4.2. Description of the Structure

The molecular structure of *N*-, *O*-dilauroylethanolamine (DLEA) is shown in the ORTEP plot given in Fig. 6.2, along with the atom numbering for all the non-hydrogen atoms. The atomic coordinates and equivalent isotropic displacement parameters for all non-hydrogen atoms and the hydrogen atom on the heteroatom (N–H) are given in Table 6.3. The bond distances and bond angles involving all the non-hydrogen atoms are given in Table 6.4 whereas the corresponding torsion angles are given in Table 6.5. It is clearly seen from Fig. 6.2, that the hydrocarbon

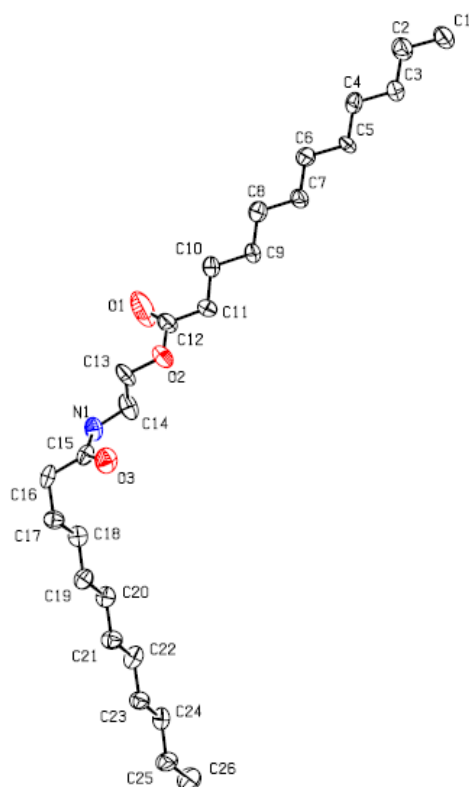


Fig. 6.2: ORTEP plot of *N*-, *O*-dilauroylethanolamine.

Table 6.3: Fractional atomic coordinates ($\times 10^4$) and equivalent isotropic displacement parameters ($\text{\AA}^2 \times 10^3$) for the *N*-, *O*- dilauroylethanolamine. $U(\text{eq})$ is defined as one third of the trace of the orthogonalized U_{ij} tensor [$U(\text{eq}) = \frac{1}{3} \sum_i \sum_j U_{ij} a_i^* a_j^* a_i a_j \cos(a_i, a_j)$].

Atom	x	y	z	U(eq)
O(1)	249(11)	3203(6)	1022(1)	79(2)
O(2)	3881(8)	3500(4)	812(1)	40(1)
O(3)	5446(6)	1464(3)	191(1)	26(1)
N(1)	1076(7)	1806(4)	298(1)	19(1)
C(1)	3081(10)	13350(5)	2848(1)	27(1)
C(2)	1893(9)	11944(5)	2736(1)	24(1)
C(3)	3090(9)	11674(5)	2505(1)	20(1)
C(4)	1886(8)	10283(5)	2389(1)	19(1)
C(5)	3108(9)	10018(5)	2160(1)	19(1)
C(6)	1890(9)	8619(5)	2043(1)	19(1)
C(7)	3151(9)	8353(5)	1813(1)	18(1)
C(8)	1983(9)	6961(5)	1693(1)	20(1)
C(9)	3289(9)	6724(5)	1467(1)	19(1)
C(10)	2103(9)	5343(5)	1341(1)	22(1)
C(11)	3506(9)	5139(5)	1118(1)	20(1)
C(12)	2320(9)	3834(5)	988(1)	22(1)
C(13)	2947(12)	2275(5)	668(1)	34(1)
C(14)	1741(9)	2963(5)	461(1)	25(1)
C(15)	3009(8)	1154(4)	171(1)	16(1)
C(16)	2008(8)	-33(4)	5(1)	18(1)
C(17)	3144(8)	278(5)	-228(1)	17(1)
C(18)	1972(8)	1744(5)	-332(1)	18(1)
C(19)	3127(8)	2036(5)	-563(1)	18(1)
C(20)	1900(8)	3442(5)	-676(1)	18(1)
C(21)	3110(8)	3739(5)	-907(1)	18(1)
C(22)	1882(8)	5134(5)	-1019(1)	19(1)
C(23)	3099(9)	5426(5)	-1251(1)	18(1)
C(24)	1889(8)	6815(5)	-1367(1)	19(1)
C(25)	3088(9)	7090(5)	-1598(1)	22(1)
C(26)	1911(10)	8505(5)	-1710(1)	27(1)

Table 6.4: Bond distances (Å) and bond angles (degrees) for N-, O-dilauroylethanolamine.

Bond distances (Å)			Bond angle (degree)		
O(1) - C(12)	1.170(7)		C(12) - O(2) - C(13)	117.3(4)	
O(2) - C(12)	1.340(5)		C(14) - N(1) - C(15)	121.8(3)	
O(2) - C(13)	1.457(6)		C(1) - C(2) - C(3)	112.6(4)	
O(3) - C(15)	1.225(5)		C(2) - C(3) - C(4)	113.2(4)	
N(1) - C(14)	1.449(6)		C(3) - C(4) - C(5)	112.8(3)	
N(1) - C(15)	1.341(5)		C(4) - C(5) - C(6)	112.8(3)	
N(1) - H(1D)	0.880(4)		C(5) - C(6) - C(7)	112.4(3)	
C(1) - C(2)	1.521(6)		C(6) - C(7) - C(8)	113.6(4)	
C(2) - C(3)	1.531(6)		C(7) - C(8) - C(9)	112.3(4)	
C(3) - C(4)	1.525(6)		C(8) - C(9) - C(10)	113.0(4)	
C(4) - C(5)	1.526(6)		C(9) - C(10) - C(11)	110.9(3)	
C(5) - C(6)	1.536(6)		C(10) - C(11) - C(12)	112.3(4)	
C(6) - C(7)	1.531(5)		O(1) - C(12) - O(2)	121.7(5)	
C(7) - C(8)	1.532(6)		O(1) - C(12) - C(11)	126.9(4)	
C(8) - C(9)	1.522(6)		O(2) - C(12) - C(11)	111.3(4)	
C(9) - C(10)	1.541(6)		O(2) - C(13) - C(14)	108.7(3)	
C(10) - C(11)	1.520(6)		N(1) - C(14) - C(13)	111.5(4)	
C(11) - C(12)	1.506(6)		O(3) - C(15) - N(1)	122.2(4)	
C(13) - C(14)	1.506(7)		O(3) - C(15) - C(16)	121.7(4)	
C(15) - C(16)	1.526(5)		N(1) - C(15) - C(16)	116.1(3)	
C(16) - C(17)	1.535(6)		C(15) - C(16) - C(17)	111.3(3)	
C(17) - C(18)	1.542(6)		C(16) - C(17) - C(18)	112.8(3)	
C(18) - C(19)	1.524(5)		C(17) - C(18) - C(19)	112.0(3)	
C(19) - C(20)	1.534(6)		C(18) - C(19) - C(20)	113.6(3)	
C(20) - C(21)	1.535(5)		C(19) - C(20) - C(21)	113.2(3)	
C(21) - C(22)	1.522(6)		C(20) - C(21) - C(22)	113.0(3)	
C(22) - C(23)	1.538(6)		C(21) - C(22) - C(23)	112.7(3)	
C(23) - C(24)	1.525(6)		C(22) - C(23) - C(24)	113.6(3)	
C(24) - C(25)	1.533(6)		C(23) - C(24) - C(25)	113.3(3)	
C(25) - C(26)	1.527(6)		C(24) - C(25) - C(26)	112.8(4)	
			C(14) - N(1) - H(1D)	114.0(2)	
			C(15) - N(1) - H(1D)	124.0(2)	

Table 6.5: Torsion angles (degrees) for *N*-, *O*-dilauroylethanolamine.

C(1)	C(2)	C(3)	C(4)	-179.1(4)
C(2)	C(3)	C(4)	C(5)	-179.6(3)
C(3)	C(4)	C(5)	C(6)	-179.9(3)
C(4)	C(5)	C(6)	C(7)	-179.4(3)
C(5)	C(6)	C(7)	C(8)	179.8(3)
C(6)	C(7)	C(8)	C(9)	-179.7(4)
C(7)	C(8)	C(9)	C(10)	-179.0(3)
C(8)	C(9)	C(10)	C(11)	-179.0(4)
C(9)	C(10)	C(11)	C(12)	-177.8(3)
C(10)	C(11)	C(12)	O(1)	14.7(7)
C(10)	C(11)	C(12)	O(2)	-168.9(4)
O(2)	C(13)	C(14)	N(1)	173.0(4)
O(3)	C(15)	C(16)	C(17)	-51.5(5)
N(1)	C(15)	C(16)	C(17)	130.0(4)
C(12)	O(2)	C(13)	C(14)	103.8(4)
C(13)	O(2)	C(12)	O(1)	-2.2(7)
C(13)	O(2)	C(12)	C(11)	-178.8(4)
C(15)	N(1)	C(14)	C(13)	-77.8(5)
C(14)	N(1)	C(15)	O(3)	2.3(6)
C(14)	N(1)	C(15)	C(16)	-179.3(4)
C(15)	C(16)	C(17)	C(18)	-67.7(4)
C(16)	C(17)	C(18)	C(19)	179.9(3)
C(17)	C(18)	C(19)	C(20)	177.1(3)
C(18)	C(19)	C(20)	C(21)	179.1(3)
C(19)	C(20)	C(21)	C(22)	179.9(3)
C(20)	C(21)	C(22)	C(23)	-179.9(3)
C(21)	C(22)	C(23)	C(24)	179.8(3)
C(22)	C(23)	C(24)	C(25)	-179.4(3)
C(23)	C(24)	C(25)	C(26)	-178.6(4)
H(1D)	N(1)	C(14)	C(13)	108(3)
H(1D)	N(1)	C(15)	O(3)	177(3)
H(1D)	N(1)	C(15)	C(16)	-5(3)

portions of the two acyl chains (C12–C1, corresponding to the *O*-acyl chain and C17–C26, corresponding to the *N*-acyl chain) of the molecule are in all-*trans* conformation. The torsion angle observed for the two acyl chain regions – excepting the C15–C16–C17–C18 angle, which is -67.7° – are all close to 180° and are fully in agreement with above observation (Table 6.5). In the region between the two acyl chains, the two torsion angles around the O2–C13 bond and the C14–N1 bond are in gauche conformation, but point in nearly opposite directions, resulting in an extension of the nearly linear arrangement until C16, which corresponds to the methylene group adjacent to the amide carbonyl. The gauche conformation at the C16–C17 bond results in a distinct change in the chain direction leading to a bending of the molecule, thus giving it an ‘L’ shape. The carbonyl group and the amide N–H are also in *trans* geometry. In NAEs such as *N*-myristoylethanolamine, *N*-palmitoylethanolamine, and *N*-stearoylethanolamine a gauche conformation at the corresponding C–C bond results in a bending of the *N*-acyl chain giving an ‘L’ shape to the molecules in the crystalline state (Dahlén et al., 1977; Ramakrishnan and Swamy, 1999; Kamlekar and Swamy, 2006; see also Chapter 2). Thus esterification of the hydroxyl group of NAE to produce *N*-, *O*-diacylethanolamine does not seem to affect the conformation of the *N*-acyl region.

6.4.3. Molecular Packing

The packing diagrams of *N*-, *O*-dilauroylethanolamine along the *b*-axis and *a*-axis are given in Figure 6.3. The DLEA molecules are packed in layers that are stacked in such a way that the methyl groups of the *O*-acyl chains from one layer face the methyl groups of the *N*-acyl chains of the layer above it. The methyl ends of the stacked layers are in van der Waals contacts with the closest methyl-methyl

distance between opposite layers and the same layer being 3.882 Å and 4.876 Å, respectively.

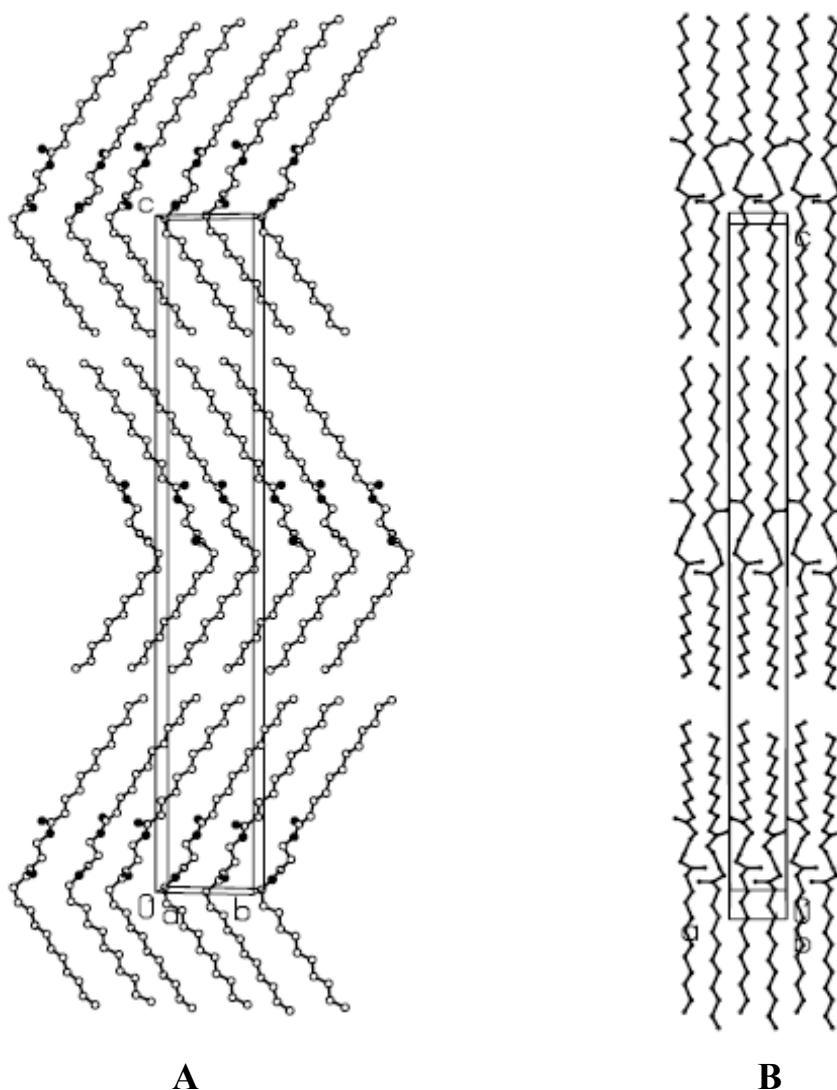


Fig. 6.3: Packing diagrams of *N*-, *O*-dilauroylethanolamine. (A) A view along with *b*-axis. (B) A view along with *a*-axis.

The layer thickness (C1–C26 distance) in the DLEA is 27.818 Å and the all-*trans* *N*- and *O*-acyl chains of the molecule are tilted by 36.5° and 34.5°, respectively.

respectively, with respect to the normal to the respective methyl end planes. These values are in the same range as the tilt angles with respect to the bilayer normal found in NMEA, NPEA and NSEA (35-37°) (Kamlekar and Swamy, 2006; Ramakrishnan and Swamy, 1999; Dahlén et al., 1977). Other long chain molecules such as long chain carboxylic acids and n-alcohols also pack in a bilayer form with tail-to-tail hydrocarbon alignment with tilted chains (Larsson, 1986).

The packing coefficient for DLEA is 68.5%, which is significantly higher than that observed for NMEA (55%) and slightly more than the packing coefficient found in NSEA (65.2%) and the two polymorphs of NPEA (both 65.3%). This suggests that the acyl chains in DLEA are packed more tightly than in NPEA and NSEA, which are in turn more tightly packed than the acyl chains in NMEA.

6.4.4. Subcell Structure

The different lateral packing modes, adopted by hydrocarbon chains in lipid crystals are generally described by subcells that specify the relations between equivalent positions within the chain and its neighbors. From an analysis of a large number of lipid crystal structures it was shown that such chain packing modes fall into a relatively small number of hydrocarbon subcells with triclinic, monoclinic, orthorhombic, and hexagonal symmetry and that their polymethylene planes can be mutually parallel or perpendicular with respect to their neighbors (Abrahamsson et al., 1978; Maulik et al., 1988). The subcells have been further divided into simple and hybrid types, with the latter involving more than two different asymmetric units in a subcell. Examination of the hydrocarbon chain packing in the *N*-acyl chain and *O*-acyl chains of DLEA revealed that the subcells in both these chains are of the orthorhombic type ($O'\perp$) in the *Pbnm* space group. The unit cell dimensions of these subcells are as follows: $a = 7.137 \text{ \AA}$, $b = 4.876 \text{ \AA}$ and $c = 2.562 \text{ \AA}$ for the *N*-acyl chain and $a = 7.225 \text{ \AA}$, $b = 4.876 \text{ \AA}$, and $c = 2.536 \text{ \AA}$ for the *O*-acyl chain.

These then yielded the areas per chain of 17.40 \AA^2 for the *N*-acyl chain and 17.61 \AA^2 for the *O*-acyl chain. These parameters are in the range that is typically observed for the orthorhombic type $O' \perp$ (Larsson, 1986).

6.4.5. Molecular Area

The area per each DLEA molecule in the bilayer plane in the crystal structures is 21.419 \AA^2 . This value is in the same range as the values of molecular area found for the NAEs whose 3-dimensional structures have been determined earlier, namely NPEA (for polymorphs α and β it is 21.99 \AA^2 and 22.03 \AA^2 , respectively), NMEA (21.95 \AA^2) and NSEA (21.99 \AA^2) as well as some other single-chain lipids such as 3(11-bromoundecanoyl)-D-glycerol, 3-lauroyl-D-glycerol and 3-Stearoyl-D-glycerol, whose molecular areas are in the range of $21.5\text{--}22.7 \text{ \AA}^2$ (Kamlekar and Swamy, 2006; Ramakrishnan and Swamy, 1999; Dahlén et al., 1977; Larsson et al., 1966; Goto et al., 1985, 1988; Pascher et al., 1992). Other single chain lipids such as lysophosphatic acid and lysophosphatidylethanolamine, have somewhat larger molecular areas (33.6 and 34.8 \AA^2 , respectively). Such large molecular areas observed in these two molecules are due to the very high tilt angle of the acyl chains with respect to the bilayer normal (Pascher et al., 1981, 1985).

6.4.6. Hydrogen Bonding and Intermolecular Interactions

The molecular packing in the crystal structure of DLEA was examined from various angles in order to understand the intermolecular interactions. The hydrogen bonding pattern observed in the crystal lattice of DLEA is shown in Fig. 6.4A. In Figures 6.4B and 6.4C, pictures of the hydrogen bonding pattern viewed along the *a*-axis and *b*-axis, respectively are shown. Fig. 6.4B gives a view of the molecular packing together with the hydrogen bonds between the amide hydrogen and the

carbonyl oxygen atoms of adjacent layers in the same leaflet of the bilayer. These N–H \cdots O hydrogen bonds are formed between the amide N–H group of one molecule and the amide carbonyl oxygen of an adjacent DLEA molecules along a-axis. The N–H and C=O groups of the amide moiety in each molecule are in *trans* geometry and point in opposite direction, thus providing proper juxtaposition to interconnect adjacent molecules by N–H \cdots O hydrogen bonds. All these H-bonds are identical, with an N–O distance of 2.835(5) Å, and H \cdots O distance of 1.84 Å and an N–H \cdots O angle of 168°. This is essentially similar to the value of 167° observed for the corresponding N–H \cdots O angle in the crystal structure of NPEA (α polymorph) (Kamlekar and Swamy, 2006) and the value of 166.7° seen in NMEA (Ramakrishnan and Swamy, 1999).

Fig. 6.4C gives a view of two weak C–H \cdots O type hydrogen bonds observed in the crystal lattice. One of these is formed between O3 (oxygen atom of the amide carbonyl group) of one molecule and one of the H-atoms on C16 (carbon atom α - to the amide carbonyl) of an adjacent molecule in the same layer. All the C–H \cdots O hydrogen bonds between O3 and C16 are identical, with a C–O distance of 3.502(5) Å, an H \cdots O distance of 2.42 Å and C–H \cdots O angle of 174°. The second C–H \cdots O bond is formed between O1 (the ester carbonyl oxygen) of one molecule and one of the H-atoms on C11 (carbon atom α - to the ester carbonyl group) of an adjacent molecule in the same layer. All these hydrogen bonds are also identical, with a C–O distance of 3.307(7) Å, H \cdots O distance of 2.48 Å and a C–H \cdots O angle of 132°.

In addition to these two intermolecular C–H \cdots O hydrogen bonds, an intramolecular C–H \cdots O bond is observed between the ester carbonyl oxygen (O1) and one of the H-atoms connected to C13 carbon in the same molecule. This bond is characterized by a C–O distance of 2.640(7) Å, H \cdots O distance of 2.23 Å and a

C–H \cdots O angle of 100° . In view of the significantly lower C–H \cdots O angle, this H-bond is expected to be considerably weaker.

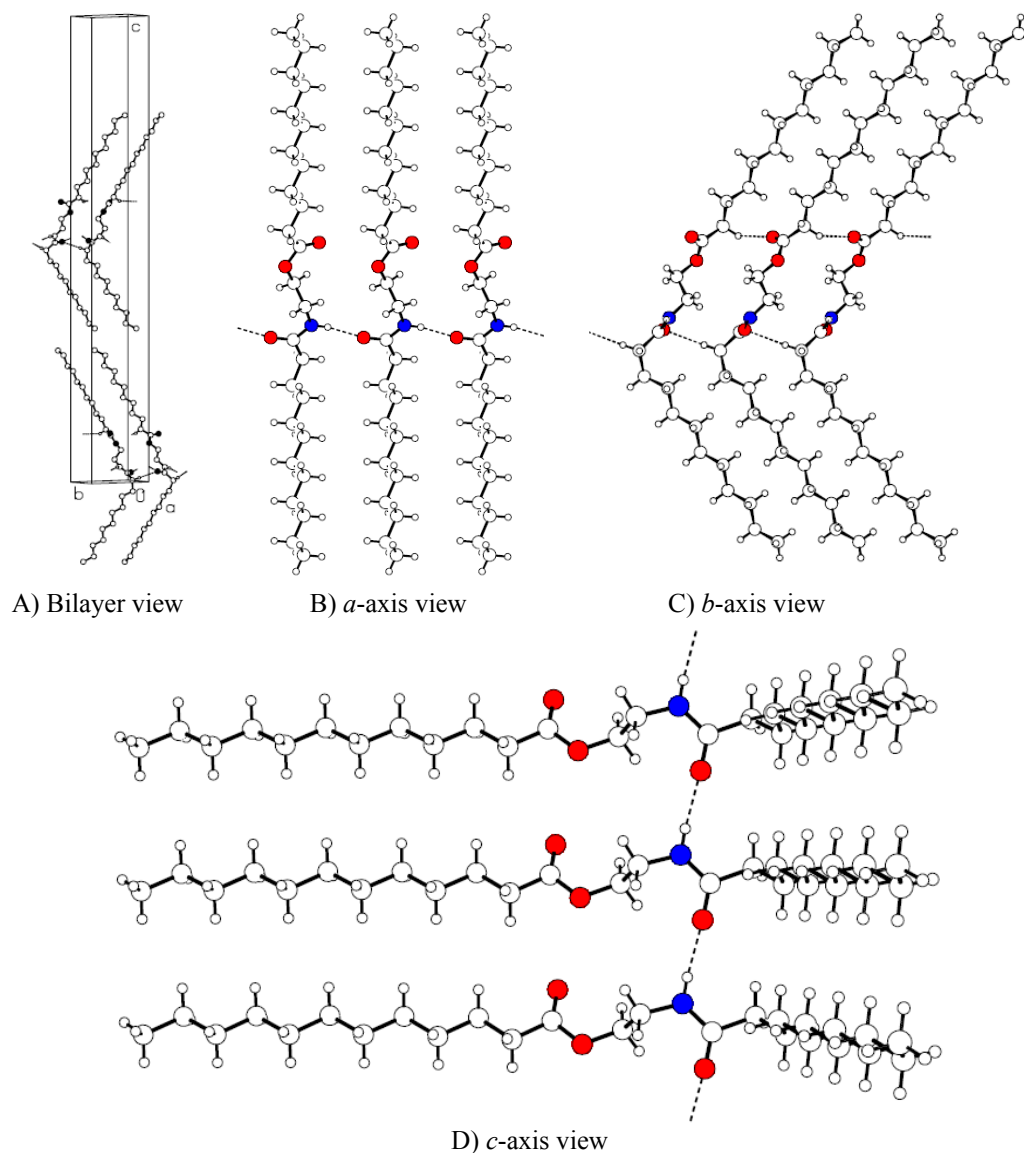


Fig. 6.4: Hydrogen bonding pattern in the crystal lattice of *N*-, *O*-dilauroylethanolamine. (A) A view of the bilayer displaying N–H \cdots O type hydrogen bonding. (B) A close view along *a*-axis displaying N–H \cdots O type hydrogen bonding. (C) A close view along *b*-axis displaying two C–H \cdots O type hydrogen bonds. (D) A close view along *c*-axis displaying two N–H \cdots O type hydrogen bonds.

6.4.7. Differential Scanning Calorimetry

DSC thermograms of heating scans of various DAEs of even, matched acyl chainlengths are shown in Fig. 6.5A and those corresponding to DAEs with matched, odd acyl chainlengths are shown in Fig. 6.5B. The corresponding cooling scans are shown in Fig. 6.6A and Fig. 6.6B, respectively. While the heating scans gave endothermic transitions, the cooling scans yielded exothermic transitions. The heating thermograms presented in Fig. 6.5A and Fig. 6.5B show that each DAE exhibits a major transition at a temperature that corresponds to the capillary melting

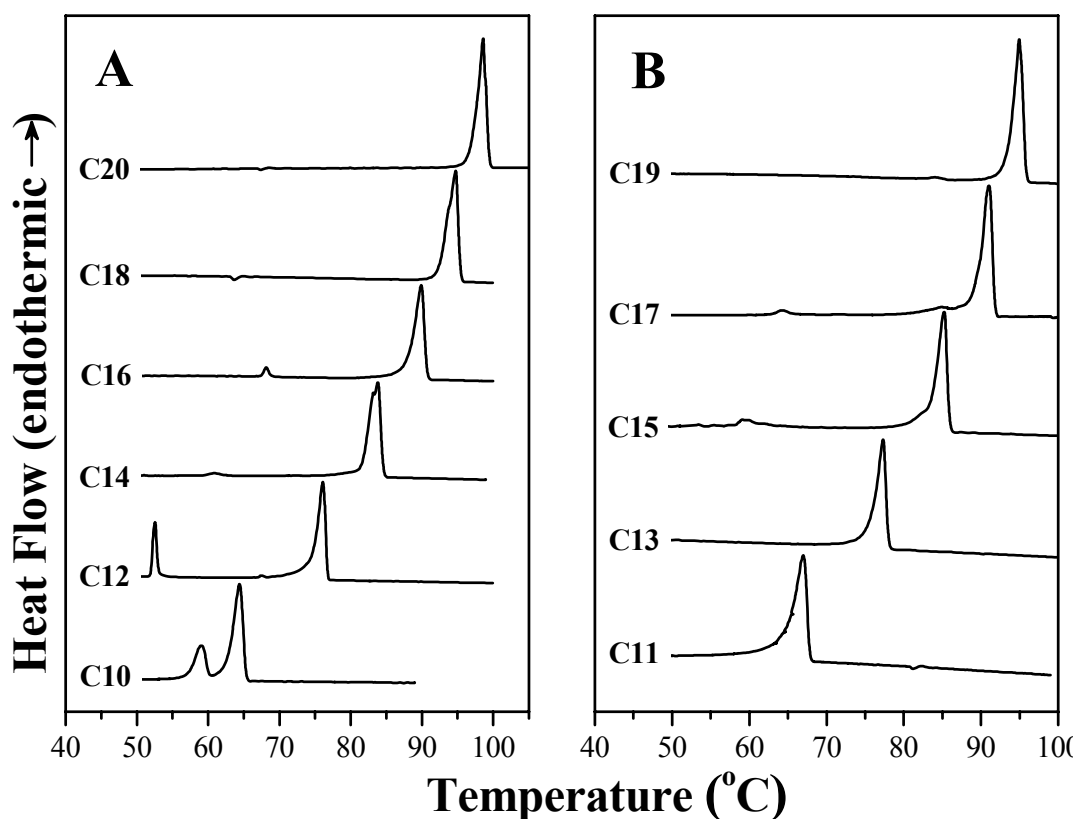


Fig. 6.5: DSC heating thermograms of *N-, O*-diacylethanolamines. A) DAEs with even number of C-atoms in the acyl chains, B) DAEs with odd number of C-atoms in the acyl chains. The number of C-atoms in the acyl chain is indicated against each thermogram.

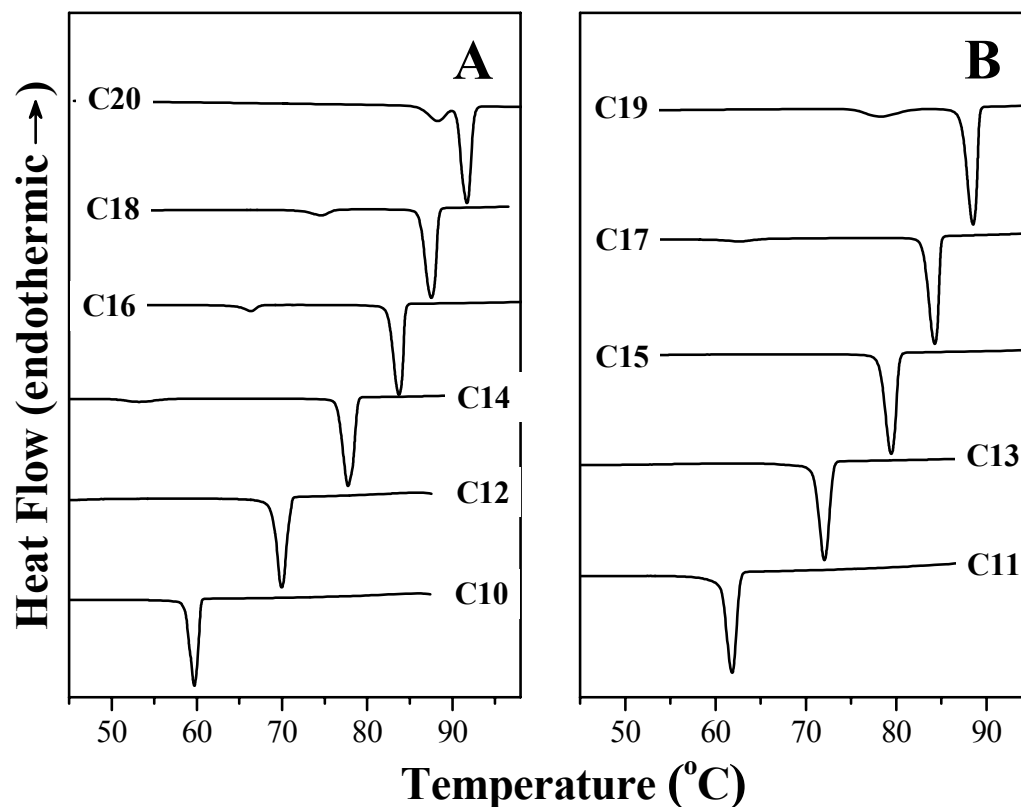


Fig. 6.6: DSC cooling thermograms of *N*-, *O*-diacylethanamines. A) DAEs with even number of C-atoms in the acyl chains, B) DAEs with odd number of C-atoms in the acyl chains. The number of C-atoms in the acyl chain is indicated against each thermogram.

point of the compound. Some of the DAEs also show one or two additional, minor transitions at lower temperatures. These transitions therefore must correspond to solid-solid phase transitions and indicate the possibility of structural polymorphism. When the samples were subjected to a second heating scan, it was observed that the additional transitions disappear in some cases and small decreases have been noted in the transition temperatures and enthalpies. Therefore, in all cases only the first heating scan is considered for further analysis and only the major transitions have

been analyzed. Transition temperatures (T_t), transition enthalpies (ΔH_t) and transition entropies (ΔS_t) obtained from the heating thermograms are presented in Table 6.6.

Table 6.6: Chain-melting phase transition temperatures (T_t), enthalpies (ΔH_t) and entropies (ΔS_t) of DAEs. Data obtained from the DSC thermograms of dry samples of N-, O-diacylethanolamines of matched acyl chainlengths ($n = 10-20$) are shown.

Acyl chainlength, n	T_t (°C)	ΔH_t	ΔS_t
C ₁₀	65.74	11.6	34.2
C ₁₁	66.99	11.7	34.3
C ₁₂	76.11	15.7	44.9
C ₁₃	77.33	16.9	48.3
C ₁₄	83.83	21.1	59.2
C ₁₅	85.21	20.5	57.2
C ₁₆	89.89	26.5	72.9
C ₁₇	91.65	26.6	72.8
C ₁₈	94.74	32.1	87.3
C ₁₉	94.94	30.1	81.6
C ₂₀	99.22	36.4	97.8

6.4.8. Chainlength Dependence of Transition Enthalpy and Transition Entropy

The chainlength dependence of transition enthalpy and transition entropy for the chain-melting phase transitions of DAEs of matched N- and O-acyl chainlengths are given in Fig. 6.7A and Fig. 6.7B, respectively. In both cases it is observed that the even and odd series independently exhibit linear dependence of the calorimetric parameters on the acyl chainlength. However, when the data obtained with the even and odd chainlength series are viewed together, a zig-zag pattern is seen with the values of enthalpy and entropy for the odd chainlength series being slightly lower than those of the even chainlength series. In other words, the calorimetric

data exhibit even-odd alternation and this aspect will be discussed in more detail below.

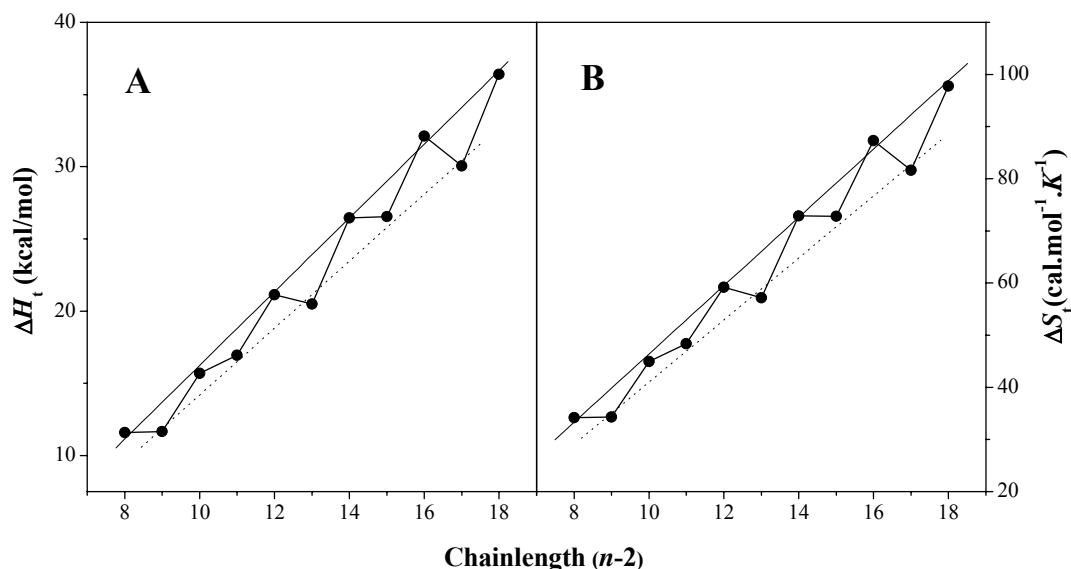


Fig. 6.7: Chainlength dependence of transition enthalpies (ΔH_t) and transition entropies (ΔS_t). Transition enthalpies (A) and transition entropies (B) obtained for the thermotropic phase transitions of *N*-, *O*-diacylethanolamines of matched acyl chainlengths are plotted against the number of methylene units ($n-2$, where n is the number of C-atoms) in each acyl chain. Data obtained from the heating scans are shown. The even-odd alternation is clearly seen in the plot.

The enthalpy and entropy data for DAEs of matched, even and odd acyl chainlengths could be fit well to expressions 2 and 3 given below (Larsson, 1986), as observed earlier with NAEs with even and odd acyl chainlengths (Ramakrishnan et al., 1997; Ramakrishnan and Swamy, 1998):

$$\Delta H_t = \Delta H_o + (n-2)\Delta H_{inc} \quad (2)$$

$$\Delta S_t = \Delta S_o + (n-2)\Delta S_{inc} \quad (3)$$

where ΔH_o and ΔS_o are the end contributions to ΔH_t and ΔS_t , respectively, arising from the terminal methyl groups and the central polar region of the DAE molecule. ΔH_{inc} and ΔS_{inc} are the incremental values of ΔH_t and ΔS_t contributed by two CH_2

groups (one from the *N*-acyl chain and the other from the *O*-acyl chain). Linear least squares analysis of the chainlength-dependent values of ΔH_t and ΔS_t for the even and odd series DAEs yielded the incremental values (ΔH_{inc} and ΔS_{inc}) and end contributions (ΔH_o and ΔS_o). These values are listed in Table 6.7.

Table 6.7: Incremental values and end contributions of transition enthalpy and entropy of DAEs. Incremental values (ΔH_{inc} , ΔS_{inc}) of chainlength dependence and end contributions (ΔH_o , ΔS_o) to the calorimetric enthalpy and entropy, for *N*-, *O*-diacylethanolamines of matched even and odd acyl chainlengths ($n = 10$ -20) are given.

Lipid	ΔH_{inc}	ΔH_o	ΔS_{inc}	ΔS_o
Even chainlength	2.552 (± 0.058)	-9.283 (± 0.782)	6.551 (± 0.157)	19.125 (± 2.112)
Odd chainlength	2.319 (± 0.107)	-9.003 (± 1.429)	5.955 (± 0.295)	18.557 (± 3.924)

A linear chainlength dependence of the transition enthalpy and transition entropy observed here for the DAEs of even chainlengths and odd chainlengths indicate that structures of the DAEs of different even and odd chainlengths are very similar in the solid state and in the liquid state. This suggests that the molecular packing and hydrogen bonding patterns in all the even chainlength DAEs are likely to be very similar to those observed in the crystal structure of DLEA (Figs. 6.3, 6.4).

The ΔH_{inc} values of 2.552 and 2.319 kcal.mol⁻¹ observed here for the DAEs with even and odd chainlengths, respectively, correspond to the contribution of two acyl chains and in order to obtain the average contribution of each CH₂ group these values should be halved. The corresponding per-chain ΔH_{inc} values would then be 1.276 and 1.16 kcal.mol⁻¹, respectively, for the DAEs with even and odd chainlengths. A comparison of these values with the corresponding values obtained previously for the NAEs show that the incremental enthalpy contributed by each CH₂ unit in the DAEs is considerably higher than that observed with the NAEs.

Analysis of the crystal structure of DLEA and comparison of the subcell structures of the *N*- and *O*-acyl chains in it with those of NMEA and NPEA, discussed above, have shown that the acyl chains in DLEA are more tightly packed than those in the NMEA and NPEA, with DLEA having a smaller area per chain (17.40 and 17.61 Å², respectively, for the *N*-acyl chain and *O*-acyl chain) than that in NPEA (18.16 and 18.25 Å², respectively, for the α and β polymorphs) (Kamlekar and Swamy, 2006). For NMEA, the corresponding value is 19.14 Å², which is considerably higher than that observed with DLEA. These observations suggest that the larger ΔH_{inc} values for the DAEs are a consequence of the closer chain packing. These observations are also in good agreement with the trends seen in the packing coefficients, discussed in Section 6.4.4.

The ΔS_{inc} values obtained here for the DAEs with matched acyl chainlengths (the per-chain values being 3.276 and 2.978 J.mol⁻¹.K⁻¹, for the even and odd chainlength series, respectively) are also considerably higher than the ΔS_{inc} values obtained for the NAEs (Ramakrishnan et al., 1997; Ramakrishnan and Swamy, 1998). This suggests that the change in the order resulting from the chain melting phase transition is higher for the DAEs than the NAEs. This is again consistent with the acyl chains in DAEs being packed more tightly.

6.4.9. Chainlength Dependence of Transition Temperatures

Although the data presented in Table 6.6 show that the transition temperatures increase with increasing acyl chainlength, the increase in the transition temperature (T_t) is not linearly proportional to the acyl chainlength. In order to understand this better the transition temperatures were plotted as a function of acyl chainlength (Fig. 6.8). From this Figure it is apparent that the T_t values exhibit an even-odd alternation, with the even chainlength series exhibiting somewhat higher transition temperatures than the odd chainlength compounds.

This aspect is discussed in more detail below. Within each series, however, the T_t values increase in a smooth progression but with decreasing increments as the chainlength is increased.

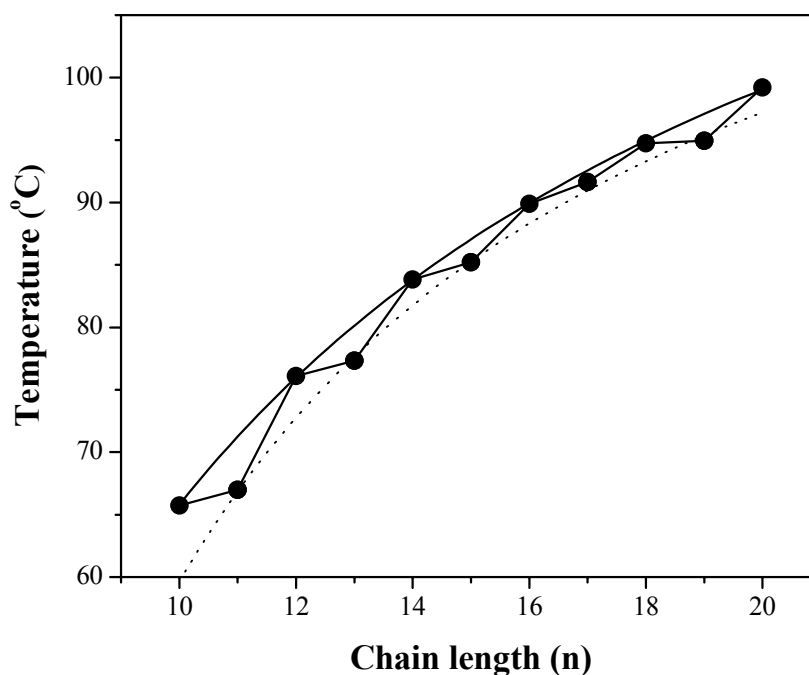


Fig. 6.8: Chainlength dependence of phase transition temperatures of N-, O-diacylethanamines of matched acyl chainlengths. Data obtained from the heating scans are shown. The even-odd alternation is clearly visible in the plot. The T_t values for even and odd series are independently fit by a non-linear least squares method to Equation (4) and the fits are shown as solid (even chainlength) and dotted (odd chainlength) lines. The fitting parameters are: $T_t = 415.5$ K, $n_o - n_o' = 3.99$, $n_o' = -3.01$ for the even chainlength series and $T_t = 403.1$ K, $n_o - n_o' = 6.07$, $n_o' = 1.3$ for the odd chainlength series.

As the acyl chainlength increases, the total contribution from the polymethylene portion $\{(\text{CH}_2)_n\}$ towards the total enthalpy and entropy of the phase transition will be sufficiently large that the end contributions are negligible in comparison. At infinite acyl chainlength, equations 2 and 3 can be reduced to (Ramakrishnan et al., 1997):

$$\Delta H_t = (n-2)\Delta H_{inc} \quad (4)$$

$$\Delta S_t = (n-2)\Delta S_{inc} \quad (5)$$

Then the transition temperature for infinite chainlength, T_t^∞ , will be given by:

$$T_t^\infty = \Delta H_{inc}/\Delta S_{inc} \quad (6)$$

From the data presented in Table 5, the T_t^∞ values for the DAEs of even and odd chainlengths have been estimated as 389.6 and 389.4 K, respectively.

The chainlength dependence of the transition temperatures of DAEs of both even and odd acyl chainlengths was fitted to equation 7, predicted from the linear dependence of transition enthalpy and transition entropy given in equations 2 and 3 (Marsh, 1982, 1991):

$$T_t^\infty = \Delta H_t/\Delta S_t = (\Delta H_{inc}/\Delta S_{inc}) [1 - (n_o - n_o')/(n - n_o')] \quad (8)$$

where n_o ($= -\Delta H_o/\Delta H_{inc}$) and n_o' ($=\Delta S_o/\Delta S_{inc}$) are the chainlengths at which the transition enthalpy and transition entropy, respectively, extrapolate to zero. From the nonlinear least squares fits shown in Fig. 6.8, it is evident that the transition temperatures of DAEs with even and odd chainlengths are described accurately by equation 8. In addition, the fitting parameters yielded the transition temperature at infinite chainlength (T_t^∞) for the DAEs of matched even and odd acyl chains as 415.5 K with χ^2 of 0.03 and 403.0 K with χ^2 of 0.39, respectively. These values are in good agreement with the values estimated from the linear regression analysis of the calorimetric data, discussed above.

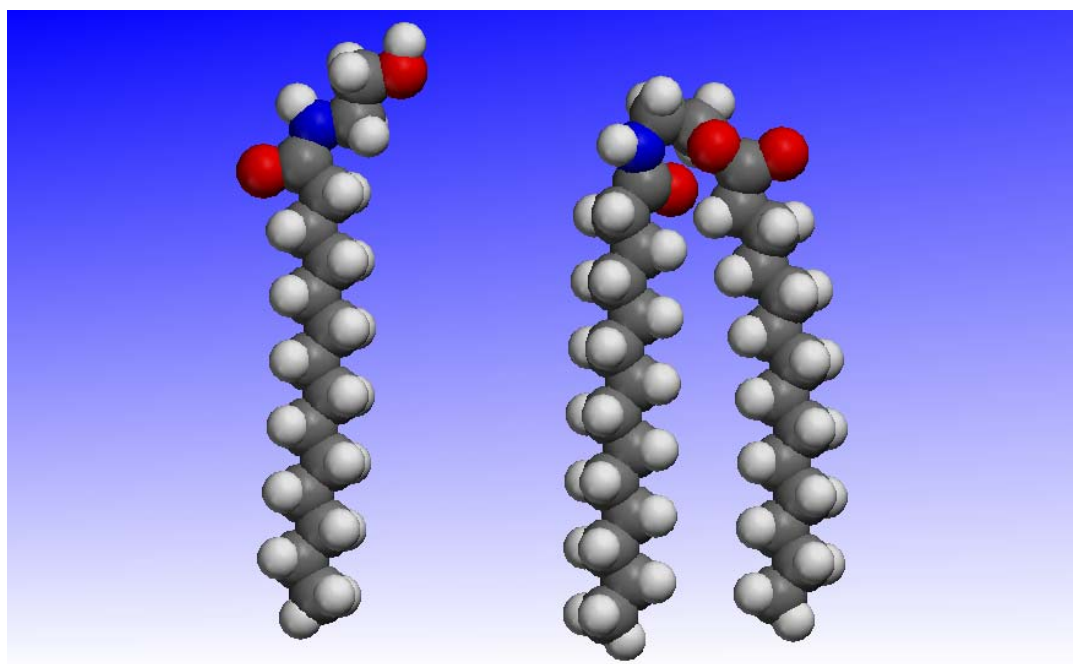
6.4.10. Even-odd Alternation in Transition Temperatures and Calorimetric Properties

It is interesting to note that the phase transition temperatures and calorimetric properties (ΔH_t and ΔS_t) of DAEs exhibit an even-odd alternation. Similar trends

were observed in the transition temperatures and physical properties of long-chain hydrocarbons, fatty acids and *N*-acylethanolamines in the solid phase, as well as for the chain melting phase transition temperatures of NAEs in the hydrated state (Larsson, 1986; Ramakrishnan and Swamy, 1998; Marsh and Swamy, 2000). Such alternation has been explained on the basis of packing of the hydrocarbon chains. In long chain fatty acids, for example, it was shown by Larsson (1986) that differences in the packing properties between the terminal methyl groups between the even and odd members can explain the differences in the physical properties. Such differences do not arise in the methyl group packing if the chains are perpendicular to the methyl group plane. However, when the hydrocarbon chains are tilted with respect to the plane of the methyl groups, their packing modes can differ leading to alternation in the physical properties. The even-odd alternation in the transition temperatures, enthalpies and entropies of DAE of matched acyl chainlengths is consistent with the tilted *N*- and *O*-acyl chains observed in the crystal structure of *N*-, *O*-dilauroylethanolamine.

Chapter 7

General Discussion and Conclusions



NAE

DAE

GENERAL DISCUSSION AND CONCLUSIONS

As indicated in the Chapter 1, the major objective of the present study was to characterize NAEs and DAEs, in order to understand their biophysical properties in the pure state and in mixtures with other membrane lipids. In pursuit of this goal single-crystal X-ray diffraction, DSC, spin-label ESR, ^{31}P -NMR, Langmuir film balance, Brewster angle microscopy (BAM), and molecular modeling studies have been carried out. The results obtained in these studies, reported in the preceding chapters (2 through 6) clearly show that the objectives have been fulfilled to a large extent. The major results obtained are discussed below and their implications towards the role of NAEs in biomembranes are considered. In addition, synthesis, characterization and differential scanning calorimetric studies of DAEs are discussed.

Earlier DSC studies on a homologous series of NAEs have indicated that long chain NAEs probably exist in several polymorphic forms (Ramakrishnan et al., 1997; Ramakrishnan and Swamy, 1998). In order to investigate this in more detail and to understand the differences between different structural polymorphs, we have carried out X-ray diffraction as well as additional DSC studies. In studies reported in Chapter 2, the crystal structure of *N*-palmitoylethanolamine has been solved in two different polymorphic forms (α and β) by single crystal X-ray diffraction. In both polymorphs the NPEA molecules adopt a bilayer-type arrangement with tail-to-tail chain packing. This supramolecular organization is governed primarily by strong intermolecular hydrogen bonds between the hydroxy groups of NPEA molecules in opposite leaflets as well as between the amide N-H and C=O groups of adjacent molecules in the same leaflet, with the van der Waals forces between acyl chains providing further stabilization. While molecular structure as well as crystal packing arrangement of NPEA in polymorph α with

$P2_1/c$ space group are very similar to the corresponding features in the crystal structures of *N*-myristylethanolamine and *N*-stearylethanolamine reported earlier, the crystal packing of NPEA molecules in polymorph β with $Pbca$ space group – which is a new form – differs from that in polymorph α . In polymorph α the supramolecular organization of the bent NPEA molecules in opposite layers yields a ‘Z’ like shape, whereas in polymorph β one of the two NPEA molecules in the above organization is rotated by about 180° , such that the two molecules are now arranged in the shape of ‘W’. Despite these differences, the hydrogen bonding patterns in the two polymorphs have been found to be very similar. Packing energy calculations indicate that the polymorph α is more stable than the β polymorph by about $2.65 \text{ kcal.mol}^{-1}$, which is comparable to the enthalpy of transition 1 seen in the DSC thermograms of α form of the dry NPEA (Ramakrishnan et al., 1997). This study has firmly established the existence of different polymorphic forms in *N*-acylethanolamines and provided a comparison of the structures of two polymorphic forms of NPEA together with a possible mechanism for their interconversion.

Previous DSC and fast-atom-bombardment mass spectrometric studies (Ramakrishnan, 2001) on the interaction of NMEA with cholesterol have provided strong evidence indicating the formation of a 1:1 (mol/mol) complex between the two components in aqueous dispersion (DSC) and in the gas phase (FAB-MS). Additional DSC studies carried out on dry mixtures of NMEA and cholesterol indicate that in the solid state also the two compounds form a 1:1 molar complex. These observations are supported by computational modeling studies, which provided a plausible structural model wherein the 1:1 complex is stabilized by several hydrogen bonds between NMEA and cholesterol besides favorable dispersive interactions. The interaction of NMEA with cholesterol to form a complex with defined stoichiometry suggested that other homologous NAEs may also interact with cholesterol and form similar complexes. To investigate this

possibility DSC studies have been carried out on hydrated mixtures of NPEA and NSEA, which indicated that both these NAEs also form 1:1 stoichiometric complexes with cholesterol. These observations taken together suggest that the ability of NAEs to interact with cholesterol and form stable complexes may be relevant to their putative role in combating stress in their parent organisms.

To investigate the interaction between NAEs and cholesterol further, Langmuir film balance and Brewster angle microscopic studies have been performed on mixtures of NMEA and cholesterol. The monolayer studies have shown that at low fractions of cholesterol, the average area per molecule is lower than that predicted for ideal mixing, whereas at high cholesterol content the experimentally obtained average molecular area is higher than the ideal value calculated from the molecular areas of NMEA and cholesterol. The experimental data shows a cross-over point at 1:1 (mol/mol) ratio. In addition, the shape of the isotherm also changes significantly at 1:1 mol ratio. When the mole fraction of NMEA is greater than that of cholesterol, the isotherms show a slow rise in pressure with compression, which is indicative of a liquid-like structure, whereas at 1:1 mol ratio and when the cholesterol content is higher, the shape of the isotherm undergoes a dramatic change, indicating a transition to a solid condensed phase at lower molecular areas. Results obtained from BAM studies provide additional support to these observations.

Several interesting observations regarding NAEs and NAEs suggest that their interaction with other membrane lipids as well as proteins are likely to be important in the roles played by them in the parent organisms (Marsh and Swamy, 2000; Swamy et al., 2003; Chapter 1). Therefore, in order to understand the mechanisms by which these two types of compounds perform their functional roles in the native tissues, it is imperative to investigate their interaction with other membrane constituents. In this context, interaction between *N*-14 DMPE and

DMPC, NPEA and DPPC, and that of different NAEs with cholesterol were investigated in this laboratory earlier (Ramakrishnan et al., 2001, 2002; Swamy et al., 2003; Chapters 3, 4). In this study, the interaction between NMEA and DMPE and NPEA and DPPE has been investigated by biophysical approaches. The two NAEs investigated here, namely NMEA and NPEA, exhibit good miscibility with phosphatidylethanolamines of equivalent acyl chainlength at contents up to only 35-40 mol%. This is considerably lower than the miscibility of NPEA and DPPC, which were found to mix well at contents up to 60 mol% of the former (Swamy et al., 2003). It is interesting to note that although the phase transition temperatures of the diacyl PEs are closer to those of the NAEs of corresponding chainlengths, the miscibility of the NAE/diacyl PE systems is less extensive than that of the NAE/diacyl PC system. Overall, these results indicate that the NAEs do not exhibit complete miscibility with either of the two major phospholipids of eukaryotic cell plasma membranes, namely phosphatidylcholine and phosphatidylethanolamine. Consequently, it appears that the NAEs may be stored in the biological membranes as their precursor lipids, namely NAPEs, which are mobilized when necessary, i.e., when subjected to membrane stress (cf. Ramakrishnan et al., 2001).

It has been reported by Schmid et al. (1990) that NAEs could be *O*-acylated by rat heart cell free preparations under suitable conditions to produce *N*-, *O*-diacylethanolamines (DAEs). In another report it was shown that different lipases could also catalyze the same reaction under appropriate conditions (Furutani et al., 1997). These observations indicated that DAEs could be present in normal biological membranes, possibly as minor constituents, but have not been detected so far. In view of this possibility, it was considered interesting to investigate the properties of *N*-, *O*-diacylethanolamines and studies on the synthesis and physico-chemical characterization of these compounds was taken up. DAEs of matched acyl chains were synthesized in good yields (55-60%) and characterized by IR and

^1H -NMR spectroscopy. X-ray diffraction studies on *N*-, *O*-dilauroylethanolamine (DLEA) show that in the solid phase molecules of DLEA pack in a bilayer type fashion similar to long-chain fatty acids. The all-*trans* *N*- and *O*-acyl chains of the molecule are tilted by 36.5° and 34.5° , respectively, with respect to the normal to the plane of the bilayer. The amide N–H and C=O groups of the *N*-acyl chain are in *trans* geometry. The packing coefficient for DLEA was found to be higher than that observed for NMEA, NSEA and NPEA, indicating that the acyl chains in DAEs are more tightly packed than those in NAEs. Hydrogen bonding interactions between the N–H and C=O groups of the amide moiety of adjacent molecules stabilize the molecular packing. These observations give molecular details of the packing and intermolecular forces that govern it and could be useful in understanding the biophysical properties of DAEs.

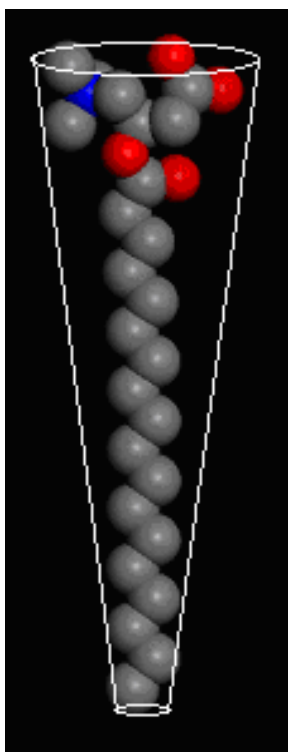
In the differential scanning calorimetric studies of DAEs, a linear dependence has been observed in the thermodynamic parameters. Transition enthalpy (ΔH_t) and transition entropy (ΔS_t), associated with the chain-melting phase transitions of homologous series of DAEs with matched, even as well as odd chainlengths ($n = 10\text{--}20$) in dry state. From the linear dependence of ΔH_t and ΔS_t , it was possible to estimate ΔH_{inc} and ΔS_{inc} , the average contribution from each CH_2 unit towards the overall transition enthalpy and entropy, respectively. When the even and odd chainlength series are compared, an alternation is observed between them in the calorimetric properties (ΔH_t , ΔS_t , T_t).

In summary, the studies presented in this thesis have widened our understanding of the biophysical properties and interaction of *N*-acylethanolamines with other membrane lipids. The existence of polymorphic forms of NAEs has been firmly established by the determination of the 3-dimensional structures of two polymorphic forms of *N*-palmitoylethanolamine. The interaction of *N*-myristoylethanolamine with cholesterol to form a 1:1 (mol/mol) complex has been

further investigated by additional DSC studies, computational modeling and Langmuir film balance measurements complemented by Brewster angle microscopy. Evidence has also been presented to show that higher homologs of NMEA, namely NPEA and NSEA also form 1:1 stoichiometric complexes with cholesterol. Studies employing DSC, ^{31}P -NMR and spin-label ESR spectroscopy have shown that NMEA/DMPE and NPEA/DPPE mixtures exhibit good mixing properties only up to 35-40 mol% of the NAE, with phase separation occurring at higher mole fractions of the NAE. This is consistent with the hypothesis that NAEs are probably stored as their precursors (NAPEs) and are generated only when required (Ramakrishnan et al., 2001). Finally, a homologous series of *N*-, *O*-diacylethanolamines of matched acyl chainlengths have been synthesized, characterized and their chain melting phase transitions have been investigated by DSC. These studies show that the calorimetric properties associated with the chain melting phase transitions of DAEs (T_t , ΔH_t , ΔS_t) exhibit odd-even alternation.

Appendix

Studies on the Critical Micellar Concentration and Phase Transitions of Stearoylcarnitine



Studies on the Critical Micellar Concentration and Phase Transitions of Stearoylcarnitine.
Kamlekar, R.K. and Swamy, M.J. 2006. *Biosci. Rep.* (In Press).

A.1. SUMMARY

The critical micellar concentration (CMC) of stearoylcarnitine was determined at different pH values at room temperature by fluorescence spectroscopy, monitoring the spectral changes of 8-anilinonaphthalene-1-sulfonate (ANS). The CMC was found to vary with pH, increasing from about 10 μM at pH 3.0 to ca. 25 μM at pH 7.0, but decreasing slightly with further increase in pH to approximately 19 μM at pH 10.0. Differential scanning calorimetry (DSC) shows that stearoylcarnitine dispersed in water at low concentration undergoes a broad thermotropic phase transition at 44.5°C, with a transition enthalpy of 15.0 kcal.mol⁻¹. The transition temperature (T_t) shifts to ca. 50.5°C in the presence of 1 mM EDTA or when the concentration is increased significantly. The turbidity of aqueous dispersions of stearoylcarnitine was found to be considerably high at low temperatures, which decreases quite abruptly over a short temperature range, indicating that a transition occurs from a phase of large aggregates to one of much smaller aggregates, most likely micelles. The phase transition temperature was determined as 29.1°C at pH 3.0, which increased with increasing pH up to a value of 55.3°C at pH 8.6 and remains nearly constant thereafter up to pH 11.2. The pH dependence of CMC and T_t suggest that the pK_a of the carboxyl group of long chain acylcarnitines shifts to higher temperatures upon aggregation (micelles or bilayer membranes).

A.2. INTRODUCTION

In mammals, fatty acid catabolism takes place in the mitochondria. For this, fatty acids have to be transported across the mitochondrial membranes and fatty acyl coenzyme A (CoA) and fatty acyl carnitine are important intermediates in this transport process. Although fatty acids exist as coenzyme A derivatives both inside and outside mitochondria, they are briefly converted into carnitine esters, which are then transported across the mitochondrial inner membrane (Voet and Voet, 1995). In addition, long chain acyl carnitines have also been implicated in a number of pathophysiological effects. For example, the serum levels of acyl carnitines and total carnitine were found to decrease significantly in cancer patients with cachexia, and it was suggested that decreased carnitine pool could contribute to the development of cachexia (Vinci et al., 2005). In patients with chronic renal failure, but not undergoing hemodialysis, acylcarnitines accumulate whereas in those undergoing hemodialysis, the plasma carnitine levels decrease significantly (Calvani et al., 2004).

A number of reports indicate that acylcarnitines induce a variety of physiological changes, e.g., activation of Ca^{2+} release channels in muscle sarcoplasmic reticulum (El-Hayek et al., 1993), fall of mitochondrial transmembrane potential (Siliprandi et al., 1992) etc. It is likely that at least some of these effects are related to the ability of acylcarnitines to modulate the membrane physical properties. Besides, acylcarnitines and their structural analogs were found to exhibit anti-proliferative activity and strong inhibitory activity of protein kinase C, an enzyme that interacts with diacylglycerols as well as anionic phospholipids such as phosphatidylserine (Kato et al., 1981; Wise and Kuo, 1983; Nakaki et al., 1984; Nakadate et al., 1986; Garcia-Huidobro et al., 1999). Therefore, considerable interest was generated in studying the biophysical properties of these two classes of

compounds. Both fatty acyl CoAs and fatty acyl carnitines, bearing long acyl chains, are amphiphilic molecules and exhibit surface active properties (Goñi et al., 1996).

In previous studies, aggregation properties of fatty acyl CoAs as well as fatty acyl carnitines have been investigated in considerable detail. Determination of critical micellar concentration (CMC) of fatty acyl CoAs of different acyl chain lengths has been the subject of several studies (Constantinides and Steim, 1985; Smith and Powell, 1986; Das and Hajra, 1992; Requero et al., 1993). In other studies the membrane perturbing properties of palmitoyl CoA and palmitoylcarnitine were compared by investigating their interaction with phosphatidylcholine large unilamellar vesicles as well as monolayers (Requero et al., 1995a, b). The effect of these two amphiphiles on the gel-fluid and lamellar-hexagonal phase transitions of phospholipids has also been investigated (Veiga et al., 1996). The CMCs of fatty acyl carnitines with even acyl chain lengths between 8 and 16 carbon atoms have also been reported (Yalkowski and Zografi, 1970a, b; Requero et al., 1993). Studies on the CMC of acyl CoAs and acyl carnitines have shown that under identical conditions the CMC decreases linearly with increasing acyl chain length (Smith and Powell, 1986; Requero et al., 1993). In addition it has been shown that the CMC values vary considerably on the properties of the medium such as buffer used, pH as well as on the method of measurement.

In an interesting report, Stinson (1990) demonstrated that palmitoyl carnitine exists in an interdigitated bilayer structure at low temperature and hexagonal phase (H_1) at high temperature, with a broad phase transition occurring between ca. 25°C and 45°C. The ability of other long chain fatty acyl carnitines to form aggregated structures other than micelles has not been investigated so far. In the present chapter, the aggregation properties of stearoylcarnitine (StCar) – which have not been hitherto characterized – have been investigated in considerable

detail; the CMC as well as the thermotropic phase transitions exhibited by this compound were investigated at different pH values and both were found to vary with change in pH.

A.3. MATERIALS AND METHODS

A.3.1. Materials

D,L-Stearoylcarnitine chloride, 8-anilinonaphthalene-1-sulphonic acid and Tris base were purchased from Sigma (St. Louis, MO, USA). Citric acid, sodium citrate, disodium hydrogen phosphate and sodium carbonate were purchased from E. Merck (Mumbai, India). Sodium bicarbonate was obtained from Ranbaxy (Mumbai, India). All other reagents and chemicals were obtained from local suppliers and were of the highest purity available. The following buffers were used for measurements at different pH values: 50 mM citric acid/sodium citrate (pH 3.0 – 6.0), 50 mM sodium phosphate (pH 7.0 – 8.0), 50 mM Tris/HCl (pH 8.0 – 9.0), 50 mM sodium carbonate/bicarbonate (pH 9.0 – 10.0) and 50 mM glycine/NaOH (pH 11.2). Double distilled water was used in all experiments.

A.3.2. Absorption Spectroscopy and Fluorescence Spectroscopy

Absorption measurements were made on a SHIMADZU model UV-3010PC UV-VIS-NIR spectrophotometer using 1 cm path length cells. Fluorescence measurements were made on a SPEX model FLUOROMAX-3 fluorescence spectrophotometer using $1 \times 1 \times 4.5$ cm quartz cells. A slit width of 3 nm was used on both excitation and emission monochromators.

A.3.3. Determination of Critical Micellar Concentration

The critical micellar concentration of stearyl carnitine was estimated by fluorescence spectroscopy using ANS as a fluorescent probe (Smith and Powell, 1986; Das and Hajra, 1992). The fluorescence studies were performed as follows. To a 2.5 ml sample of 10 μ M ANS, small aliquots of D,L-stearyl carnitine were added from a 1 mM stock solution using a Hamilton microliter syringe. After each addition, the fluorescence spectrum was recorded between 440 nm and 600 nm, keeping the excitation wavelength at 390 nm. The fluorescence intensity at 500 nm was then plotted as function of amphiphile concentration and the CMC was estimated as the concentration where a distinct break in the slope was observed.

A.3.4. Turbidimetry

Changes in the aggregation state of stearyl carnitine as a function of temperature at different pH values were investigated by turbidimetry. For this, samples were prepared by dispersing stearyl carnitine in the buffer of desired pH at ca. 1 mM concentration. The sample was then hydrated fully by heating to about 65-70°C in a warm water bath, with intermittent vortexing, followed by at least five cycles of freeze thawing, using liquid nitrogen and hot water (ca. 65°C). After the last incubation in hot water, the sample tube was incubated overnight at ca. 4°C and the cold solution was transferred to a spectrometer cuvette. Sample turbidity was measured at 325 nm at various temperatures between 15 and 60°C, while increasing the temperature.

A.3.5. Differential Scanning Calorimetry

Samples for DSC were prepared by suspending solid stearyl carnitine with double distilled water or with 50 mM sodium phosphate buffer, pH 7.4, containing 1 mM

EDTA. Samples were hydrated by heating the above suspension to ~65°C in a warm water, with intermittent vortexing. The hydrated samples were then incubated overnight at 4°C and then the lipid suspension and buffer were loaded into the sample and reference cell, respectively, of a VP-DSC differential scanning calorimeter (MicroCalTM, Inc., Northampton, MA, USA). A scan rate of 10°/hour or 30°/hour in the Celcius scale was used in different experiments. Three to five heating scans were performed for each sample and the scans were found to be reproducible. Transition temperatures, enthalpies and width at half height were determined using the Origin 7.0 software provided with the calorimeter. Transition entropies (ΔS_t) were determined from the transition enthalpy (ΔH_t) assuming a first order transition according to the expression (Marsh, 1990):

$$\Delta S_t = \Delta H_t / T_t \quad (1)$$

where T_t refers to the transition temperature.

A.4. RESULTS AND DISCUSSION

In view of their involvement in fatty acid transport across the inner mitochondrial membrane, the properties of acylcarnitines are investigated with considerable interest. Among the various acylcarnitines, palmitoylcarnitine has been investigated extensively, whereas other acylcarnitines have been characterized to a significantly lesser extent. While the CMC values of acylcarnitines with 8 to 16 C-atoms in the acyl chain have been determined, to the best of our knowledge the aggregation properties of stearoylcarnitine – which contains 18 C-atoms in the acyl chain – have not been studied so far. Because stearoyl chain is a major component of the membrane phospholipids, it was considered important to investigate the aggregation and phase properties of StCar. Therefore, in this study, we have

investigated the CMC as well as phase transitions exhibited by StCar in considerable detail and results of these studies are discussed here.

A structural diagram of StCar is given in Fig. A.1A and its space-filling model is shown in Fig. A.1B. From these two figures it can be seen that this molecule has a larger cross-sectional area at the head group region and a significantly smaller area of cross-section in the acyl chain.

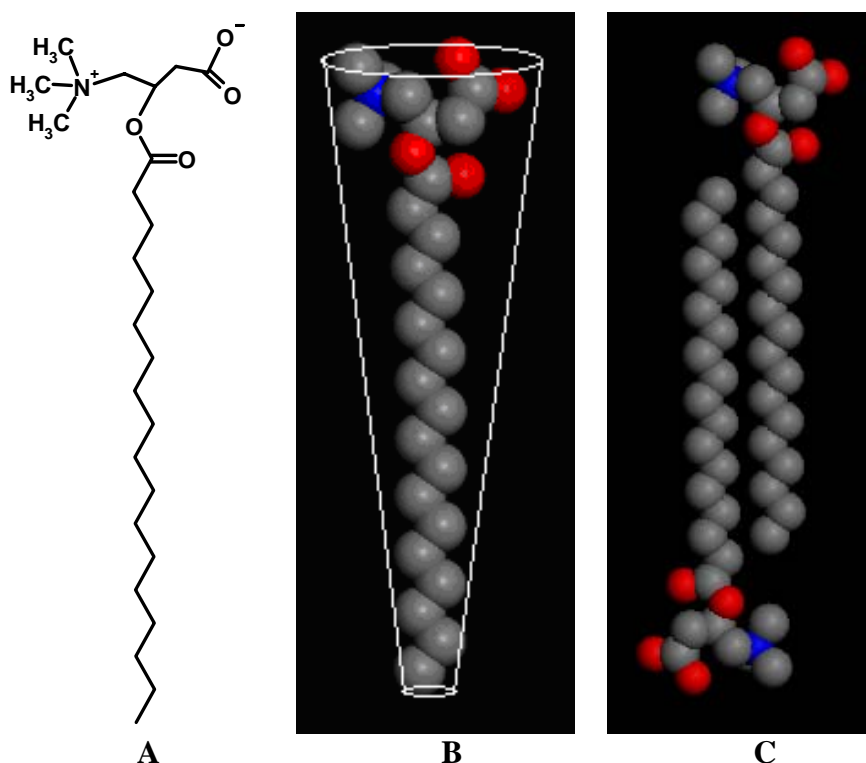


Fig. A.1: Structure and space-filling model of stearoylcarnitine. The chemical structure is shown in A and a space-filling model is shown in B. A schematic representation of two molecules of stearoylcarnitine in an interdigitated bilayer form is shown in C. The acyl chain is shown in all-trans conformation expected for the gel phase. The space-filling molecular models were generated using Accelrys MS Modeling 3.0.1 program (Accelrys Inc., San Diego, CA, USA; website: <http://www.accelrys.com>).

As shown schematically in Fig. A.1B, StCar may be considered to have a truncated conical shape. Such molecules usually adopt one of the following

structures depending on the other factors such as temperature, pressure and hydration: interdigitated gel phase, hexagonal phase (H_I) and micelles. In an earlier study, it was reported that palmitoylcarnitine forms an interdigitated structure in the gel phase, which undergoes a broad thermotropic phase transition to hexagonal structure (Stinson, 1990). Also, turbidimetric and FTIR studies suggested that palmitoylcarnitine dispersed in water at low concentration undergoes a phase transition from an ordered state to a disordered state, which is most likely micellar (Eschabe et al., 1995; Veiga et al., 1996). Since these two molecules are very similar in their structures, with the acyl chain of StCar being only slightly longer, it may be expected that it will also form an interdigitated structure in the gel phase (see Fig. A.1C), although at very low concentrations, it is likely to form micelles.

A.4.1. Critical Micellar Concentration of Stearoylcarnitine

The CMC of stearoylcarnitine was determined by fluorescence spectroscopy using 8-anilinonaphthalene-1-sulfonate (ANS) as the fluorescent probe. In these studies, the fluorescence intensity of the probe was monitored as a function of the acylcarnitine concentration. Representative plots of ANS fluorescence intensity as a function of StCar concentration, for the measurements made at pH 3.0, pH 6.0 and pH 9.0 are given in Fig. A.2. In each plot two distinct breaks are observed in the slope and each break indicates a change in the aggregation state of StCar. The first break should indicate the aggregation of StCar molecules that are solubilized in the buffer to form micelles and thus yield information on the critical micellar concentration of StCar, whereas the second break is expected to correspond to a transition of the micelles to another structural form. From the data presented in Fig. A.2, the CMC of StCar at pH 3.0, 6.0 and 9.0 were determined as 9.2, 15.0 and 22.5 μM , respectively. Two or three independent experiments yielded average values of $9.9 (\pm 0.7)$, $17.4 (\pm 2.7)$ and $22.3 (\pm 0.2)$ μM , at pH 3.0, 6.0 and 9.0, respectively.

These values are broadly in the same range as the values observed for palmitoylcarnitine (5-18 μM ; see Requero et al., 1993) and indicate that the CMC of StCar increases with pH in the range studied. In order to investigate the pH dependence of the CMC, measurements were also carried out at several other pH values and average values obtained from two or three separate experiments, carried out at each pH value, are listed in Table A.1.

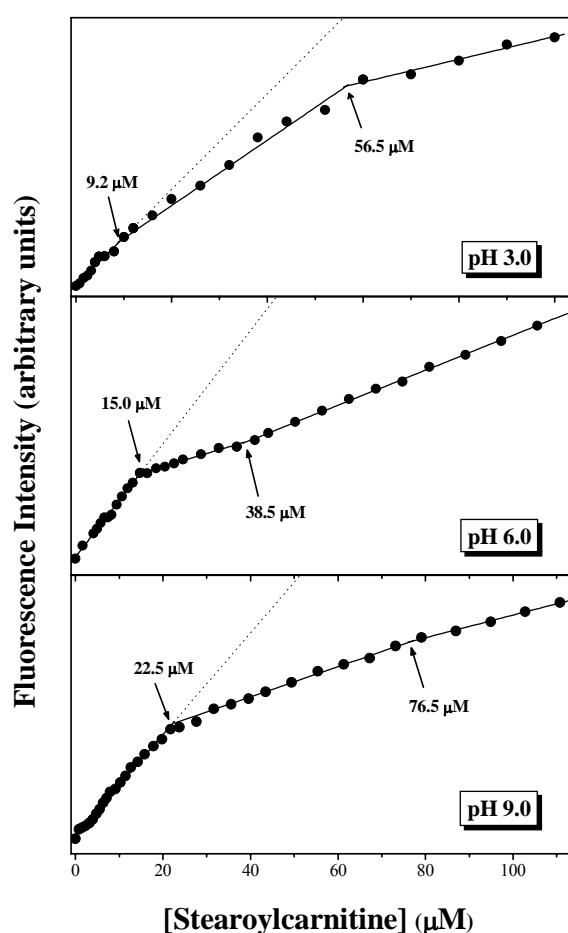


Fig. A.2: Determination of CMC of stearoylcarnitine by fluorescence spectroscopy. Fluorescence intensity of ANS is plotted as a function of StCar concentration at different pH as indicated in the figure. For each plot, concentration of StCar corresponding to the first break in the slope was taken as the CMC. The dotted line is an extrapolation of the initial linear part. Results from measurements performed at different pH values are given in Table A.1.

Table A.1: Critical micelle concentration (CMC) of stearylcarntine at different pH values. CMC values given are the averages obtained from two or three independent experiments. See text for further details.

pH	CMC (μM)
3.0	9.9 (± 0.7)
4.0	12.1 (± 1.3)
5.0	17.6 (± 0.1)
6.0	17.4 (± 2.7)
7.0	24.9 (± 0.9)
8.0	23.0 (± 0.6)
9.0	22.3 (± 0.2)
10.0	19.2 (± 0.1)

It is seen from the data presented in this Table that the CMC of stearylcarntine increases with increase in pH, reaching a maximum of ca. 25 μM at pH 7.0, but decreases slightly thereafter and reaches a value of 19.2 at pH 10.0. An approximately linear increase in the CMC was also observed for palmitoylcarntine when the pH of the medium was increased from 4.0 to 8.5 (Requero et al., 1993). The present results indicate that StCar also exhibits a similar behavior; our studies further show that the CMC value reaches a maximum around pH 7.0 and remains more or less stable up to pH 9.0 and decreases slightly at higher pH values.

A.4.2. Phase Transitions of Stearylcarntine – Turbidimetric and DSC Studies

Previous studies on palmitoylcarntine indicated that when dispersed in water it exists in an interdigitated bilayer phase at low temperature and converts to a normal hexagonal phase (H_I) as the temperature is increased (Stinson, 1990). The phase transition occurred over a broad temperature range with considerable coexistence of the two phases (ca. 20 degrees) and was essentially complete by 40°C. In DSC studies palmitoylcarntine dispersed in 100 mM PIPES buffer, pH 7.4, containing 140 mM NaCl, exhibited an endothermic phase transition at 47°C, which coincided with results of turbidimetric studies that indicated a transition from a phase of

larger aggregates to one of smaller aggregates, whereas aqueous dispersions of acylcarnitines of shorter acyl chains (containing up to 14 C-atoms) did not exhibit any phase transition (Veiga et al., 1996), clearly indicating that the phase properties of acylcarnitines depend on the acyl chainlength. However, thermotropic phase transitions of acyl carnitines with longer acyl chains have not been investigated. In the light of this, an investigation of the phase behavior of stearoylcarnitine was taken up in this study.

When hydrated at room temperature StCar yielded turbid suspensions which became optically clear upon heating to high temperature. This suggested that this compound undergoes a phase transition from a phase of high turbidity to a phase where the aggregates are small and do not scatter visible light. Therefore, detailed studies on the phase transitions of stearoylcarnitine were carried out by turbidimetric analysis by monitoring the sample turbidity at 325 nm as a function of temperature using a spectrophotometer. Since stearoylcarnitine has a quaternary ammonium group (the betaine) and a free carboxyl group, which can undergo protonation/deprotonation, the amphiphile can exist in the cationic form at low pH and in a zwitterionic form at high pH. It is most likely that the charge state can affect the phase transition temperature because the charged lipid molecules will experience repulsion when they aggregate, whereas the zwitterionic species will not (cf. Träuble et al., 1976). Indeed for some of the negatively charged lipids such as phosphatidylglycerols, *N*-biotinylphosphatidylethanolamines and *N*-acylphosphatidylethanolamines, it has been shown that screening the charge repulsion by high ionic strength leads to an increase in their phase transition temperature (Cevc et al., 1980; Swamy et al., 1994, 1997). In view of this, it is interesting to investigate the phase transitions of stearoylcarnitine at different pH values and such measurements were carried out between pH 3.0 and pH 11.2.

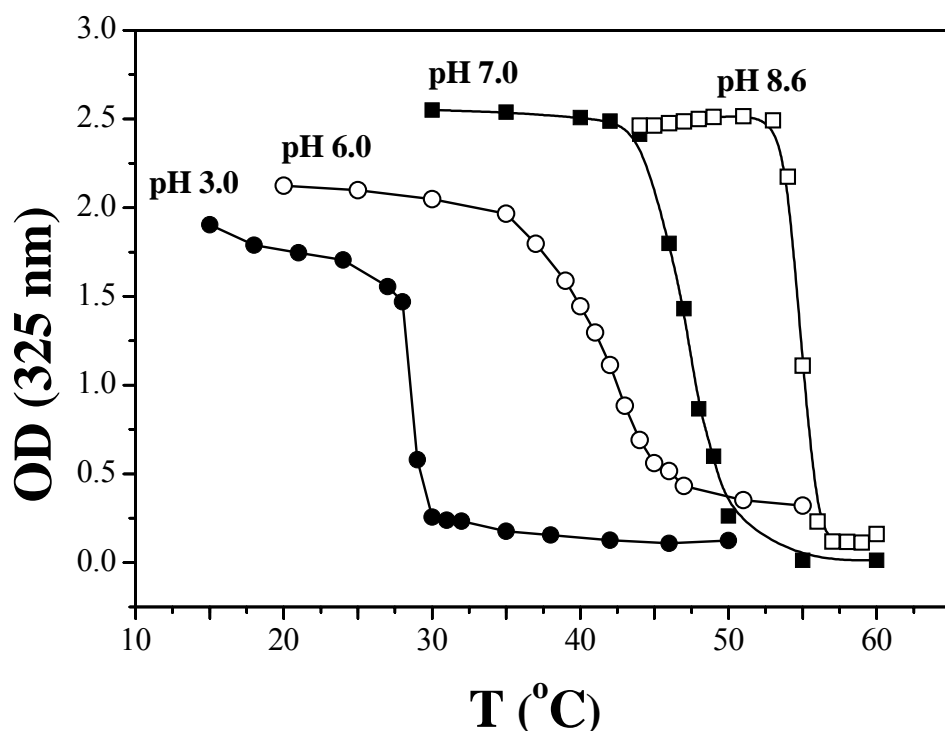


Fig. A.3: Turbidimetric study of thermotropic phase transitions in hydrated dispersions of stearyl carnitine at different pH values. The pH value corresponding to each phase transition profile is indicated. See text for further details.

Representative plots depicting change in the turbidity of StCar at pH 3.0, 6.0, 7.0 and 8.6 are shown in Fig. A.3. In each plot the turbidity values are relatively high at low temperature, remain so up to a certain temperature and exhibit a sharp decrease upon further increase of temperature and thereafter remain low. The midpoint of the steeply declining region was taken as the phase transition temperature. The T_t values determined at different pH are plotted as a function of pH in Fig. A.4. From this figure it can be seen that the phase transition temperatures show an increasing trend with increasing pH up to 8.6, with the T_t value of 29°C at pH 3.0 increasing to 55.7°C at pH 8.6. The T_t values then remain relatively high up to pH 11.2 (Fig. A.4).

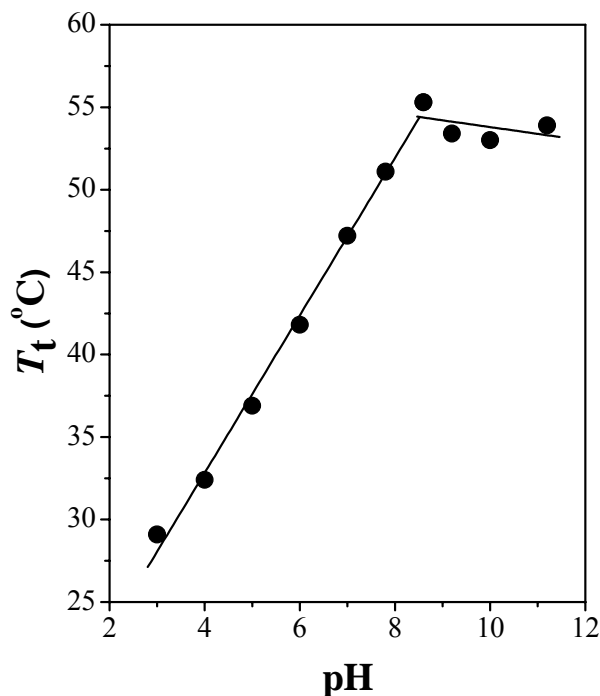


Fig. A.4: pH dependence of the phase transition temperature of hydrated dispersions of stearoylcarnitine.

The dependence of the phase transition temperature (T_t) on the sample pH indicates that the ionization state of the carboxylate influences the phase transition. While the protonated form of StCar is cationic, upon dissociation of the carboxyl group it becomes zwitterionic. This change in the charge state is expected to affect the phase transition and shift the T_t to higher temperature because the electrostatic repulsion between the positively charged StCar molecules will be reduced when the carboxyl group is deprotonated. This ionization of the carboxylate is described by the acid dissociation constant, pK_a .

The pK_a of carnitine in water at 25°C has been reported to be 3.72 whereas that of both acetylcarnitine and propionylcarnitine was found to be 3.58 (De Maria et al., 1994), suggesting that increasing the acyl chainlength does not alter the pK_a if the acylcarnitine is present as a monomer in water. However, the pK_a of the

carboxyl group of long chain acylcarnitines will be different because they aggregate in aqueous solution and hence their pK_a values will be affected by both the polarity of the interface as well as the surface electrostatics (cf. Cevc and Marsh, 1987). The titration of the carboxylate of StCar here may be compared with the titration behavior of stearic acid (SA) in the zwitterionic phosphatidylcholine (PC) membranes (Ptak et al., 1980) and stearic acid spin-labeled on the 5th C atom (5-SASL) in the negatively charged dimyristoylphosphatidylglycerol (DMPG) membranes (Sankaram et al., 1990). While the pK_a of SA was shifted from about 5.0 to 7.4 in the zwitterionic PC membranes, in the negatively charged DMPG it shifts further to about 8.0, which correspond to shifts of approximately 2.4 and 3.0 pH units in the zwitterionic and negatively charged membranes, respectively. Since the change in the phase transition temperature of StCar with pH does not show any sharp change, but increases somewhat gradually over the pH range between 3.0 and 9.0, it may be expected that the carboxyl group of StCar titrates over a broad pH range with a midpoint around 6.0 – 6.5; this indicates a shift in the pK_a of StCar by about 2.5 – 3.0 pH units, a value that is in good agreement with the shifts in pK_a observed for SA/5-SASL in the zwitterionic (PC) and negatively charged (DMPG) membranes.

The results of the turbidimetric experiments presented above clearly indicate that the sample turbidity decreases quite dramatically at the phase transition, and suggest that the aggregates formed above the phase transition are very small as compared to those formed below the phase transition. Visual inspection indicated that above phase transition the samples are clear to the naked eye, suggesting that the aggregates are likely to be some sort of micelles. Further work is necessary to characterize the structures of the aggregates.

In order to obtain further evidence regarding the phase transitions exhibited by the aqueous dispersions of StCar and to determine the enthalpy and entropy

associated with the phase transitions, differential scanning calorimetric experiments were carried out. DSC heating scans of fully hydrated stearoylcarnitine under different conditions are shown in Fig. A.5. Thermogram **A** gives a heating scan of a 1 mg/ml StCar sample dispersed in distilled water. A broad transition centered at 45.5°C with a half-width of about 6° is seen in this thermogram. The change in enthalpy and entropy associated with this transition were -15.0 kcal/mol and -33.7 cal/mol/K, respectively. The ΔH° value is slightly larger than the value of -14.1 kcal/mol reported for palmitoylcarnitine (Veiga et al., 1996), which is consistent with the increased acyl chain length of StCar.

This thermogram was not reversible in the sense that reheating of the sample immediately upon cooling to low temperature (10°C) did not yield the endothermic transition. However, long incubation at low temperature (overnight) resulted in a complete reappearance of the phase transition. This is also consistent with the above turbidimetric studies as well as with the results of Veiga et al. (1996) with palmitoylcarnitine.

Thermogram **B** with a narrower transition (half-width = 2.4°) centered at 50.6°C corresponds to a 1 mM sample of StCar dispersed in 50 mM phosphate buffer, pH 7.4, containing 1 mM EDTA (PBS-EDTA). This transition was found to be completely reversible, but the associated changes in enthalpy (-11.3 kcal/mol) and entropy (-22.3 cal/mol/K) are considerably smaller in magnitude than those obtained for the sample hydrated with water alone (see above). Veiga et al. (1996) have reported that palmitoylcarnitine gave a thermotropic phase transition that was irreversible when dispersed in buffer without EDTA but could be made reversible

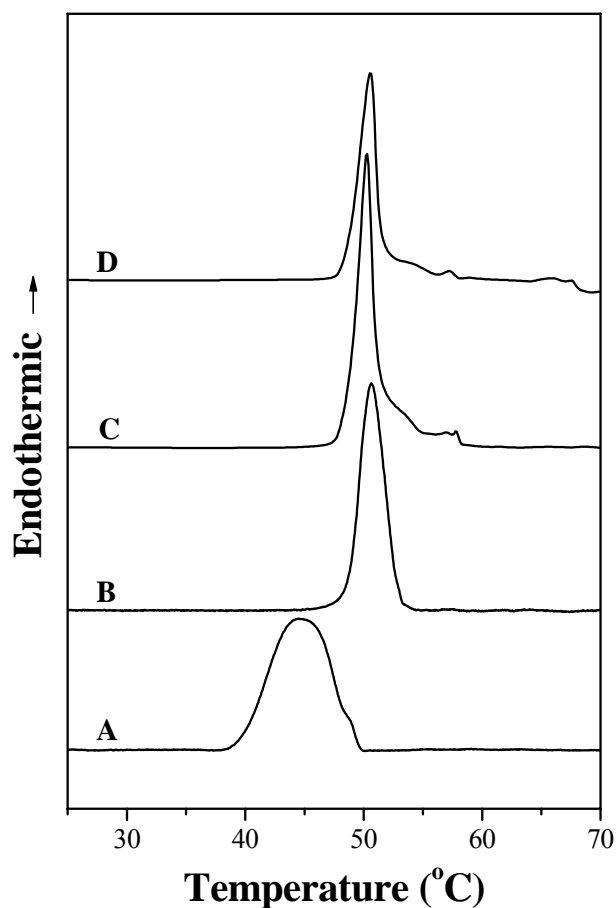


Fig. A.5: Differential scanning calorimetric heating scans of stearylcarbitine. A) 1 mg/ml in excess water; B) 1 mM in 50 mM phosphate buffer, pH 7.4, containing 1 mM EDTA; C) 108 mM in 50 mM phosphate buffer, pH 7.4; D) 98 mM in 50 mM phosphate buffer, pH 7.4, containing 1 mM EDTA. Scan rate = 10°/hr.

by the addition of EDTA, suggesting that the (presumably) micellar structures formed upon heating are stabilized by complexation with divalent metal ions. If this is true and if no divalent cations are added in the buffer, the trace amount of divalent metal ions present in the sample will be too small to complex much of the amphiphile if the concentration of acylcarbitine is increased significantly (e.g., 100 fold); in such a situation one should see practically no difference in the transitions observed in the presence and absence of EDTA. This is found to be true as shown

in thermograms **C** and **D**. While thermogram **C** was obtained with 108 mM StCar in PBS, thermogram **D** was obtained by adding EDTA from a 10 mM stock solution to give a final concentration of 1 mM. This resulted in a decrease in the final concentration of StCar to about 98 mM. Both **C** and **D** gave essentially identical endothermic transitions, which are centered at ca. 50.4°C with a half-width of 1.5-1.6°, validating the above interpretation. The phase transition temperatures obtained from the DSC measurements are in good agreement with the values obtained from the turbidimetric measurements described above and validate the extensive measurements on the pH dependence of the phase transition temperatures. The ΔH° values obtained were -11.2 kcal/mol and -9.8 kcal/mol, for samples **C** and **D**, respectively, with the corresponding ΔS° values being -22.3 and -19.4 cal/mol/K, respectively.

The significantly larger change in enthalpy obtained for StCar dispersed in water as compared to the dispersions in buffer (both without and with EDTA) suggests that the transition involves large disordering of the amphiphile aggregates in this sample as compared to the other samples. This can be interpreted as being due to the formation of more disordered structures upon phase transition in the case of the aqueous dispersions whereas in the dispersions of StCar in different buffers, the aggregates could be relatively more ordered. The larger change in the transition enthalpy for the sample hydrated with distilled water as compared to those hydrated with buffer is also consistent with this interpretation. This is qualitatively similar to the interpretation proposed by Veiga et al. (1996) for their results with palmitoylcarnitine. Structural characterization of the aggregates formed in the different samples is necessary to understand this better and we plan to investigate this aspect in our future work.

In summary, in the present study the pH dependence of the critical micellar concentration and phase transitions exhibited by stearoylcarnitine have been

investigated. The results obtained indicate that both the CMC and phase transition temperature are significantly influenced by the pH and increase with increase in the pH of the medium, but remain relatively stable at higher pH values. The pH dependence of the CMC and phase transition temperature suggests that the pK_a of the carboxyl group of acylcarnitines shifts to a significantly higher pH value upon aggregation. These observations provide a structural basis for understanding the role of acylcarnitines in different physiological processes.

References



REFERENCES

- Abrahamsson, S., Dahlén, B., Löfgren, H. and Pascher, I. 1978. Lateral packing of hydrocarbon chains. *Progr. Chem. Fats Lipids* **16**: 125-143.
- Akoka, S., Tellier, C., LeRoux, C. and Marion, D. 1988. A phosphorus magnetic resonance and a differential scanning calorimetry study of the physical properties of *N*-acylphosphatidylethanolamines in aqueous dispersions. *Chem. Phys. Lipids* **46**: 43-50.
- Ambrosoni, A., Bertoli, E., Mariani, P., Tanfani, E., Wozniak, M. and Zolese, G. 1993. *N*-Acylethanolamines as membrane topological stress compromising agents. *Biochem. biophys. Acta* **1148**: 351-355.
- Berdyshev, E.V., Schmid, P.C., Dong, Z. and Schmid, H.H.O. 2000. Stress-induced generation of *N*-acylethanolamines in mouse epidermal JB6 P⁺ cells. *Biochem. J.* **346**: 369-374.
- Bezuglov, V., Bobrov, M., Gretskeya, N., Gonchar, A., Zinchenko, G., Melck, D., Bisogno, T., Di Marzo, V., Kuklev, D., Rossi, J. C., Vidal J.P. and Durand, T. 2001. Synthesis and biological evaluation of novel amides of polyunsaturated fatty acids with dopamine. *Bioorg. Med. Chem. Lett.* **11**: 447-49.
- Bomstein, R.A. 1965. A new class of phosphatides isolated from soft wheat flour. *Biochem. biophys. Res. Commun.* **21**: 49-54.
- Brown, D.A. and London, E. 1998. Functions of lipid rafts in biological membranes. *Ann. Rev. Cell Dev. Biol.* **14**: 111-136.
- Brown, D.A. and Rose, J.K. 1992. Sorting of GPI-anchored proteins to glycolipid-enriched membrane subdomains during transport to the apical cell surface. *Cell* **68**: 533-544.
- Calvani, M., Benatti, P., Mancinelli, A., D'Iddio, S., Giordano, V., Koverech, A., Amato, A. and Brass, E.P. 2004. Carnitine replacement in end-stage renal disease and hemodialysis. *Ann. N. Y. Acad. Sci.* **1033**: 52-66.
- Campbell, I.D. and Dwek, R.A. 1984. Biological Spectroscopy. Benjamin/Cummings, Menlo Park, California, U.S.A.
- Cevc, G. and Marsh, D. 1987. Phospholipid bilayers. Physical principles and models. pp. 182-184, Wiley-Interscience, New York.
- Cevc, G., Watts, A. and Marsh, D. 1980. Non-electrostatic contribution to the titration of the ordered-fluid phase transition of phosphatidylglycerol bilayers. *FEBS Lett.* **120**: 267-270.

- Chapman, K.D. 2000. Emerging physiological roles for *N*-acylphosphatidylethanolamine metabolism in plants: signal transduction and membrane protection. *Chem. Phys. Lipids* **108**: 221-230.
- Chapman, K.D. 2004. Occurrence, metabolism, and prospective functions of *N*-acylethanolamines in plants. *Prog. Lipid Res.* **43**: 302-327.
- Chapman, K.D., Tripathy, S., Venables, B. and Desouja, A.D. 1998. *N*-Acylethanolamines: Formation and molecular composition of a new class of plant lipids. *Plant Physiol.* **116**: 1163-1168.
- Chapman, K.D., Venables, B.J., Markovic, R., Blair, R.W. and Bettinger, C. 1999. *N*-Acylethanolamines in seeds. Quantification of molecular species and their degradation upon imbibition. *Plant Physiol.* **120**: 1157-1164.
- Clarke, N.G., Hazlewood, G.P. and Dawson, R.M.C. 1976. Novel lipids of *Butyrivibrio* sp. *Chem. Phys. Lipids* **17**: 222-232.
- Constantinides, P.P. and Steim, J.M. 1985. Physical properties of fatty acyl-CoA. Critical micelle concentrations and micellar size and shape. *J. Biol. Chem.* **260**: 5773-5780.
- Cravatt, B.F. and Lichtman, A.H. 2003. Fatty acid amide hydrolase: an emerging therapeutic target in the endocannabinoid system. *Curr. Opin. Chem. Biol.* **7**: 469-475.
- Dahlén, B., Pascher, I. and Sundell, S. 1977. The crystal structure of *N*-(2-hydroxyethyl)-octadecanoate. *Acta Chem. Scand. A.* **31**: 313-320.
- Das, A.K. and Hajra, A.K. 1992. Critical micellar concentrations of palmitoyl dihydroxyacetone phosphate and 1-palmitoyl-rac-glycerol-3-phosphate. *J. Biol. Chem.* **267**: 9731.
- Dawson, R.M.C., Clarke, N. and Quarles, R.H. 1969. *N*-Acylphosphatidylethanolamine, a phospholipid that is rapidly metabolized during the early germination of pea seeds. *Biochem. J.* **114**: 265-270.
- De Maria, P., Fontana, A., Frascari, S., Gargaro, G., Spinelli, D. and Tinti, M.O. 1994. Effect of the addition of electrolytes on the partition coefficients, activity coefficients, and acid dissociation constants of carnitine and its acetyl and propionyl derivatives. *J. Pharmaceutical Sci.* **83**: 742-746.
- Devane, W.A., Hanus, L., Breuer, A., Pertwee, R.G., Stevensen, L.A., Griffin, G., Gibson, D., Mandelbaum, A., Etinger, A. and Mechoulam, R. 1992. Isolation and structure of a brain constituent that binds to the cannabinoid receptor. *Science* **258**: 1946-1949.

- Domingo, J., Mora, M. and De Madariaga, M.A. 1993. Incorporation of *N*-acylethanolamine phospholipids into egg phosphatidylcholine vesicles: characterization and permeability properties of the binary systems. *Biochim. Biophys. Acta* **1148**: 308-316.
- El-Hayek, R., Valdivia, C., Valdivia, H.H., Hogan, K. and Coronado, R. 1993. Activation of the Ca^{2+} release channel of skeletal muscle sarcoplasmic reticulum by palmitoyl carnitine. *Biophys. J.* **65**: 779-789.
- Ellingson, J.S. 1974. Changes in the phospholipid composition in the differentiating cellular slime mold, *Dictyostelium discoideum*. *Biochim. Biophys. Acta* **337**: 60-7.
- Ellingson, J.S. 1980. Identification of *N*-acylethanolamine phosphoglycerides and acylphosphatidylglycerol as the phospholipids which disappear as *Dictyostelium discoideum* cells aggregate. *Biochemistry* **19**: 6176-6182.
- Epps, D.E., Natarajan, V., Schmid, P.C. and Schmid, H.H.O. 1980. Accumulation of *N*-acylethanolamine glycerophospholipids in infarcted myocardium. *Biochim. Biophys. Acta* **618**: 420-430.
- Epps, D.E., Palmer, J.W., Schmid, H.H.O. and Pfeiffer, D.R. 1982. Inhibition of permeability-dependent Ca^{2+} release from mitochondria by *N*-acylethanolamines, a class of lipids synthesized in ischemic heart tissue. *J. Biol. Chem.* **257**: 1383-1391.
- Epps, D.E., Schmid, P.C., Natarajan, V. and Schmid, H.H.O. 1979. *N*-acylethanolamine accumulation in infarcted myocardium. *Biochem. Biophys. Res. Commun.* **90**: 628-633.
- Eschabe, I., Requero, M.A., Goñi, F.M., Arrondo, J.L. and Alonso, A. 1995. An infrared investigation of palmitoyl-coenzyme A and palmitoylcarnitine interaction with perdeuterated-chain phospholipid bilayers. *Eur. J. Biochem.* **231**: 199-203.
- Etter, M.C. 1990. Encoding and decoding hydrogen-bond patterns of organic compounds. *Acc. Chem. Res.* **23**: 120-126.
- Facci, L., Dal Toso, R., Romanello, S., Buriani, A., Skaper, S.D. and Leon, A. 1995. Mast cells express a peripheral cannabinoid receptor with differential sensitivity to anandamide and palmitoylethanolamide. *Proc. Natl. Acad. Sci. U.S.A.* **92**: 3376-3380.
- Fahy, E., Subramaniam, S., Brown, H.A., Glass, C.K., Merrill, A.H., Murphy, Jr., R. C., Raetz, C.R.H., Russell, D.W., Seyama, Y., Shaw, W., Shimizu, T., Spener, F., van Meer, G., VanNieuwenhze, M.S., White, S.H., Witztum, J.L. and Dennis, E.A. 2005. A comprehensive classification system for lipids. *J. Lipid Res.* **46**: 839-861.

- Feingold, L. 1993. Cholesterol in Membrane Models. CRC Press, Ann Arbor, MI.
- Furutani, T., Ooshima, H. and Kato, J. 1997. Preparation of *N*-, *O*-diacylethanolamine from *N*-acylethanolamine using lipase preparations. *Enzyme Microbial Technol.* **20**: 214-220.
- Ganley, O.H., Graessle, O.E. and Robinson, H.J. 1958. Anti-inflammatory activity of compounds obtained from egg yolk, peanut oil, and soybean lecithin. *J. Lab. Clin. Med.* **51**: 709-714.
- Gennis, R.B. 1989. Biomembranes. Molecular structure and function. Springer-Verlag, New York.
- Garcia-Huidobro, T., Valenzuela, E., Leisewitz, A.V., Valderrama, J. and Bronfman, M. 1999. Anti-proliferative effect of two novel palmitoyl-carnitine analogs, selective inhibitors of protein kinase C conventional isoenzymes. *Eur. J. Biochem.* **266**: 855-864.
- Goñi, F.M., Requero, M.A. and Alonso, A. 1996. Palmitoylcarnitine, a surface active metabolite. *FEBS Lett.* **390**: 1-5.
- Goto, M. and Takiguchi, T. 1985. The crystal structure of the β -form of α -monolaurin. *Bull. Chem. Soc. Jpn.* **58**: 1319-1320.
- Goto, M., Kozawa, K. and Uchida, T. 1988. The crystal structure of the β_1 ' form of optically active α -monostearin. *Bull. Chem. Soc. Jpn.* **61**: 1434-1436.
- Grell, E. 1981. Membrane spectroscopy. Springer-Verlag, New York.
- Gunstone, F.D., Harwood, J.L. and Padley, F.B. (Eds.). 1986. The lipid handbook. Chapman and Hall, London.
- Hack, M.H., and Helmy, F.M. 1975. Bis-phosphatidic acid plasmalogen in brain of *Amia calva* and its correlation with the infarct plasmalogen and the cardiolipin (diphosphatidyl glycerol) series of phosphatides. *Comp. Biochem. Physiol.* **52C**: 139-65.
- Hack, M.H. and Helmy, F.M. 1982. A reappraisal of the dog-heart infarct plasmalogen, its conception as a bis-phosphatidic acid and current recognition as an *N*-acylphosphatidylethanolamine. *Comp. Biochem. Physiol.* **73B**: 873-879.
- Hansen, H.H., Ikonomidou, C., Bittigau, P. and Hansen, H.S. 2001a. Accumulation of the anadamide precursor and other *N*-acylethanolamine phospholipids in infant rat models of *in vivo* necrotic and apoptotic neural death. *J. Neurochem.* **76**: 39-46.
- Hansen, H.H., Schmid, P.C., Bittigau, P., Lastres-Becker, I., Berrendero, F., Manzanares, J., Ikonomidou, C., Schmid, H.H.O., Fernandez-Ruiz, J.J. and Hansen,

- H.S. 2001b. Anandamide, but not 2-arachidonoylglycerol, accumulates during *in vivo* neurodegeneration. *J. Neurochem.* **78**: 1415-1427.
- Hansen, H.S., Moesgaard, B., Hansen, H.H. and Petersen, G. 2000. *N*-Acylethanolamines and precursor phospholipids – relation to cell injury. *Chem. Phys. Lipids* **108**: 135-150.
- Hargin, K.D. and Morrison, W.R. 1980. The distribution of acyl lipids in the germ, aleurone, starch and non-starch endosperm of our wheat varieties. *J. Sci. Fd. Agric.* **31**: 877-888.
- Hazlewood, G.P. and Dawson, R.M.C. 1975. Intermolecular transacylation of phosphatidylethanolamine by a *Butyrivibrio* sp. *Biochem. J.* **150**: 521-525.
- Hesketh, T.R., Kornberg, H.L., Metcalfe, J.C. and Northcote, D.H., Pogson, C.I. and Tipton, K.F. (Eds). 1982. Techniques in Lipid and Membrane Biochemistry, Elsevier, Ireland.
- Hönig, D. and Möbius, D. 1992. Reflectometry at the Brewster angle and Brewster angle microscopy at the air–water interface. *Thin Solid Films* **210/211**: 64-68.
- <http://en.wikipedia.org/wiki/Biomembrane>.
- Jain, M.K. 1988. Introduction to Biological Membranes. Wiley, New York.
- Janusz, J.M., Buckwalter, B.L., Young, P.A., LaHann, T.R., Farmer, R.W., Kasting, G.B., Loomans, M.E., Kerckaert, G.A., Maddin, C.S., Berman, E.F., Bohne, R.L., Cupps, T.L. and Milstein, J.R. 1993. Vanilloids 1: Analogs of capsaicin with antinociceptive and antiinflammatory activity. *J. Med. Chem.* **36**: 2595-2604.
- Kamlekar, R.K and Swamy, M.J. 2006. Molecular packing and intermolecular interactions in two structural polymorphs of *N*-palmitoylethanolamine, a Type-2 cannabinoid receptor agonist. *J. Lipid Res.* **47**: 1424-1433.
- Katoh, N., Wren, R.W., Wise, B.C., Shoji, M. and Kuo, J.F. 1981. Substrate proteins for calmodulin-sensitive Ca^{2+} -dependent protein kinases in heart, and inhibition of their phosphorylation by palmitoylcarnitine. *Proc. Natl. Acad. Sci. U.S.A.* **78**: 4813-4817.
- LaFrance, D., Marion, D. and Pézolet, M. 1990. Study of the structure of *N*-acyldipalmitoylphosphatidylethanolamines in aqueous dispersion by infrared and Raman spectroscopies. *Biochemistry* **29**: 4592-4599.
- Larsson, K. 1966. The crystal structure of the L-1-monoglyceride of 11-bromodecanoic acid. *Acta Crystallogr.* **21**: 267-272.

- Larsson, K. 1986. Physical properties—structural and physical characteristics. *In* The lipid Handbook (Gunstone, F. D., Harwood, J. L. and Padley, F. B., Eds.), Chapman and Hall, London, pp. 321-384.
- Lehninger, A.L., Nelson, D.L. and Cox, M.M. 1993. Principles of Biochemistry, CBS Publishers & Distributors, Delhi, 1013pp.
- Li, X-M., Ramakrishnan, M., Brockman, H.L., Brown, R.E. and Swamy, M.J. 2002. *N*-Myristoylated phosphatidylethanolamine: Interfacial behavior and interaction with cholesterol. *Langmuir* **18**: 231-238.
- Mackie, K., Devane, W.A. and Hille, B. 1993. Anandamide, an endogenous cannabinoid, inhibits calcium currents as a partial agonist in N18 neuroblastoma cells. *Mol. Pharmacol.* **44**: 498-503.
- MacMurray, T.A. and Morrison, W.R. 1970. Composition of wheat flour lipids. *J. Sci. Food. Agric.* **21**: 520-528.
- Markey, S.P., Dudding, T. and Wang, T.L. 2000. Base- and acid-catalyzed interconversions of O-acyl and N-acyl-ethanolamines: a cautionary note for lipid analyses. *J. Lipid Res.* **41**: 657-662.
- Marsh, D. 1988. Molecular mobility in membranes. *In* Physical properties of biological membranes and their functional implications, (Hidalgo, C., Ed.), Plenum, New York.
- Marsh, D. 1990. Handbook of Lipid Bilayers. CRC Press, Boca Raton, Florida, 387pp.
- Marsh, D. and Watts, A. 1982. Spin labeling and lipid-protein interactions in membranes. *In* Lipid-Protein Interactions (Jost, P. C., and Griffith, O. H., Eds.), Wiley-Interscience, New York. **2**: 53-126.
- Marsh, D. and Swamy, M.J. 2000. Derivatized lipids in membranes. Physico-chemical aspects of *N*-biotinyl phosphatidylethanolamines, *N*-acylphosphatidylethanolamines and *N*-acylethanolamines. *Chem. Phys. Lipids* **105**: 43-69.
- Maulik, P.R., Ruocco, M.J. and Shipley, G.G. 1988. Hydrocarbon chain packing modes in lipids: effect of altered sub-cell dimensions and chain rotation. *Chem. Phys. Lipids* **56**: 123-133.
- Mercadal, M., Domingo, J.C., Bermudez, M., Mora, M. and De Madariaga, M.A. 1995. *N*-Palmitoylphosphatidylethanolamine stabilizes liposomes in the presence of human serum: effect of lipidic composition and system characterization. *Biochim. Biophys. Acta* **1235**: 281-288.

- Moesgaard, B., Jaroszweski, J.W. and Hansen, H.S. 1999. Accumulation of *N*-acylethanolamine phospholipid in rat brains during post-decapitative ischemia: a ^{31}P NMR study. *J. Lipid Res.* **40**: 515-521.
- Mouritsen, O.G. 2005. Life-as a Matter of Fat. The Emerging Science of Lipidomics. Springer-Verlag, Berlin, 276 pp.
- Nakadate, T., Yamamoto, S., Aizu, E. and Kato, R. 1986. Inhibition of 12-*O*-tetradecanoyl phorbol-13-acetate-induced tumor promotion and epidermal ornithine decarboxylase activity in mouse skin by palmitoylcarnitine. *Cancer Res.* **46**: 1589-1593.
- Nakaki, T., Mita, S., Yamamoto, S., Nakadate, T. and Kato, R. 1984. Inhibition by palmitoylcarnitine of adhesion and morphological changes in HL-60 cells induced by 12-*O*-tetradecanoyl phorbol-13-acetate. *Cancer Res.* **44**: 1908-1912.
- Natarajan, V., Schmid, P.C. and Schmid, H.H.O. 1986. *N*-Acylethanolamine phospholipid metabolism in normal and ischemic rat brain. *Biochim. Biophys. Acta* **878**: 32-41.
- Natarajan, V., Schmid, P.C., Reddy, P.V., Zuzarate-Aungustin, M.L. and Schmid, H.H.O. 1985. Occurrence of *N*-acylethanolamine phospholipids in fish brain and spinal chord. *Biochim. Biophys. Acta* **835**: 426-433.
- Ohvo-Rekilä, H., Ramstedt, B., Leppimäki, P. and Slotte, J.P. 2002. Cholesterol interactions with phospholipids in membranes. *Prog. Lipid. Res.* **41**: 66-97.
- Okamoto, Y., Morishita, J., Tsuboi, K., Tonai, T. and Ueda, N. 2004. Molecular characterization of a phospholipase D generating anandamide and its congeners. *J. Biol. Chem.* **279**: 5298-5305.
- Pascher, I. and Sundell, S. 1985. Interactions and space requirements of the phosphate head group in membrane lipids. The crystal structure of disodium lysophosphatidate dihydrate. *Chem. Phys. Lipids* **37**: 241-250.
- Pascher, I., Lundmark, M., Nyholm, P. and Sundell, S. 1992. Crystal structures of membrane lipids. *Biochim. Biophys. Acta* **1113**: 339-372.
- Pascher, I., Sundell, S. and Hauser, H. 1981. Polar group interaction and molecular packing of membrane lipids. The crystal structure of lysophosphatidylethanolamine. *J. Mol. Biol.* **153**: 807-824.
- Pertwee, R.G. 1972. Ring test - quantitative method for assessing cataleptic effect of cannabis in mice. *Br. J. Pharmacol.* **46**: 753.
- Porter, A.C., Sauer, J-M., Knierman, M.D., Becker, G.W., Berna, M.J., Bao, J., Nomikos, G.G., Carter, P., Bymaster, F.P., Leese, A.B. and Felder, C.C. 2002.

- Characterization of a novel endocannabinoid, virodhamine, with antagonist activity at the CB1 receptor. *J. Pharmacol. Exp. Ther.* **301**: 1020-1024.
- Prince, R.C. 1987. Hopanoids: The world's most abundant biomolecules? *TIBS* **12**: 455-456.
- Ptak, M., Egret-Charlier, M., Sanson, A. and Bouloussa, O. 1980. A NMR study of the ionization of fatty acids, fatty amines and *N*-acylamino acids incorporated in phosphatidylcholine vesicles. *Biochim. Biophys. Acta* **600**: 387-397.
- Radhakrishnan, A. and McConnell, H.M. 1999a. Cholesterol-phospholipid complexes in membranes. *J. Am. Chem. Soc.* **121**: 486-487.
- Radhakrishnan, A. and McConnell, H.M. 1999b. Condensed complexes of cholesterol and phospholipids. *Biophys. J.* **77**:1507-1517. Erratum in: 2001. *Biophys. J.* **80**: 2037
- Radhakrishnan, A., Li, X-M., Brown, R. E. and McConnell, H. M. 2001. Stoichiometry of cholesterol-sphingomyelin condensed complexes in monolayers. *Biochim. Biophys. Acta* **1511**: 1-6.
- Radhakrishnan, A. and McConnell, H.M. 2000. Chemical activity of cholesterol in membranes. *Biochemistry* **39**: 8119-8124.
- Radhakrishnan, A., Anderson, T.G. and McConnell, H.M. 2000. Condensed complexes, rafts, and the chemical activity of cholesterol in membranes. *Proc. Natl. Acad. Sci. U.S.A.* **97**: 12422-12427.
- Ramakrishnan, M. 2001. Calorimetric and spectroscopic studies on *N*-acylethanolamines, *N*-acylphosphatidylethanolamines and their mixtures with phosphatidylcholine and cholesterol. Ph. D thesis, University of Hyderabad.
- Ramakrishnan, M. and Swamy, M.J. 1998. Differential scanning calorimetric studies on the thermotropic phase transitions of *N*-acylethanolamines of odd chainlengths. *Chem. Phys. Lipids* **94**: 43-51.
- Ramakrishnan, M. and Swamy, M.J. 1999. Molecular packing and intermolecular interactions in *N*-acylethanolamines: crystal structure of *N*-myristoylethanolamine. *Biochim. Biophys. Acta* **1418**: 261-267.
- Ramakrishnan, M., Sheeba, V., Komath, S.S. and Swamy, M.J. 1997. Differential scanning calorimetric studies on the thermotropic phase transitions of dry and hydrated forms of *N*-acylethanolamines of even chainlengths. *Biochim. Biophys. Acta* **1329**: 302-310.
- Ramakrishnan, M., Marsh, D. and Swamy, M.J. 2001. Interaction of *N*-myristoyldimyristoylphosphatidylethanolamine with dimyristoylphosphatidyl-

- choline investigated by differential scanning calorimetry: binary phase diagram. *Biochim. Biophys. Acta* **1512**: 22-26.
- Ramakrishnan, M., Kenoth, R., Kamlekar, R.K., Chandra, M.S., Radhakrishnan, T.P. and Swamy, M.J. 2002. *N*-Myristoylethanolamine -Cholesterol (1:1) complex: First evidence from differential scanning calorimetry, fast-atom-bombardment mass spectrometry and computational modelling. *FEBS Lett.* **531**: 343-347.
- Requero, M.A., Goñi, F.M. and Alonso, A. 1993. The critical micellar concentrations of fatty acyl coenzyme A and fatty acyl carnitines. *J. Colloid Interface Sci.* **161**: 343-346.
- Requero, M.A., Goñi, F.M. and Alonso, A. 1995a. The membrane-perturbing properties of palmitoyl-coenzyme A and palmitoylcarnitine. A comparative study. *Biochemistry* **34**: 10400-10405.
- Requero, M. A., González, M., Goñi, F.M., Alonso, A. and Fidelo, G. 1995b. Differential penetration of fatty acyl-coenzyme A and fatty acylcarnitines into phospholipid monolayers. *FEBS Lett.* **357**: 75-78.
- Romão, R.I.S and da Silva, A.M.G. 2004. Phase behaviour and morphology of binary mixtures of DPPC with steaonitrile, stearic acid, and octadecanol at the air–water interface. *Chem. Phys. Lipids* **131**: 27-39.
- Romero, J., Garcia, L., Cebeira, M., Zadrozny, D., Fernandez-Ruiz, J.J. and Ramos, J.A. 1995. The endogenous cannabinoid receptor ligand, anandamide, inhibits the motor behavior: role of nigrostriatal dopaminergic neurons. *Life Sci.* **56**: 2033-2040.
- Sanderson, J.M. 2005. Peptide–lipid interactions: insights and perspectives. *Org. Biomol. Chem.* **3**: 201-212.
- Sankaram, M.B., Brophy, P.J., Jordi, W. and Marsh, D. 1990. Fatty acid pH titrations and the selectivity of interaction with extrinsic proteins in dimyristoylphosphatidylglycerol dispersions. Spin label ESR studies. *Biochim. Biophys. Acta* **1021**: 63-69.
- Scheul, H., Goldstein, E., Mechoulam, R., Zimmerman, A.M. and Zimmerman, S. 1994. Anandamide (arachidonylethanolamide), a brain cannabinoid receptor agonist, reduces sperm fertilizing capacity in sea urchins by inhibiting the acrosome reaction. *Proc. Natl. Acad. Sci. U.S.A.* **91**: 7678-7682.
- Schmid, H.H.O., Schmid, P.C., and Natarajan, V. 1990. *N*-acylated glycerophospholipids and their derivatives. *Prog. Lipid Res.* **29**: 1-43.

- Schmid, H.H.O., Schmid, P.C. and Natarajan, V. 1996. The *N*-acylation-phosphodiesterase pathway and signalling. *Chem. Phys. Lipids* **80**:133-42.
- Schmid, H.H.O., Schmid, P.C. and Berdyshev, E.V. 2002. Cell signaling by endocannabinoids and their congeners: questions of selectivity and other challenges. *Chem. Phys. Lipids* **121**: 111-134.
- Seltzman, H.H., Fleming, D.N., Thomas, B.F., Gilliam, A.F., McCallion, D.S., Pertwee, R.G., Compton, D.R. and Martin, B.R. 1997. Synthesis and pharmacological comparison of dimethylheptyl and pentyl analogs of anandamide. *J. Med. Chem.* **40**: 3626-3634.
- Sheets, E.D., Holowka, D. and Baird, B. 1999. Membrane organization in immunoglobulin E receptor signaling. *Curr. Opin. Chem. Biol.* **3**: 95-99.
- Sheldrick, G.M. 1997. SHELXL97. Program for the refinement of crystal structures, University of Göttingen, Göttingen, Germany.
- Siliprandi, D., Biban, C., Testa, S., Toninello, A. and Siliprandi, N. 1992. Effects of palmitoyl CoA and palmitoyl carnitine on the membrane potential and Mg^{2+} content of rat heart mitochondria. *Mol. Cell. Biochem.* **116**: 117-123.
- Simons, K. and Ikonen, E. 1997. Functional rafts in cell membranes. *Nature* **387**:569-72
- Singer, S.J. and Nicholson, G.L. 1972. The fluid mosaic model of the structure of cell membranes. *Science* **175**: 720-731.
- Smith, R.H. and Powell, G.L. 1986. The critical micelle concentration of some physiologically important fatty acyl coenzyme A's as a function of chain length. *Arch. Biochem. Biophys.* **244**: 357-360.
- Stinson, R.H. 1990. Palmitoyl carnitine can exist in lamellar and hexagonal phases. *Chem. Phys. Lipids* **52**: 29-39.
- Sun, Y-X., Tsuboi, K., Okamoto, Y., Tonai, T., Murakami, M., Kudo, I. and Ueda, N. 2004. Biosynthesis of anandamide and *N*-palmitoylethanolamine by sequential actions of phospholipase A₂ and lysophospholipase D. *Biochem. J.* **380**: 749-756.
- Swamy, M.J., Angerstein, B. and Marsh, D. 1994. Differential scanning calorimetry of thermotropic phase transitions in vitaminylated lipids. Aqueous dispersions of *N*-biotinyl phosphatidylethanolamines. *Biophys. J.* **66**: 31-39.
- Swamy, M.J., Marsh, D. and Ramakrishnan, M. 1997. Differential scanning calorimetry of chain-melting phase transitions of *N*-acylphosphatidylethanolamines. *Biophys. J.* **73**: 2556-2564.

- Swamy, M.J., Ramakrishnan, M., Marsh, D. and Würz, U. 2003. Miscibility and phase behaviour of binary mixtures of *N*-palmitoylethanolamine and dipalmitoylphosphatidylcholine. *Biochim. Biophys. Acta* **1616**: 174-183.
- Tanford, C. 1973. The Hydrophobic Effect. Wiley, New York.
- Träuble, H., Teubner, M., Woolley, P. and Eibl, H. 1976. Electrostatic interactions at charged lipid membranes. I. Effects of pH and univalent cations on membrane structure. *Biophys. Chem.* **4**: 319-342.
- Tsuboi, K., Sun, Y-X., Okamoto, Y., Araki, N., Tonai, T. and Ueda, N. 2005. Molecular characterization of *N*-acylethanolamine-hydrolyzing acid amidase, a novel member of the choloylglycine hydrolase family with structural and functional similarity to acid ceramidase. *J. Biol. Chem.* **280**: 11082-11092.
- Tulenko, T., Chen, M., Mason, P.E. and Mason, R.P. 1998. Physical effects of cholesterol on arterial smooth muscle membranes: evidence of immiscible cholesterol domains and alterations in bilayer width during atherogenesis. *J. Lipid Res.* **39**: 947-956.
- Veiga, M.P., Requero, M.A., Goñi, F.M. and Alonso, A. 1996. Effect of long-chain acyl-CoAs and acylcarnitines on gel-fluid and lamellar-hexagonal phospholipid phase transitions. *Mol. Membr. Biol.* **13**: 165-172.
- Venance, L., Piomelli, D., Glowinski, J. and Giaume, C. 1995. Inhibition of anandamide of gap junctions and intercellular calcium signaling in striatal astrocytes. *Nature* **376**: 590-594.
- Vinci, E., Rampello, E., Zanolli, L., Oreste, G., Pistone, G. and Malaguarnera, M. 2005. Serum carnitine levels in patients with tumoral cachexia. *Eur. J. Intern. Med.* **16**: 419-423.
- Voet, D. and Voet, J.G. 1995. Biochemistry, John Wiley & Sons, New York, pp. 668-669.
- Vogel, Z., Barg, J., Levy, R., Saya, D., Heldman, E. and Mechoulam, R. 1993. Anandamide, a brain endogenous compound, interacts specifically with cannabinoid receptors and inhibits adenylate cyclase. *J. Neurochem.* **61**: 352-355.
- Wise, B.C. and Kuo, J.F. 1983. Modes of inhibition by acylcarnitines, adryamycin and trifluoroperazine of cardiac phospholipid-sensitive calcium-dependent protein kinase. *Biochem. Pharmacol.* **32**: 1259-1265.
- Wouters, J., Vandevoorde, S., Culot, C., Docquir, F. and Lambert, D.M. 2002. Polymorphism of *N*-stearoylethanolamine: differential scanning calorimetric,

vibrational spectroscopic (FTIR), and crystallographic studies. *Chem. Phys. Lipids* **119**: 13-21.

Yalkowsky, S.H. and Zografi, G. 1970a. Some micellar properties of long-chain acylcarnitines. *J. Colloid Interface Sci.* **34**: 525-533.

Yalkowsky, S.H. and Zografi, G. 1970b. Potentiometric titration of monomeric and micellar acylcarnitine. *J. Pharmaceutical Sci.* **59**: 798-802.

Curriculum Vitae



CURRICULUM VITAE

K. Ravikanth was born in the MahabubNagar in 1974. After his schooling and Intermediate studies at MahabubNagar, he joined M.V.S College for Arts and Science, MahabubNagar, Andhra Pradesh and obtained his B. Sc. degree in 1995. He received his B. Ed. degree from Kakatiya University in 1996. He received his M. Sc. degree in 1999 from Centre for Post-Graduate Studies, Sri Krishna Devaraya University, Kurnool. In July 2000, he was qualified for Lectureship in UGC-CSIR-NET, All India Joint Entrance Examination. In July 2001 he was awarded M. Phil degree from School of chemistry, University of Hyderabad, and subsequently joined the same department for the Ph. D program in August 2001. JRF (2001) and SRF (2003) was awarded by Council for Scientific and Industrial Research, India. Besides membrane biophysical studies, lipid-protein interaction, his areas of research interests include small molecule synthesis, Liposome drug delivery and protein biochemistry.

List of Publications

(* = work pertinent to this thesis)

- *1. *N*-Myristoylethanolamine—Cholesterol (1:1) Complex: First Evidence from Differential Scanning Calorimetry, Fast-Atom-Bombardment Mass Spectrometry and Computational Modelling.
Ramakrishnan, M., Kenoth, R., **Kamlekar, R.K.**, Chandra, M.S., Radhakrishnan, T.P. and Swamy, M.J. (2002) *FEBS Lett.* **531**, 343-347.
- *2. Molecular Packing and Intermolecular Interactions in Two Structural Polymorphs of *N*-Palmitoylethanolamine, a Type-2 Cannabinoid Receptor Agonist.
Kamlekar, R. K. and Swamy, M. J. (2006) *J. Lipid Res.* **47**: 1424-1433.
- *3. Studies on the Critical Micellar Concentration and Phase Transitions of Stearoylcarnitine.
Kamlekar, R. K. and Swamy, M. J. (2006) *Biosci. Rep.* (Published online: DOI 10.1007/s10540-006-9027-7).

- *4. Miscibility and Phase Behavior of *N*-Acylethanolamine/ Diacylphosphatidylethanolamine Binary Mixtures of Matched Acyl Chainlengths ($n = 14, 16$).
Kamlekar, R.K., Satyanarayana, S., Marsh, D. and Swamy, M.J. (2006) (Communicated).
- *5. Monolayer and Brewster-Angle Microscopic Studies on the Interaction of *N*-Myristoylethanolamine with Cholesterol.
Kamlekar, R.K., Chandra, M.S., Radhakrishnan, T.P. and Swamy, M.J. (2006) (Manuscript under preparation).
- *6. Synthesis and Characterization of *N*-, *O*-Diacylethanolamines of Matched Acyl Chainlengths ($n = 10-20$) and Crystal Structure and Molecular Packing of *N*-, *O*-Dilauroylethanolamine.
Kamlekar, R.K., Tarafdar, P.K. and Swamy, M.J. (2006) (Manuscript under preparation).
- 7. *N*-Acyldopamines: Synthesis, Characterization and DSC Studies.
Kamlekar, R.K. and Swamy, M.J. (2006) (Manuscript under preparation).

Symposium Attended

- 1. Paper presented (Poster) in the International Conference on Chemistry Biology Interface Synergistic New Frontiers, Dr. B. R. Ambedkar Centre for Biomedical Research during 21 – 26, November (2004). “*Miscibility and Phase behavior of binary mixtures of NMEA/DMPE and NPEA/DPPE: The DSC and ESR spectral study*”.
Kamlekar, R.K., Marsh, D. and Swamy, M.J.
- 2. Paper presented (Poster) in the CHEMFEST-2005, School of Chemistry, University of Hyderabad in March (2005). “*Miscibility and Phase Behavior of N-Acylethanolamine/ Phosphatidylethanolamine Binary Mixtures of Matched Acyl Chains. Calorimetric and ESR Spectral Studies*”.
Kamlekar, R.K., Marsh, D. and Swamy, M.J.
- 3. Paper presented (Oral & Poster) in the CHEMFEST-2006, School of Chemistry, University of Hyderabad on 04, March (2006). “*N-Acylethanolamines: Structural Polymorphism and Interaction with Cholesterol*”.
Kamlekar, R.K., Chandra, M.S., Radhakrishnan, T.P. and Swamy, M.J.
- 4. Paper presented (Poster) in the Asia-Pacific Workshop on Biological Physics, National University of Singapore, Singapore, 3-5 July (2006). “*Crystal Structure and Intermolecular Interactions of Two Polymorphs of N-Palmitoylethanolamine, A Type-2 Cannabinoid Receptor Agonist*”.
Kamlekar, R.K. and Swamy, M.J.